MIXED MODE DELAMINATION OF

GLASS FIBER/POLYMER MATRIX COMPOSITE MATERIALS

by

Pancasatya Agastra

A thesis submitted in partial fulfillment
of the requirements for the degree

of

Master of Science

in

Chemical Engineering

MONTANA STATE UNIVERSITY—BOZEMAN
Bozeman, Montana

March 2004

APPROVAL

of a thesis submitted by

Pancasatya Agastra

This thesis has been read by each member of the thesis committee and has been found to be satisfactory regarding content, English usage, format, citations, bibliographic style, and consistency, and is ready for submission to the college of Graduate Studies.

Dr. John F. Mandell ____

Chairperson, Graduate Committee Date

Approved for the Department of Chemical Engineering

Dr. Ronald W. Larsen ____

Department Head Date

Approved for the College of Graduate Studies

Dr. Bruce R. McLeod ____

Graduate Committee Date

STATEMENT OF PERMISSION TO USE

In presenting this thesis in partial fulfillment of the requirements for a master's degree at Montana State University-Bozeman, I agree that the Library shall make it available to borrowers under rules of the Library.

If I have indicated my intention to copyright this thesis by including a copyright notice page, copying is allowable only for scholarly purposes, consistent with "fair use" as prescribed in the U.S. Copyright Law. Request for permission for extended quotation from or reproduction of this thesis in whole or in parts may be granted only by the copyright holder.

Signature ____

Date ____

ACKNOWLEDGEMENTS

First, I would like to thank Allah, The Almighty God, for giving me the strength courage to endlessly pursue what is so called knowledge. I would like to thank my parents for sacrificing their life for their children so that we can go to school to become someone. I want to thank my brothers, sisters, niece and nephews, my housemaid, who have given me moral support from afar.

Now, in no particular order, I would like to thank—in my most humble self—Dr. John Mandell, who has taught and guided me through the years of graduate school. He also has put up with me during my disoriented times; I owe him much of my gratitude. I want to thank Dr. Douglas Cairns, also for teaching me and giving moral support during graduate school. I want to thank Dr. Ron Larsen, whom I have known for a long time, for willing to be in the Graduate Committee.

I also would like to thank Daniel Samborsky, Miles Buechler, William Ritter, and Shelley Thomas for their often-hidden support and guidance. I also would like to thank my Indonesian friends, Orin Aulia, Rinaldi Santoso, Ardinan Santoso, Rian Pulunggono and my benevolent roommate Nabil El-Ferradi for their endless support. Last, but not least, I would like to thank my dear girlfriend, Rachel Webster, who has always been there for me. Thank you also to those people whose names I have not mentioned, but have helped me academically, morally, financially, and so on; you know who you are. This thesis was supported by Sandia National Laboratories under subcontract BC7159.

TABLE OF CONTENTS

TABLE OF CONTENTS - CONTINUED

TABLE OF CONTENTS - CONTINUED

LIST OF TABLES

LIST OF TABLES - CONTINUED

LIST OF FIGURES

LIST OF FIGURES - CONTINUED

LIST OF FIGURES - CONTINUED

ABSTRACT

Delamination between layers in composite materials is a major source of structural failure. Delamination resistance is quantified by the critical strain energy release rate, G. The strain energy release rate in the opening mode (mode I) is symbolized by G_I and in the shearing mode (mode II) by G_{II}. In service, most failures occur by mixed mode delamination cracks. The Mixed-Mode Bending test has been developed to produce a wide range of mixed-mode conditions for composite materials specimens.

Unidirectional stitched fabric E-glass composites with three different resins, isophthalic polyester, vinyl ester and epoxy, were tested for their delamination resistance. The resins represent the types of resins commonly used for the wind turbine blades. Seven G_I/G_{II} ratios were tested. In descending order, the toughest composite materials used: epoxy, vinyl ester, and isophthalic polyester resins.

Finite element models of the three different test geometries, each with three different resins, were also created to validate the data reduction and experimental methods. The G-values were calculated using the one-step virtual crack closure method (VCCT1). The first validation was a comparison between the experimental deflection and that from modified beam theory and finite element models. The second validation was a comparison between the modified beam theory and finite element G-values.

The final step was to explore mixed-mode delamination criteria. All three resin systems produced a maximum in the G_I component at failure, for some intermediate G_I/G_{II} ratio. Several different types of failure criteria, implicit and explicit forms, were fitted to the mixed mode test results. The power interaction criterion, an explicit form, fit the data best according to the R^2 value. The updated failure criterion is now available for implementation in finite element models of complex structures.

INTRODUCTION

Demands for Megawatt Wind Turbine Blades

Renewable energy will gain importance as the fossil fuel is depleted, and people have to find other sources of renewable energy. Wind energy is one of many options for renewable energy. In the world, the US is the second largest producer of wind power after Germany. A lot of the technology originates from Denmark. The leading energy company, GE, is currently testing a prototype of a 3.6 MW wind turbine blade, with a colossal rotor diameter of 104 m. The largest operating wind turbine in North America is operating in Big Spring, Texas, Vestas 1.65 MW V-66 spanning 66 meters in rotor diameter, owned by York Research Corporation.

In relation to the growing size of wind turbine blades, the fundamentals of understanding the constitutive materials must also grow. Montana State University has done extensive research on the behavior of materials used in wind turbine blades [1,2]. The most common materials for wind turbine blades are fiberglass composites. Composites are superior because their strength can be tailored to meet the required application, lightweight, and the specific strength (strength per weight) is high.

One major drawback of composite materials is delamination—separation of a laminate into layers. One major US Company, Kenetech, failed partly because of delamination failure at the trailing edge [3]. The size of the wind turbine blades, without the proper understanding of the material behavior, is likely to produce failure due to delamination.

Many ways have been found to resist delamination, for example weaving the fibers increases the toughness, but introduces micro-buckling modes, which is detrimental to the compressive strength; toughening the resin suppresses delamination but often decreases the modulus, an inherent trade-off in increasing toughness in the resins. Toughened resins are commonly used in aerospace preimpregnated materials, to resist delamination [4]. However, the cost of using prepreg materials in wind turbine manufacture can be high. Hence, low cost composite materials are sought for building wind turbine blades, such as fiberglass, where delamination has not been studied in detail.

There are three fundamental ways delamination can happen: opening mode, shearing or sliding mode, and tearing mode. More often than not, delamination occurs under mixed opening and shearing modes, which is the subject of this study.

This study is the extension of researches by Darrin Haugen [5] and Robert Morehead [6], who studied delamination of the skin-stiffener intersection geometry which is common in composite materials structures like wind turbine blades. This work combines, adds to, and revises their earlier work.

This research has explored the delamination of resin transfer molded (RTM) composites under mixed mode conditions, modes I and II, which occurs more commonly in applications than pure modes. The test method used for mixed mode fracture is the Mixed Mode Bending (MMB) Test. At the time this paper is written, the ASTM Standard for MMB had only recently been published [7]. Mixed mode conditions can occur in places where there is a change of geometry, i.e. a ply drop, an inevitable design characteristic of tapered structures. A ply drop is a geometric variation where one or more plies are discontinued because of design requirements. At the ply drop, a stress concentration is formed at the corner of the dropped ply. The stress concentration generally contains a mixed mode condition; however, the mode components are unknown without a detailed analysis, as by FEA.

In the Double Cantilever Beam (DCB) specimen, a pure mode I test, the End-Notched Flexure (ENF) specimen, a pure mode-II test, and the MMB test geometries, the modal components are known; therefore, the strain energy release rates can easily be calculated. In this study, the test specimens are modeled by finite element analysis and the G's are calculated using a numerical approach, the Virtual Crack Closure Technique, VCCT [8-11]. These models are the basis for calculating G-values at ply drops.

Once the test specimen models are validated, that is, the experimental values match the numerical values, then a mixed mode failure criterion is established. This criterion can then be used to predict the critical load of a complex structure, i.e., ply drops. The author hopes to establish a new level of analysis of delamination in composite materials structures using finite element analysis.

BACKGROUND

Delamination

Delamination between layers or plies of a composite laminate is a major weakness in composite materials. Delamination may reduce the stiffness of components and cause a catastrophic failure. A source of delamination is a stress concentration, which usually appears at a geometric discontinuity, i.e. edges and ply drops.

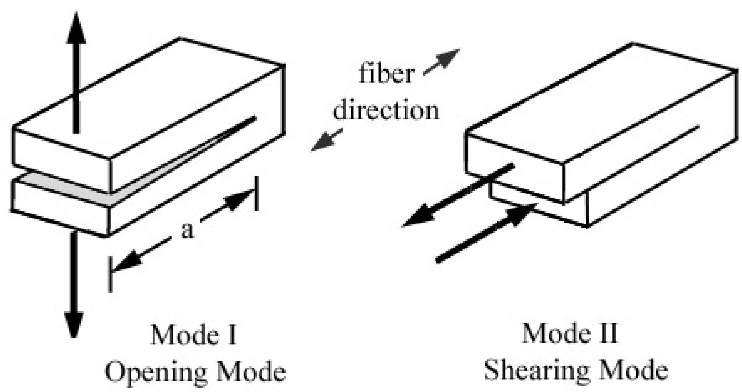

Figure 1 Two modes of crack propagation.

Delamination can occur in three modes:

1. Mode-I, opening mode, referred to as the out-of-plane delamination;
2. Mode-II, shearing mode, in-plane delamination;
3. Mode-II, tearing mode (not illustrated), anti-plane delamination.

Mode I and II are illustrated in Figure 1. The two modes of interest are mode-I and mode-II, as they are the most common modes of composite fracture. The most common approach to delamination analysis is the calculation of the strain energy release rate, SERR, with the symbol G, based on linear elastic fracture mechanics, LEFM. This method is limited to "brittle matrices"; for tough matrices, another method like elastic-plastic fracture mechanics may be employed, i.e., J-integral [12,13]. G is a measure of how tough the material is in resisting delamination and can be calculated from the load-deflection curve.

The criterion for the critical load used for metals is the 5% offset load from a load-deflection curve as prescribed in ASTM E399 [14]. The five percent method lumps nonlinear effects of small crack extension and material response into a modified linear calculation. Delamination is dominated by the resin property; as the resin gets tougher, the delamination becomes less brittle, which may limit the linear analysis of toughness [12]. In the load-deflection curve, crack extension is sometimes indicated by a sudden drop in load, under displacement controlled testing.[1]

The most common criterion for mode-I fracture toughness for metals is the critical stress intensity factor, K_{Ic}, and this value can be related to the corresponding energy based criterion G_{Ic}. The two criteria are not independent, but are related through the elastic constants [12]. The choice of criteria is generally a matter of convenience for the particular test method, with energy being easily calculated for compliant specimens as used for ply delamination.

[1] If the test were under load control, the load would not drop, instead the displacement would increase. Displacement control is most commonly used for testing.

Crack Interface

The most vulnerable lay-up to delamination is one where the crack is located at the interface between two 0° plies, (0/0) [5]. Tests of coupons with the (+45/-45) lay-up may be complicated because coupling effects, such as bending-twisting, may arise, and due to intra-ply matrix cracking within the plies [5].

In addition, fracture at +45/-45 interface is not a simple bi-modal fracture, but tri-modal, because mode-III can be induced at the crack interface where the orientations of the fibers are different [15]. In this study, only unidirectional materials with varying matrices are tested to check the toughness of laminates with these matrices.

When delamination test specimens are prepared, a Nylon starter-strip is incorporated as a crack starter. Originally, the resin rich area that forms at the tip of the Nylon strip was avoided by ignoring the initial step of crack growth [6]. Based on data with materials used in this study, the crack extending from starter crack tip is found to give the lowest G values, and so is the focus of this study.

Strain Energy Release Rate

Strain energy, covered in many mechanics textbooks [16], is the underlying origin of the strain energy release rate. The SERR will be referred to as G; G_I for SERR in mode I, and G_{II} for mode II. G_{Ic} refers to the critical SERR for crack extension under pure mode-I loading and G_{IIc}, pure mode-II. The G calculations are based on beam theory and, and, because of corrections, the theory is then called modified beam-theory, MBT. The corrections are discussed in more detail under DCB, ENF, and MMB subheadings.

Delamination in E-glass composites similar to those used in this study has been studied previously by Haugen [5] and Morehead [6]. They both predicted the critical load for delamination in the skin stiffener geometry by using mixed mode failure criteria with G_{Ic} and G_{IIc} values obtained from pure mode-I and -II tests, and finite element results.

In subsequent reports [5,17] based on these results, two methods were presented for predicting mixed mode delamination. Method A used measured G_{Ic} values from the actual (90/45) and (45/45) interfaces involved, and G_{IIc} values from (90/45) interface. Crack extensions corresponding to the observed crack extension in the skin-stiffener experiments were used to determine G_{Ic} and G_{IIc}. Method B used initiation G_{Ic} and G_{IIc} values from (0/0) crack interface in order to simplify the data requirements, since these were the minimum values obtained for various interfaces and crack extensions [5,17].

The MMB results from this study provide mixed mode data, which can be applied to the earlier studies. Available mixed mode failure criteria are empirical in nature, and are the subject of many studies, primarily for prepreg materials [18,24]. Studies reported in the literature [18-31] are based on both linear and nonlinear analysis. A nonlinear relationship between G_I and G_{II} suggests that there may be an interaction between the two [18,21,24,32]; an appropriate model to include this interaction will be sought in this study.

Testing for Pure Modes and Mixed Mode

The most established toughness criterion for mode-I delamination is G_{Ic}, determined using a double cantilever beam (DCB) test, which has been standardized in ASTM 5528 [33]. G_{IIc} is most commonly obtained using an end-notched flexure (ENF) [34-38] test, which is similar to a three-point bending test but with a crack at one end. Figure 2 and Figure 3 illustrate the DCB and ENF test specimens, respectively.

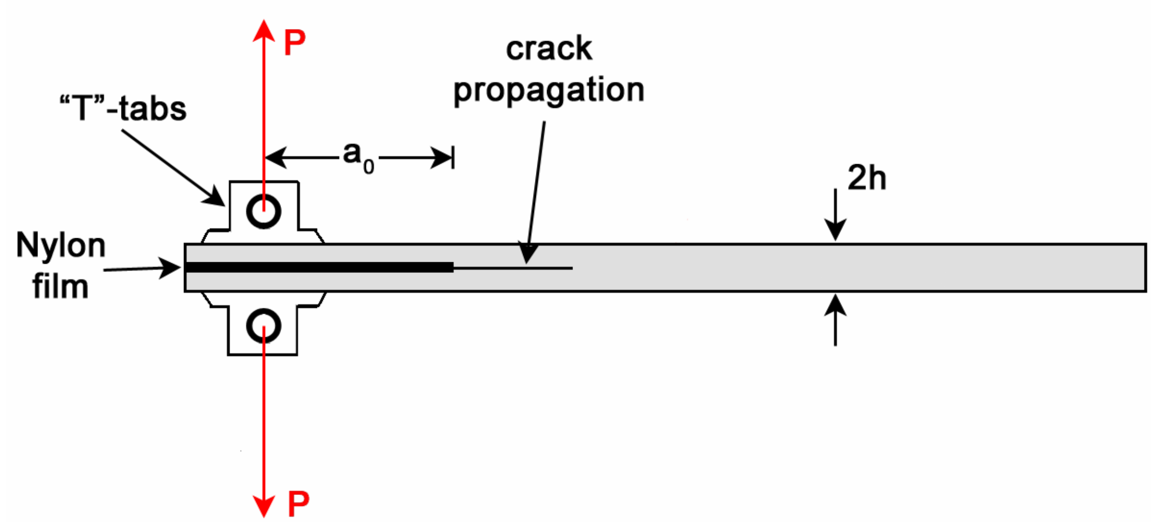

Figure 2 Double Cantilever Beam Test

Several other methods of calculating G_{Ic} from the DCB test, exemplified in ASTM 5528, were not used here because they lack accuracy, i.e. the area method. The compliance calibration method is not applicable because it involves significant crack extension, which causes fiber bridging. This method is also not applicable for G_{II} because the crack is unstable.

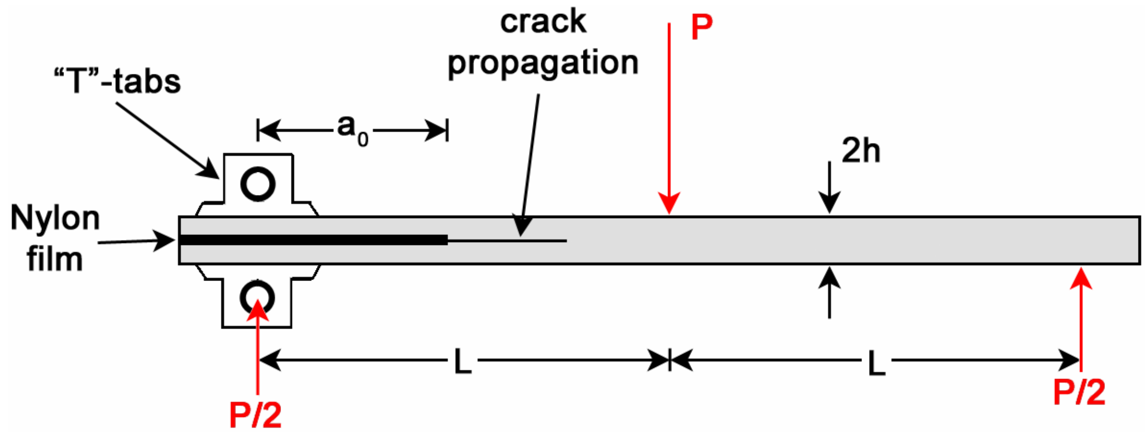

Figure 3 End-Notched Flexure Test

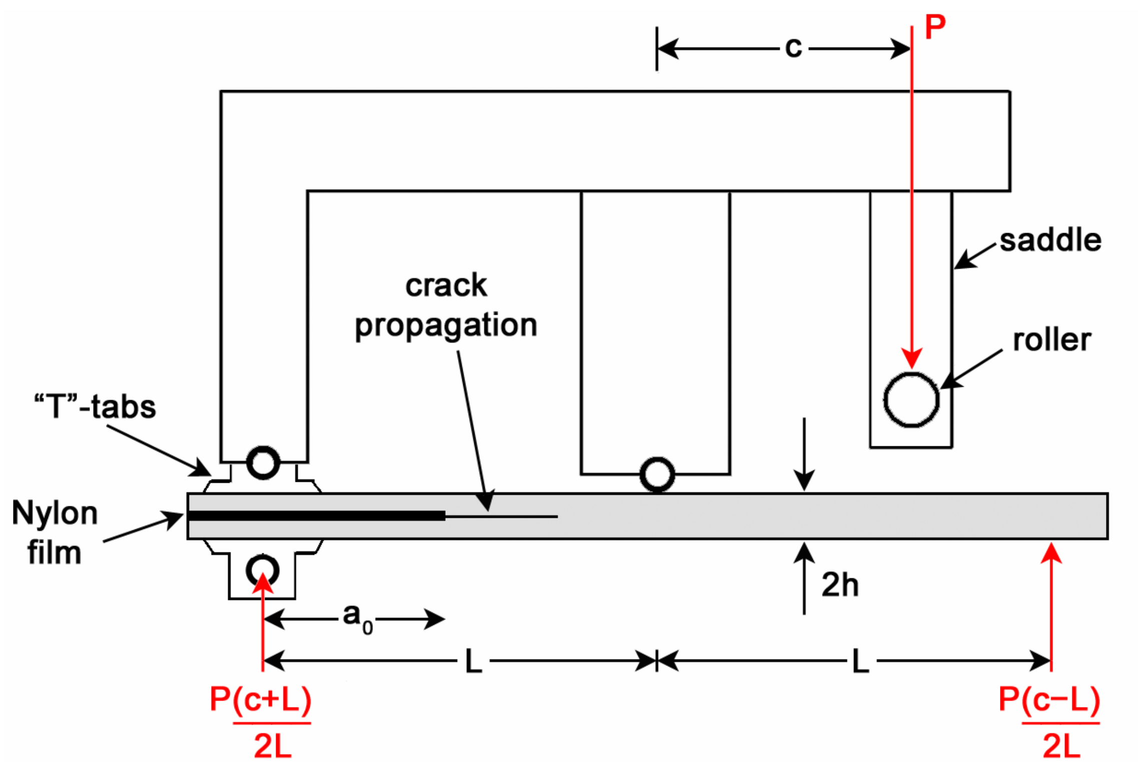

Figure 4 Schematic of mixed mode bending apparatus with the applied load and reactions.

The ENF test has not yet been standardized; complications due to friction between the beams may have prevented it from being standardized, because more detailed studies are needed [35,36]. Significant friction would affect the G_{IIc} calculation. Finite element analysis can be used to study friction effects in ENF tests using contact elements, a special type of elements that are available in the finite element analysis package ANSYS 7.0.

The mixed mode bending (MMB) test developed by Reeder and Crews [18,19] allows SERR calculation under mixed mode conditions. This test is reported to be superior to many already existing mixed mode tests, because the mixed mode ratio, G_I/G_{II}, can be varied by a single adjustment. Figure 4 illustrates the mixed mode bending test.

SERR Corrections

The derivation of SERR for various tests is available in several references [12, 40-43]. Corrections for SERR have been developed by several researchers; Timoshenko for shear deformation [45,46], Kanninen for elastic foundation [47], and Williams for large deflection and beam-root rotation [48,49].

In their analysis of this test, Reeder & Crews incorporated effects of both shear deformation and elastic foundation [18-20,22-24,30,31]. The Reeder and Crews analysis is used in this study, and an analysis by Williams [21,48-53] that includes large rotation and beam-root rotation, is discussed.

Shear deformation must be considered if the shear modulus is relatively small compared to the longitudinal modulus, as in most polymer matrix composites. Shear deformation is a function of specimen thickness (h), longitudinal modulus (E_{11}), and shear modulus in the 1-2 or 1-3 planes (G_{12} or G_{13}). The shear moduli G_{12} and G_{13} are taken to be the same, based on the usual transversely isotropic assumption. As the beams become shorter, this correction becomes more significant. This correction applies to both DCB and ENF tests.

Elastic foundation analysis is required for the DCB specimen because the two beams are supporting each other and act elastically, instead of acting as a rigid body [47]. The elastic foundation correction is a function of thickness, and longitudinal and transverse moduli.

A large deflection correction can be applied to pure modes when deflection can be obtained experimentally. In the MMB test, large deflection correction is not applicable because the deflection contributed by each mode is not measurable. While the mode-II deflection may be determined, the mode-I deflection component (in mixed mode) is no longer symmetric as in pure mode-I [27,28,31]. Since the modal deflections cannot be determined, corrections for them are unavailable prior to the test.

The rotation correction will render the testing substantially more difficult and the accuracy is limited by the accuracy of the equipment as well as the measurements. Rotation of the beam root can be measured approximately, but not at the accuracy of the other measurements. The accuracy of the toughness determination is not any better than the least accurate measurement. Large deflection and beam-root rotation corrections are not used in this study.

The SERR values formulated by Reeder and Crews are the following:

$$G_I = \frac{12P_I^2}{b^2h^3E_{11}}\left(a_o{}^2 + \frac{2a_o}{\lambda} + \frac{1}{\lambda^2} + \frac{h^2E_{11}}{10G_{13}}\right) \quad (1)$$

$$G_{II} = \frac{9P_{II}^2}{16b^2h^3E_{11}}\left(a_o^{\ 2} + \frac{h^2E_{11}}{5G_{13}}\right) \tag{2}$$

$$\lambda = \frac{1}{h}\sqrt[4]{\frac{6E_{22}}{E_{11}}} \tag{3}$$

$$P_I = P_C\left(\frac{3c - L}{4L}\right) \tag{4}$$

$$P_{II} = P_C\left(\frac{c + L}{L}\right) \tag{5}$$

where,

a_o = initial crack length

b = width of specimen

c = geometric variable that changes the G_I/G_{II} ratio

E_{11}, E_{22} = longitudinal and transverse moduli, respectively

G_{13} = inplane shear modulus

G_I, G_{II} = strain energy release rate in mode I and II, respectively

h = half-thickness of specimen

L = half-length of the bottom support

P_C = critical loading determined from load-deflection curve

$P_{I,}$ P_{II} = mode I and II loadings, respectively

λ = elastic foundation correction

See the illustration of the apparatus in Figure 4 for the geometric variables a_o, c, h and L. Lambda is the parameter in the elastic foundation correction and is a function of h, E_{11} and E_{22}.

Tensile vs. Flexural Modulus

There is a discrepancy in the Reeder and Crews method in using the flexural modulus to replace the tensile modulus. Flexural modulus can be used to account for fiber stacking, but strain energy is derived using the tensile modulus, therefore consistency must be exercised. If the flexural modulus is determined using a simple three-point bending test, the equation does account for shear deformation [16].

$$\delta = \frac{PL^3}{4bh^3E_{11}^f} \tag{6}$$

where,

δ = experimental deflection

b = width of specimen

E_{11}^f = flexural longitudinal modulus

h = half-thickness of specimen

P = experimental load

This equation is derived without the shear term and is the most common alternative to finding the tensile modulus experimentally. Another equation, which includes additional deflection due to shear, is the following [15,45,46]:

$$\delta = \frac{PL^3}{4bh^3E_{11}} + \frac{3PL}{8G_{13}bh} \tag{7}$$

The shear correction should only be used if tensile modulus is used. If the flexural modulus is determined from equation (6), then the shear correction should not be used in conjunction, as it is inherent in E_{11}^f.

Hackle Formation

On a local scale, the crack propagates normal to the direction of the maximum tensile stress, but on the global scale, the crack propagates between the lamina. As a result, for mode II, hackles are formed when the crack propagates. The direction of these hackles is perpendicular to the plane of principal stresses, which is at a 45° angle from the plane of principal stresses. In addition, as the crack propagates, a certain volume of matrix between lamina is removed. In pure mode-I, only formation of cusps is evident and there is essentially no removal of material, only separation. In mode II, the removal of voluminous material is confirmed by the presence of matrix grains in the crack interface. These grains often prevent the beam from completely closing and returning to the original position.

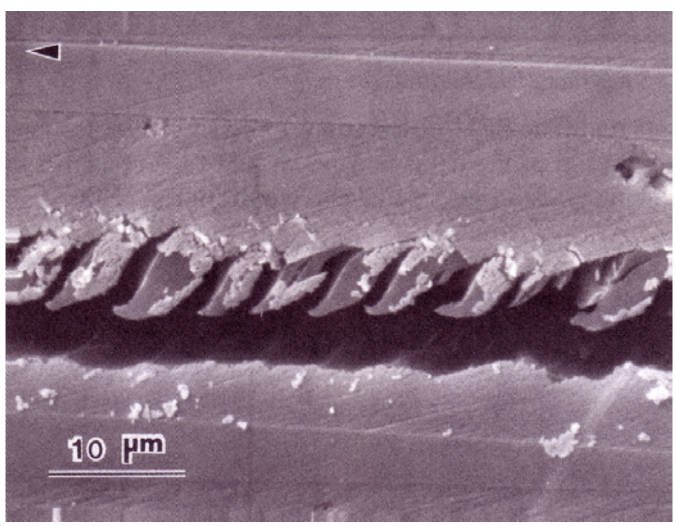

Figure 5 The formation of hackles between lamina during mode-II crack propagation. The arrow represents the direction of crack propagation [37]

A tremendous amount of energy is also dissipated instantaneously during crack propagation in mode II, such that the crack jumps past the loading point. Even though the mode-II crack is much harder to induce (higher G-value than mode I), once initiated, the result can be catastrophic, because of the available strain energy. For a tough matrix, high G_{IIc} is caused by yielding of the material at the crack tip and on the crack interface [37,38]. Figure 5 illustrates the formation of hackles between lamina.

Finite Element Modeling

Finite element modeling is first applied to the test specimens and then extended to other geometries such as ply drops, where analytical formulations are not available. Three methods are exemplified in the ANSYS manual to calculate fracture toughness: K_{Ic}, the stress intensity factor, G, the strain energy release rate (using Virtual Crack Extension, not the Virtual Crack Closure Technique), and J-integral, also an energy approach but more applicable to ductile fracture [54]. A macro to calculate K_{Ic} is already available in ANSYS, but it is restricted to isotropic materials. Codes for G and J calculation must be formulated by the user.

The ANSYS SERR calculation is different from the one given by Raju [9]. ANSYS virtual crack extension calculates the difference of strain energy at two different crack lengths, a and a+Δa, where a is the crack length, and Δa is the incremental crack extension. There are two distinct methods of the virtual crack closure technique (VCCT): one-step and two-step. One-step VCCT (VCCT1) calculates the strain energy instantaneously before the crack extends, and hence only uses initial crack length. The two-step VCCT (VCCT2) uses two different runs, similar to VCE by ANSYS, but unlike VCE, VCCT2 only uses the displacements of nodes around the crack tip. A more elaborate explanation is available in Reference 5.

VCCT1 determines the SERR using nodal displacements and forces around the crack tip. A schematic representation of the elements around the crack tip is given in Figure 6. VCCT1 is deemed sufficient to calculate the SERR [5], and is the only method used in this study.

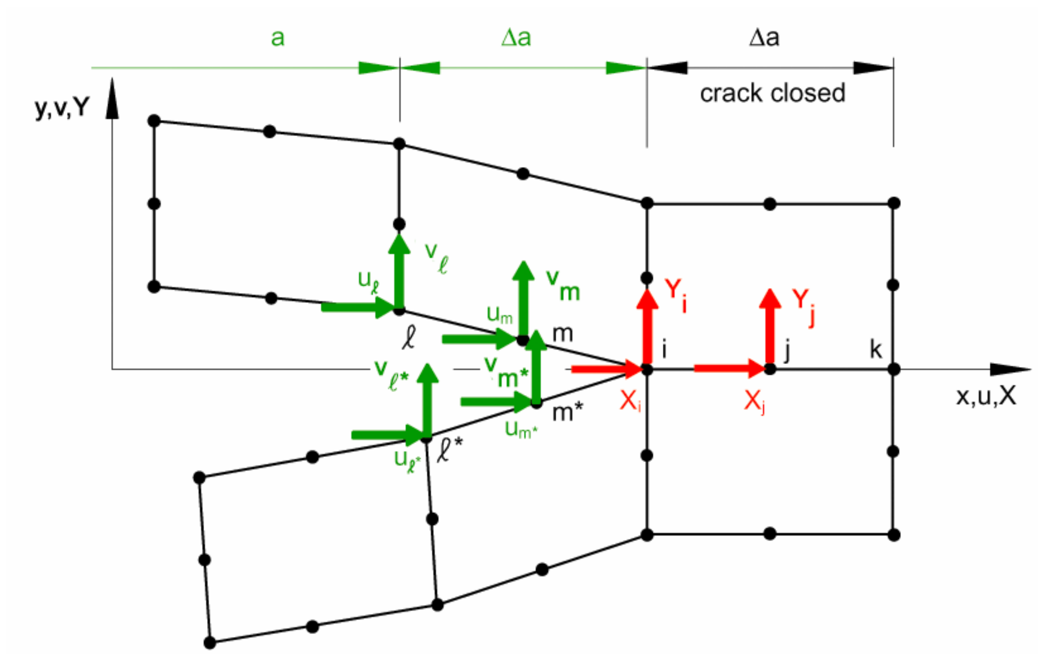

Figure 6 Illustration of the nodal reactions and displacement to calculate SERR using VCCT

VCCT1 formulas to calculate SERR:

$$G_I = -\frac{\left[Y_i(v_l - v_{l*}) + Y_j(v_m - v_{m*})\right]}{2\Delta a} \quad (8)$$

$$G_{II} = -\frac{\left[X_i(u_l - u_{l*}) + X_j(u_m - u_{m*})\right]}{2\Delta a} \quad (9)$$

where,

Δa = infinitesimal crack propagation

G_I, G_{II} = strain energy release rate in mode I and II, respectively

u and v = nodal displacements in x- and y-directions, respectively

Y and X = nodal forces in y- and x-directions, respectively

subscripts i, j, l, l*, m, and m* = node designations

The input for the finite element model (i.e. geometry, material properties, and critical loads) is based on experimental values. From the deformed result, nodal forces and displacements around the crack tip are extracted and substituted in the SERR calculation (Equations 8 and 9).

The derivation of the SERR using VCCT1 is feasible because of Irwin's fundamental assumption. It states that for an infinitesimal crack propagation, the crack opening at a distance of Δa behind the new crack tip (crack front for 3-D, crack tip for 2-D) is the same as the crack opening at a distance Δa from the previous crack tip [8-11]. Hence, the energy required to open a crack is the same as the energy to close the crack for length Δa. This allows the multiplication of the nodal displacement behind the crack tip and the nodal reaction in front of the crack tip.

Raju has also formulated the equation for other types of elements, i.e. shell, solid and a special element called a Quarter-Point element [9,10,55,56]. The model is done in 2D using an 8-node-quadrilateral-quadratic element, PLANE82, with plane strain option. Linear elements are not used because they are less accurate than quadratic elements and require twice as many elements. Furthermore, convergence to the true value with quadratic elements is much faster than with linear elements [57].

An independent convergence study to determine the size of the elements around the crack tip is required. The ANSYS manual suggests that for crack tip elements, the element size should be between 0.005 and 0.02 of crack length. An independent convergence study and the ANSYS suggestion are compared for consistency in this study.

Failure Criteria

Failure Criterion Background

The failure envelope for combinations of G_I and G_{II} must be fitted with a model for design purposes. Since most of the criteria lack theoretical derivation, only empirical models are available for curve fitting. Several papers have presented various mixed mode delamination criteria for composites. Reeder suggested several criteria for fitting, but after his own review, only the linear interaction criterion, bilinear criterion, and exponential hackle [24] are appropriate for his data, which are high fiber content carbon fiber prepreg materials. Reeder's qualified criteria are fitted to the MMB data in this paper.

Although these models have worked for carbon fiber prepreg composites, they may not work for E-glass composites with more heterogeneous, lower fiber content structures. Therefore, a more general failure criterion that works for a wide range of composite materials is more desirable.

$$\left(\frac{\sigma_{I}}{\sigma_{Iult}}\right)^{m}+\left(\frac{\sigma_{II}}{\sigma_{IIult}}\right)^{n}=1 \tag{10}$$

$$\left(\frac{K_{I}}{K_{Ic}}\right)^{m}+\left(\frac{K_{II}}{K_{IIc}}\right)^{n}=1 \tag{11}$$

$$\left(\frac{G_{I}}{G_{Ic}}\right)^{\frac{m}{2}}+\left(\frac{G_{II}}{G_{IIc}}\right)^{\frac{n}{2}}=1 \tag{12}$$

The most intuitive failure criterion follows the strength of material approach as in Equation 10 and then the strengths are changed to K_{Ic} as in Equation 11. Since, for isotropic material, the strain energy is proportional to K^2, the ½ power is substituted into the equation as in Equation 12. This paper will revise this conventional power law failure criterion used by Haugen and Morehead to a more appropriate model that accounts for the maximum in the G_I component. Several models by Reeder, one of the pioneers in exploring many types of failure criteria, are presented: bilinear, exponential hackle and linear interaction and are discussed in the later section.

Challenges in Finding the Best Failure Criterion

Several foundations must first be established before a model can be formulated, because, in fitting a curve, virtually any function can be used if there are enough parameters. Two important considerations are as follows:

1. The number of parameters. The number of parameters must be minimized for practical purposes. Fewer parameters would make models easy to use and understand. However, more parameters mean increased flexibility of the criterion.

2. The type of parameters. Parameters should include "all" variables, implying that the criterion should be maximized with respect to the parameter. The parameters should also have physical meaning.

The first step in finding the best model seems to require experience and creativity, because the behavior of the function must first be known apriori. The models considered are those that can include a maximum in the G_I component. Reeder has provided several models; in graphical form, his data showed a G_I-maximum. However, the G_I increase with increasing G_{II} in his data was small compared to the present data.

The two considerations bring up two types of model:

a) Implicit. The variables used in the criterion, i.e. G_I, G_{II}, R_G, and/or G_T, where $R_G=G_I/G_{II}$ and $G_T=G_I+G_{II}$, can make a difference on the model. An implicit model means that G_I cannot be expressed explicitly as a function of G_{II}. This is usually because of using R_G and G_T as the initial variables and then changing all the variables in terms of G_I and G_{II}. Implicit models may fit the data well, but are not easy to work with because an iterative calculation must be done to solve for the G_I and G_{II} components.

b) Explicit. Explicit models allow the expression of G_I (explicitly) as a function of G_{II}. Compared with implicit models, explicit models are easier to use, because of the direct relationship between G_I and G_{II}. If a single G_{II} is known, then the R_G and G_I can automatically be calculated. Because there is a maximum in the G_I component, for a given G_I, there are two possible G_{II}'s.

Therefore, the overall purpose of this section is to optimize the failure criterion model with respect to the number of parameters and the type of model. Reeder's view of failure criteria is available in reference 18; the author's review of Reeder's models follows.

The Power Law Criterion

The conventional criteria can be traced back to the power law criterion based on K_{Ic} and K_{IIc} [32]. In the form of the SERR:

$$\left(\frac{G_I}{G_{Ic}}\right)^{\frac{m}{2}} + \left(\frac{G_{II}}{G_{IIc}}\right)^{\frac{n}{2}} = 1 \tag{13}$$

The division by two is redundant, because the constant ½ can be included in the parameters. The criterion simplifies to

$$\left(\frac{G_{II}}{G_{Ic}}\right)^{m} + \left(\frac{G_{II}}{G_{IIc}}\right)^{n} = 1 \tag{14}$$

This model has been shown to work for tough polymer matrices, where m=n=1, a linear criterion in G [24]. For tough polymers, the matrix between plies of the composite is completely yielded, and G_{Ic} approaches G_{IIc} [24].

Exponential Hackle Criterion

The exponential hackle model (Equation 15) follows the general behavior of the mixed mode result, but the derivation of this model is based on R_G and G_T, and is, hence, implicit. The advantage of this model is that it involves only a single parameter, γ. The single-parameter inherently limits the use of the model, even though it is very practical, especially if the G_I maximum is as much as three times G_{Ic}.

$$G_I + G_{II} = (G_{Ic} - G_{IIc})\exp(\gamma\,(1 - N)) + G_{IIc}$$
$$N = \sqrt{1 + \left(\frac{G_{II}}{G_I}\right)\sqrt{\frac{E_{11}}{E_{22}}}} \tag{15}$$

$$\sqrt{1 + \left(\frac{K_{IIc}}{K_{Ic}}\right)} \tag{16}$$

The variable N is related to the hackle angle, which is originally in terms of the K components as in Equation 16 [18]. In Equation 15, the hackle angle is expressed in terms of the G components. It is unclear why the modulus ratio is included in N. The square root of E_{11}/E_{22} is only useful if the effect of the ratio is to be studied. Currently, the interest is finding "a good fit" to the data. Hence, this ratio can be lumped with the parameter gamma.

The origin of this criterion can be traced back to a slightly different form using "the derived variables". The simplified version of Equation 15 is called the modified exponential hackle criterion, which contains no moduli ratio in N.

$$G_I + G_{II} = (G_{Ic} - G_{IIc})\exp(\gamma_m\,(1 - N)) + G_{IIc}$$
$$N = \sqrt{1 + \left(\frac{G_{II}}{G_I}\right)} \tag{17}$$

The variable N is defined because it fits the data. The author is unclear as to the background of the parameter N, whether it is theoretical or simply empirical. Equation 17 was used to fit the mixed mode data.

It is suspected that an attempt has been made to include R_G into the model. This attempt must first establish the relationship between R_G and G_{II}. Nonetheless, it is appropriate to use G_{II} as the independent variable, because G_{II} does not have a maximum as revealed by the mixed mode results. However, the inclusion of inverse-R_G creates a singularity, because in pure mode-II, R_G becomes infinitely large. Equation 17, expressed in terms of the derived variables R_G and G_T, is the following:

$$G_T = \left(G_{Ic} - G_{IIc}\right)\exp\left(\gamma\,(1 - N)\right) + G_{IIc}$$
$$N = \sqrt{1 + \left(\frac{1}{R_G}\right)} \tag{18}$$

Linear Interaction

The linear interaction model originated from the fact that there is an interaction between G_I and G_{II} [21]. There is another term that includes $G_I \times G_{II}$, since, without these terms, there would not be any multiplicative interaction between G_I and G_{II} and the interaction is simply linear. The model has two parameters that reside in a linear-polynomial coefficient of $G_I \times G_{II}$. This model is greatly limited by the value of maximum G_I it can achieve; therefore, more modification is also done on this model.

This model can be better understood using factored quadratic polynomials. Below is the illustration: Assume that $y=G_I/G_{Ic}$ and $x=G_{II}/G_{IIc}$.

$$(y-1)(x-1) = 0$$
$$yx - x - y + 1 = 0 \tag{19}$$

To assume an interaction between normalized G_I and G_{II}, a parameter should be placed in front of the G_I-G_{II} interaction term. The parameter is added into the equation. It must be noted that the interaction has already existed in the first term (y-1)(x-1). Another interaction term is added with a parameter (in the original interaction term). Linear refers to the form of equation that acts as the coefficient of the interaction term.

$$
\begin{aligned}
&(y-1)(x-1)-\kappa\, yx = 0 \\
&yx - x - y + 1 - \kappa\, yx = 0
\end{aligned}
\tag{20}
$$

When κ is equal to one, the form will turn into a "linear" relation between G_I and G_{II}. This is the same as having the simplified conventional failure criterion (Eq. 14) with both m and n exponents equal to one.

Since there is an inflection point in the mixed mode results [18], the interaction parameter cannot be constant. Therefore, κ, a zeroth order coefficient, is changed into a first order coefficient—a coefficient that can vary linearly. Nevertheless, since there is a maximum in G_I, it is assumed that the linear coefficient will follow a climactic trend. This climactic trend is represented in the increasing value of G_I/G_T. G_I/G_T will be the variable that provides ranges of the linear coefficient from positive to negative (or the reverse). This varying coefficient allows the curvature to change the location of the inflection point in the G_I-vs.-G_{II} graph.

G_I is normalized by G_{Ic} and G_{II} by G_{IIc}. This equation is created using G_I and R_G as the variables; therefore, when converted to G_I and G_{II}, the equation becomes implicit, which requires two iterative calculations: one to find the parameters using experimental G's, and one more to calculate predicted G_I iteratively using previously calculated parameters.

The G_I/G_T ratio (with no exponent) cannot accommodate the maximum properly. The exponent of G_I/G_T is raised to a fourth power to improve the fit of the equation to the data. This equation works for Reeder's data, but his data have a relatively small maximum compared to the current data. The original interaction criterion follows:

$$\left(\frac{G_I}{G_{Ic}}-1\right)\left(\frac{G_{II}}{G_{IIc}}-1\right)-\left[\kappa+\varphi\left(\frac{G_I}{G_I+G_{II}}\right)\right]\left(\frac{G_I}{G_{Ic}}\right)\left(\frac{G_{II}}{G_{IIc}}\right)=0 \quad (21)$$

The modified linear interaction criterion with G_I/G_T to the fourth power is:

$$\left(\frac{G_I}{G_{Ic}}-1\right)\left(\frac{G_{II}}{G_{IIc}}-1\right)-\left[\kappa_m+\varphi_m\left(\frac{G_I}{G_I+G_{II}}\right)\right]^4\left(\frac{G_I}{G_{Ic}}\right)\left(\frac{G_{II}}{G_{IIc}}\right)=0 \quad (22)$$

Bilinear Criterion

The Bilinear Criterion is the simplest among all the models in the sense that it is easy to apply and understand. One of the most intuitive failure criteria would be a linear criterion, implying that there is no interaction between G_I and G_{II}. The result for mixed mode failure proved that a linear criterion is an oversimplification; it may have worked for the data presented by Reeder, but it does not work for the data currently under consideration. The Bilinear Criterion equations are the following:

$$\begin{aligned} G_I &= \xi\, G_{II} + G_{Ic} \\ G_I &= \zeta\, G_{II} - \zeta\, G_{IIc} \end{aligned} \quad (23)$$

where, ξ is the parameter for increasing G_I, and ζ is the parameter for decreasing G_I. This criterion has two linear criteria, at $R_G>1$ (increasing G_I) and $R_G<1$ (decreasing G_I); Reeder suggested that there is a change of mechanism in crack propagation at $R_G\sim1$. Each criterion contributes one parameter, giving a total of two parameters, ξ and ζ.

The two different linear equations create a piecewise function, which consequently causes another variable to be defined, because a single G_{II} cannot be used to calculate G_I, unless the critical R_G, the ratio where a change of fracture mechanism occurs, is known. The critical R_G can be used to calculate the critical G_{II} that determines which of the two equations, the decreasing G_I or the increasing G_I, to use.

In spite of the model's simplicity, it has a problem at R_G=1; an inherent problem in piecewise functions. The function is continuous at R_G=1, but not its derivative. The actual maximum of G_I is less likely to be a sharp point than a curve, showing a transition in fracture mechanism. Hence, at R_G=1, the prediction may overestimate the mixed mode toughness.

Determining which data points should be used for creating the linear criterion can also be a problem. The criterion is greatly affected by how many points are used to determine the parameters. This kind of complication does not exist with continuous functions.

Since the only background behind creating the failure criterion originated from the conventional (empirical) K_{Ic} criterion (Eq. 11) and until further theory has been developed, other models should be explored. The author realizes that the maximum could be modeled by a probability distribution function, which contains the function e^x, sine function, or higher order polynomials.

Sinusoidal Criterion

The sinusoidal empirical model is the following:

$$\frac{G_I}{G_{Ic}} = \alpha \sin\left(\beta \pi \exp\left(1 - \frac{G_{II}}{G_{IIc}}\right) + \chi\right) \tag{24}$$

The advantage of having a sinus form is that it can include linear interaction or any interaction with a maximum in the explicit form. This criterion has three parameters: α, β, and χ.

Power Interaction Criterion

The Power Interaction criterion originated from the beta probability distribution function. This is similar to the linear interaction, but with variable powers as the interaction parameters.

$$\left(\frac{G_I}{G_{Ic}}\right)=\left(\frac{G_{IIc}}{2G_{Ic}}\right)\left(\frac{G_{II}}{G_{IIc}}+\delta\right)^{\varepsilon}\left(1-\frac{G_{II}}{G_{IIc}}\right)^{\varphi} \tag{25}$$

This form has the same advantage as the sine function but with a more meaningful interpretation of the parameters, which are δ, ε, and φ. This form is similar to the linear interaction form, since it contains interactive parameters, only difference is that this form is explicit.

EXPERIMENTAL PROCEDURES

Test Specimen Preparation

Specimens for delamination testing require that a thin Nylon strip be molded into the material to serve as a starter crack. Plates of material were molded by resin transfer molding (RTM). Ten layers of unidirectional, stitched D155 fabric (E-glass fibers), with dimension of 80-cm × 50-cm were placed in an RTM mold. Three strips of 70 mm wide by 40 μm thick Nylon films (Richmond Aircraft Products HS8171-6) were placed between 5^{th} and 6^{th} layers as a crack starter approximately 25 cm apart as shown in Figure 7.

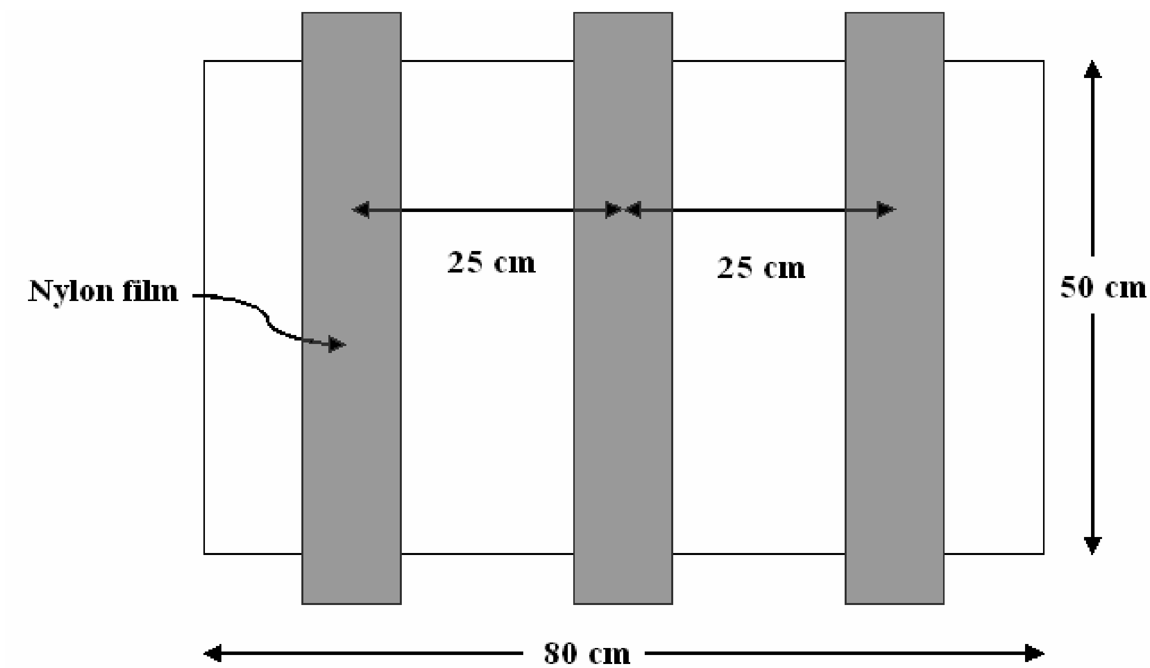

Figure 7 The layout of the mold

The mold was clamped and injected with isophthalic polyester resin, which had already been catalyzed by 1.5 %-volume of methyl-ethyl-ketone-peroxide (MEKP). The injection method is the same for vinyl ester, but for epoxy, no catalyst is required. Epoxy is usually a two-part system that only requires mixing of the two parts to cure.

The total thickness of laminate was 6 mm to achieve a fiber volume content of 36%. The injection required about two minutes; once the injection was done, the mold was left overnight at room temperature (about 20°C) for curing. Figure 8 illustrates an RTM process in progress.

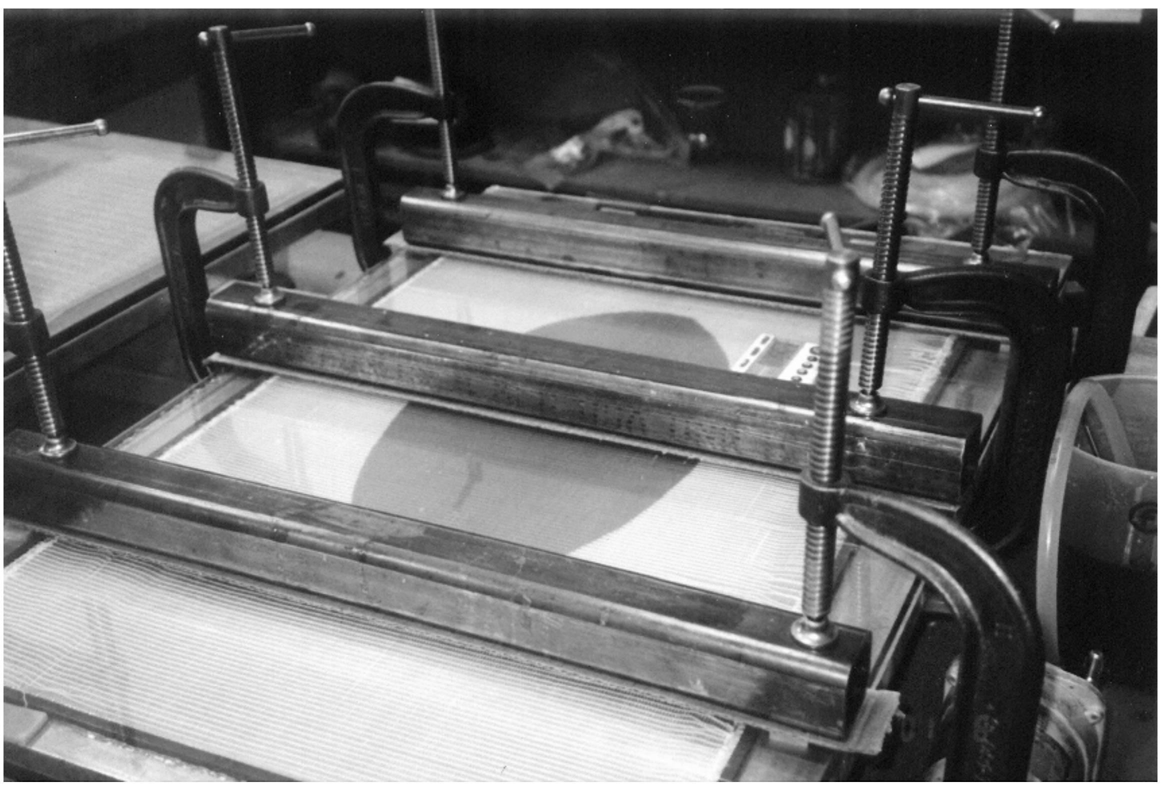

Figure 8 An RTM process in progress

Once the laminate was fully cured, it was cut into specimens with a water-cooled diamond impregnated blade. Specimen dimensions were 2.5 cm × 12 cm, as shown in

Figure 12. About 80 specimens could be created from one plate depending on the level of perfection of the laminate; flawed areas, by visual inspection, were not used for test specimens. While piano hinges are commonly used for load introduction into DCB test specimens, for this study, it was required for the MMB geometry to use aluminum "T"-tabs as shown in Figure 9, because piano hinges would peel off at higher loads.

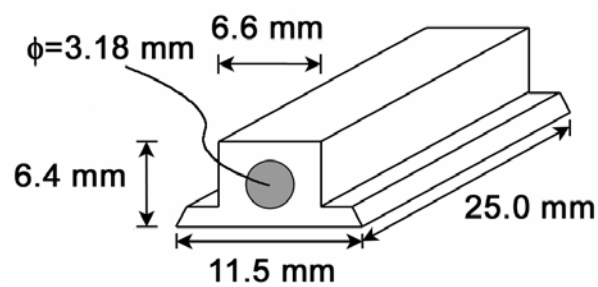

Figure 9 Sketch of T-tabs

The crack length measured from the edge of the specimen (not from the load point) was approximately 30 mm. This length is important to reduce the effect of the tabs on the beam stiffness. Williams [58] used similar tabs, but with a different geometry, with a higher point of load introduction to reduce any mode-III (tearing) introduction. However, too high a point of rotation may cause, due to friction, a local moment that is opposite to the intended moment for the cantilever beams and this is why the point of rotation must be as close as possible to the specimen surface. The base of the tabs must also be as small as possible to reduce the stiffening effect on the beams, without introducing failure of the adhesive.

The tabs are numbered in pairs and then bonded to the specimen using Hysol 9301. The bonding of the tabs onto the specimens must be done carefully, because misalignment of tabs may introduce some unknown mode-III component. A jig, shown in Figure 10, and a clamp were used to ensure proper alignment of the tabs. After the bonding process, the entire specimen was cured in an oven for 6 hours at 65ºC; this provided a cure for the adhesive and a postcure for the laminate. The pins for the tabs are 3.18 mm in diameter and made of steel.

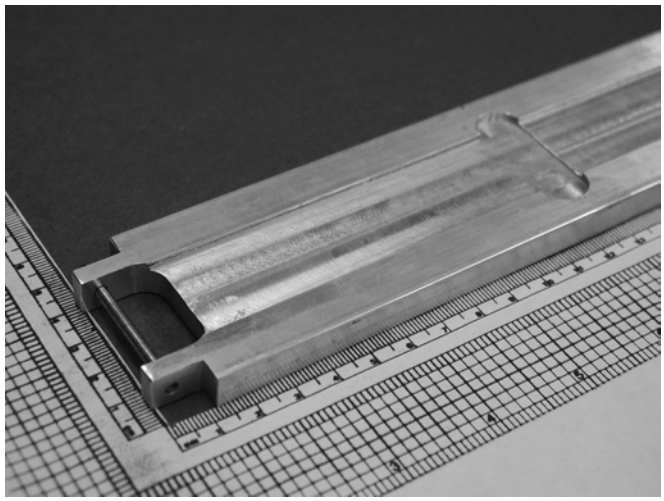

Figure 10 A jig used to glue the tabs onto the test specimen

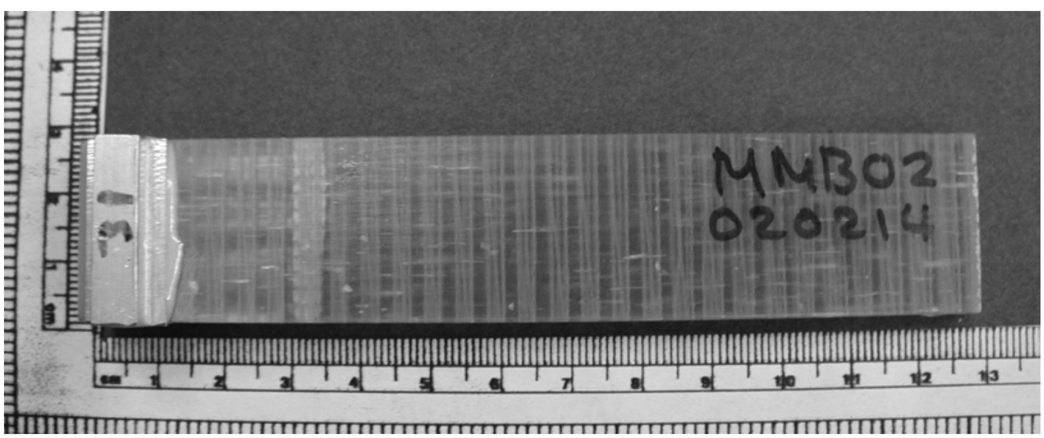

Figure 11 A test specimen after T-tab bonding (top view)

With the epoxy matrix specimens, the resin sometimes adheres to the Nylon strip, which may peel during the experiment and can be mistaken for a crack propagation. In this case, the crack is first opened very carefully with a very sharp blade until the tip of the crack is visible. Once the crack is open, the crack length is then marked as shown in Figure 12 and the specimen is ready for testing.

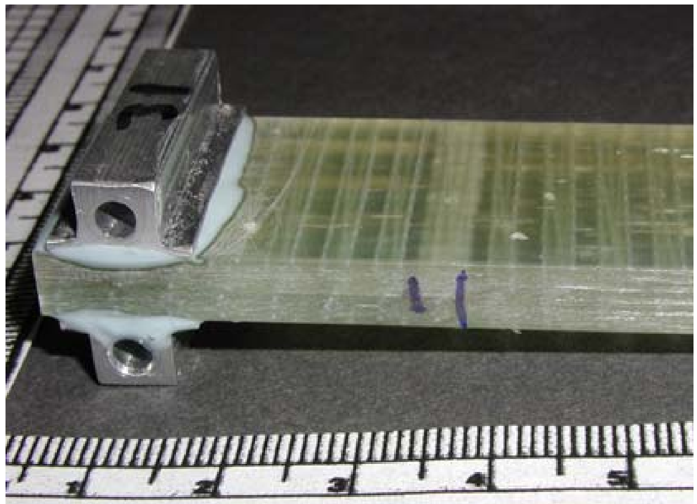

Figure 12 A test specimen with "T"-tabs and markings of the initial and final crack tip positions.

Testing Equipment

The mixed mode bending apparatus (shown later in Figure 15) was fabricated as part of this study. A roller was used at the point load introduction (on the saddle) to reduce nonlinearity in the load versus displacement graph [20-22,28,29]. The height of the loading point above the specimen was an issue; Reeder and Crews [20,22,30,31] explained that an error of 30% could be induced due to incorrect height of the loading point from the specimen. This height has been investigated in the finite element modeling.

The base of the apparatus is steel, including the rollers. The tab adapter is also steel with adjustable height and lateral rotation. The loading lever is aluminum, with steel fulcrum and steel tab adapter. To apply the load on the saddle, a steel yoke is placed on the Instron grip.

Testing Procedures

Material Properties

All materials were tested for the elastic constants on an Instron machine model 8562 with a 100-kN load cell; the longitudinal (E_{11}) and the transverse (E_{22}) moduli were averages of three to four specimens. G_{12}, ν_{12}, and ν_{23} were obtained from DOE/MSU Database [1]. G_{23} was calculated using the (transversely) isotropic equation [15]

$$G_{23} = \frac{E_{22} \text{ or } E_{33}}{2(1+\nu_{23})} \tag{26}$$

G_{23} is calculated, because it is not easily determined experimentally; therefore, it should be subjected to further study. The fiber volume fractions were determined using the matrix burn-off method following ASTM Test Standard [59] and the equations developed by Mandell and Samborsky [1,2].

DCB, ENF, and MMB Testing

All tests were done on the Instron machine model 8562 with a 100-kN load cell. The procedure for running the Instron machine is available in APPENDIX A. The speed of the actuator was 0.02 mm/s for ENF and 0.04 mm/s for DCB and MMB tests. The possible introduction of mode-III was reduced by ensuring that the pins could easily slide in and out of the tabs and the tab adapter when a small load was applied. The pins were lubricated to reduce friction. The crack tip position was marked with a pen on both sides of the specimen. All crack propagation was accomplished in the testing machine, including precracking when included.

The specimens were then loaded to produce a short length of crack extension, and unloaded. The complete load-versus-deflection curves (loading and unloading) were obtained from the testing. The critical loads were determined using the 5%-slope-offset from the linear part of the loading curve [14]. The critical load was determined as the maximum load within the 5% offset, or the load where the curve intersects the offset line. This method is elaborated in the Experimental Results chapter, subheading Critical Load Determination.

All dimensions and material properties required to calculate the SERR were recorded as input for the finite element model. The crack length was taken as the average between two sides, for both initial and arrested crack tip positions. DCB, ENF, and MMB tests in progress are illustrated in Figures 13, 14, and 15, respectively.

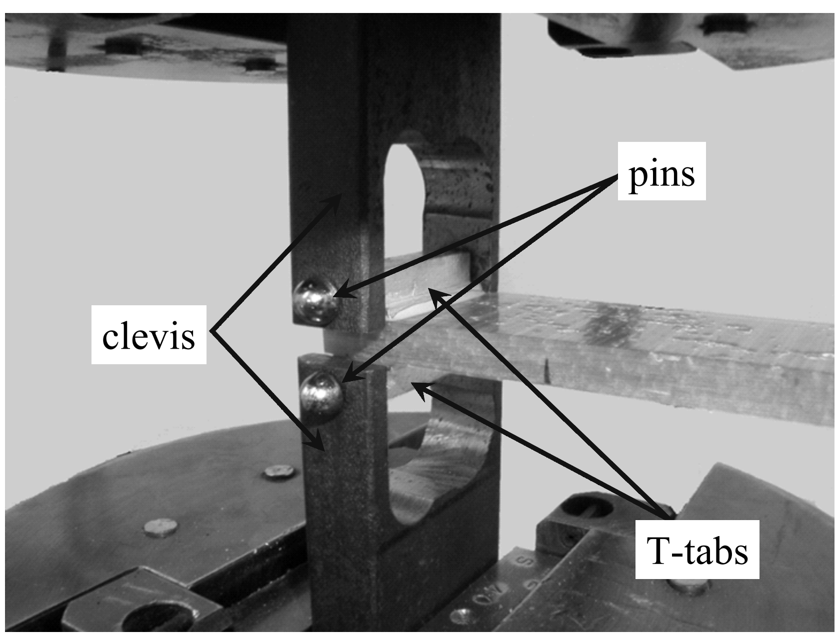

Figure 13 DCB test in progress

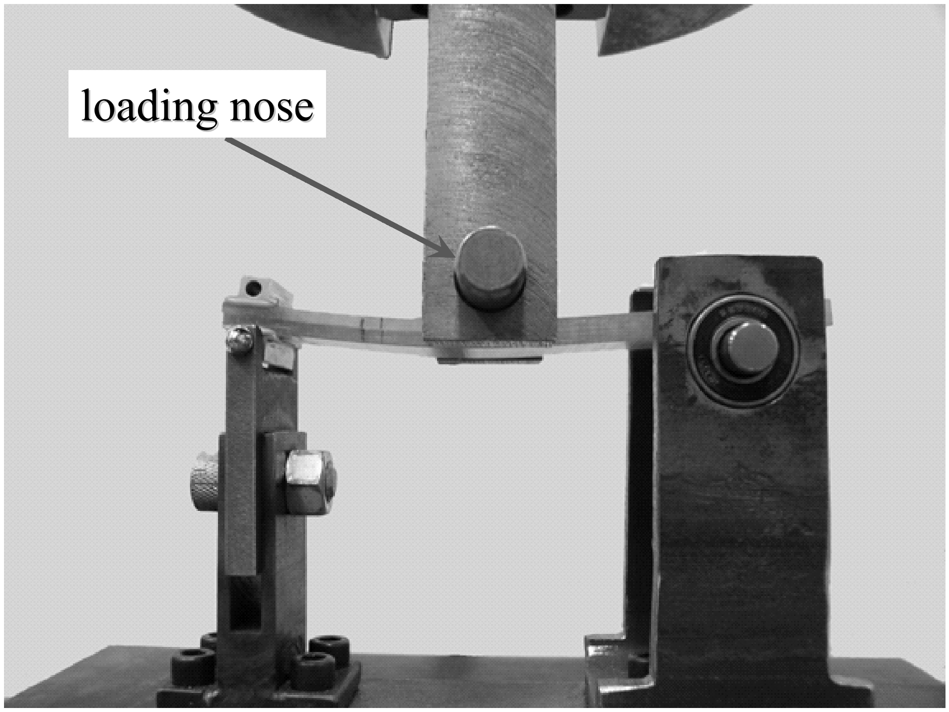

Figure 14 ENF test in progress

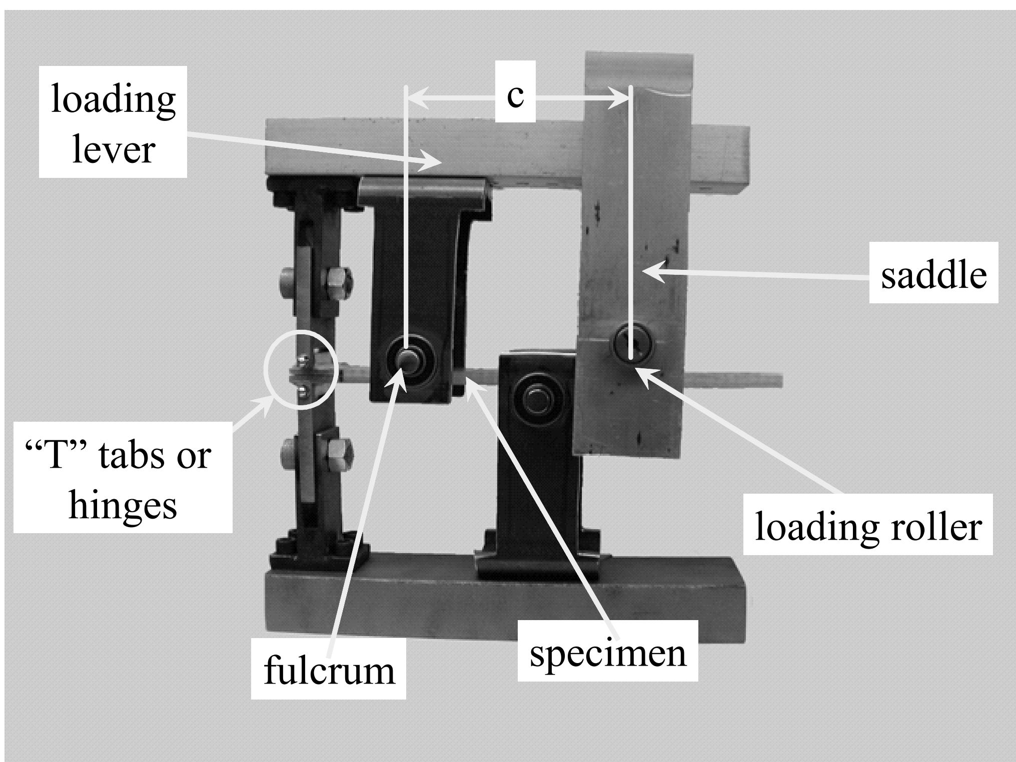

Figure 15 The MMB apparatus

Precracking

Precracking includes the propagation of the crack from the tip of the Nylon strip. Precracking was originally used to avoid testing the resin rich area which forms ahead of the Nylon strip [5,6]. This method was also used in original papers of Reeder and Crews. They were using carbon-fiber composite and they assumed that fiber bridging was insignificant. However, this is not the case with this specimen using glass fabrics; fiber bridging has been shown to be important as the crack extends for these materials [5,6, 41]. The initiation G (G data determined for initial crack extension from the Nylon strip) has been found to be the lowest value in previous studies [5,6] and is used as a conservative value for design [5]. The effect of precracking is studied in this paper for the mixed mode condition.

NUMERICAL PROCEDURES

Finite Element Preprocessing

ANSYS 7.0 was used to model all specimens, DCB, ENF, and MMB. PLANE82, an 8-noded quadratic-rectangular element with plane strain option, was used [60]. Geometry was created using solid modeling—an option in ANSYS that allows the finite element creation from volumes, instead of directly from nodes. Material properties were determined from both experimental tests and DOE/MSU database as noted earlier. The specimen is assumed transversely isotropic.

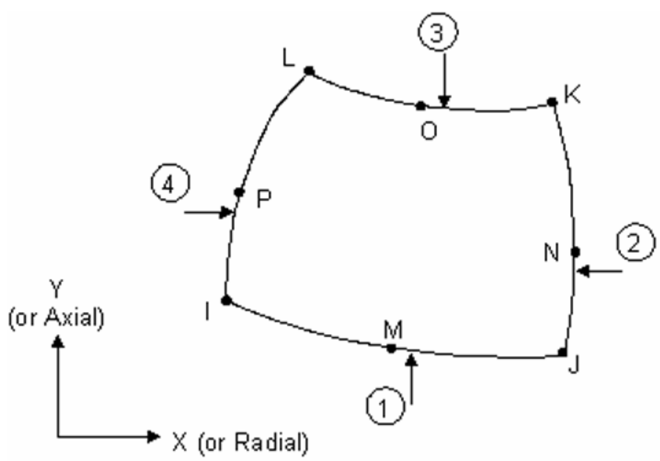

Figure 16 PLANE82 2-D 8-Node Structural Solid

A convergence study for elements through the thickness was done to find the minimum number of elements. This convergence study was done only on the DCB model and the result was used for the remaining models. The objective of the convergence study was to reduce the sum squared-of-difference between deflections from the experiments and the finite element model prediction.

Another type of convergence study is the optimization of element size around the crack tip. Optimization was done to find the best configuration of element sizes around the crack tip, as well as the minimum element size for SERR calculation. The SERR calculated using VCCT1 is sensitive to the mesh density and size. It is of paramount importance that the size of elements around the crack tip be small enough to calculate the SERR accurately [9].

The elements around the crack tip could be sized using two different methods: changing the spacing ratio or refining the elements around the crack tip node [61]. Spacing ratio is more desirable because it gives a smoother transition from the larger to smaller size elements. Another method is the refinement of elements around keypoints. This method simply creates small elements around the crack tip, consequently adding more elements. The disadvantage of this method is that more variables must be determined to refine the elements surrounding the crack tip: the level of refinement, distance of refinement from the crack tip, and smoothing of elements after refinement [62].

Spacing ratio is the chosen method, because only two variables are involved, the size around crack tip and the spacing ratio. This method creates a smoother transition in mesh density.

Finite Element Models as Verification of Assumptions

Finite element modeling is also used to verify validity of assumptions in the modified beam theory:

1. "T"-tabs. "T"-tabs and the loading lever are modeled. The effect of "T"-tabs on the result was also studied, because they may stiffen the beam.

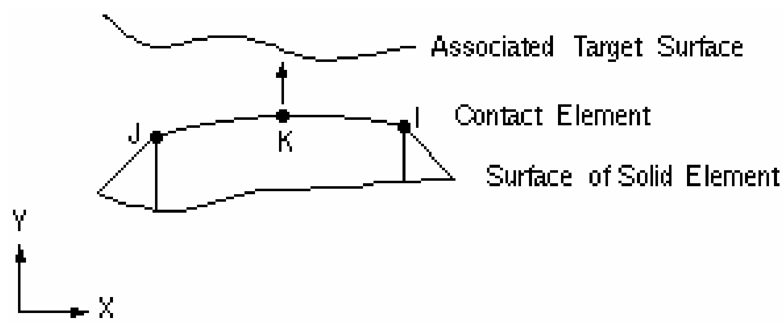

Figure 17 CONTA172 2-D Surface-to-Surface Contact Element (3 nodes)

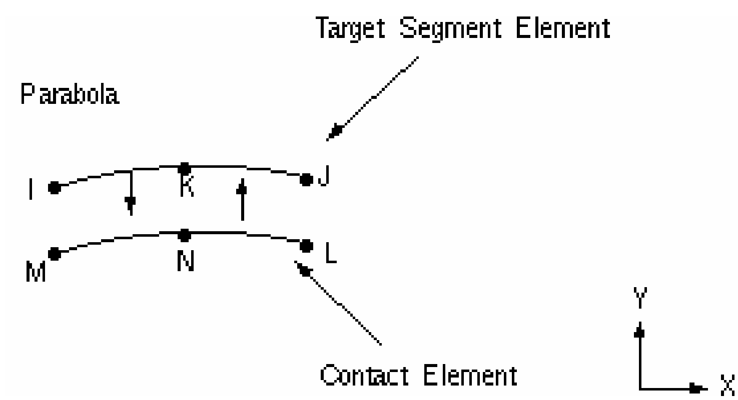

Figure 18 TARGE169 Target Surface Element

2. Friction existing in ENF tests. The presence of contact requires contact elements to be used in the finite element model. Otherwise, the beam halves would overlap. Two contact elements are used, CONTA172 and TARGE169, illustrated in Figure 17 and Figure 18, respectively. Contact elements are cumbersome to work with, because several parameters have to be defined properly to achieve an efficient convergence rate [63]. Friction is certainly present, but ignored by setting the coefficient of friction very small, 0.01.

3. Linear solution. Linear and nonlinear solutions were obtained, to check how much the specimen geometry, including the "T"-tabs, would cause nonlinearity.
4. VCCT1 is a sufficient method to calculate SERR [5]. The model was created to be as simple as possible without elimination of the important details. Fiber misalignment and porosity cannot be modeled easily using finite elements. All imperfections are lumped together in the "smeared" material mechanical properties.

EXPERIMENTAL RESULTS

Elastic Constants

Table 1 summarizes the elastic constants measured in this study and taken from the DOE/MSU Database [1]. None of the properties varied significantly with matrix material, as expected, since all matrix modulus values are similar [1].

Table 1 Elastic Constants of Unidirectional Composites

Material Properties	Isophthalic Polyester		Vinyl Ester		Epoxy		Source
	avg	std	avg	std	avg	std	
E_{11}	27.9	2.3	31.1	0.7	31.9	1.1	Experimental
E_{22}, E_{33}	7.44	---	7.96	0.68	7.38	0.19	Experimental
G_{12}, G_{13}	3.05	0.29	3.05	0.29	3.05	0.29	DOE/MSU Database
G_{23}	2.58	---	2.76	0.34	2.56	0.24	Calculated (Eq. 10)
ν_{12}, ν_{13}	0.33	0.02	0.33	0.02	0.33	0.02	DOE/MSU Database
ν_{23}	0.44	0.04	0.44	0.04	0.44	0.04	DOE/MSU Database
fiber volume fraction	36.7%	---	34.2%	0.6%	32.4%	---	Experimental

Modulus units are in GPa

Critical Load Determination

The critical load was determined using the 5% slope offset method following metals standard ASTM E399 [14] as illustrated below. The results from an MMB test of the E-glass/isophthalic-polyester system are shown in Figure 19. In this case, the load was determined as the actual maximum load at the onset of crack propagation, since the maximum occurred to the left of the 5% offset line. However, sometimes crack propagation is more stable, indicated by deviation from linear response, so that the

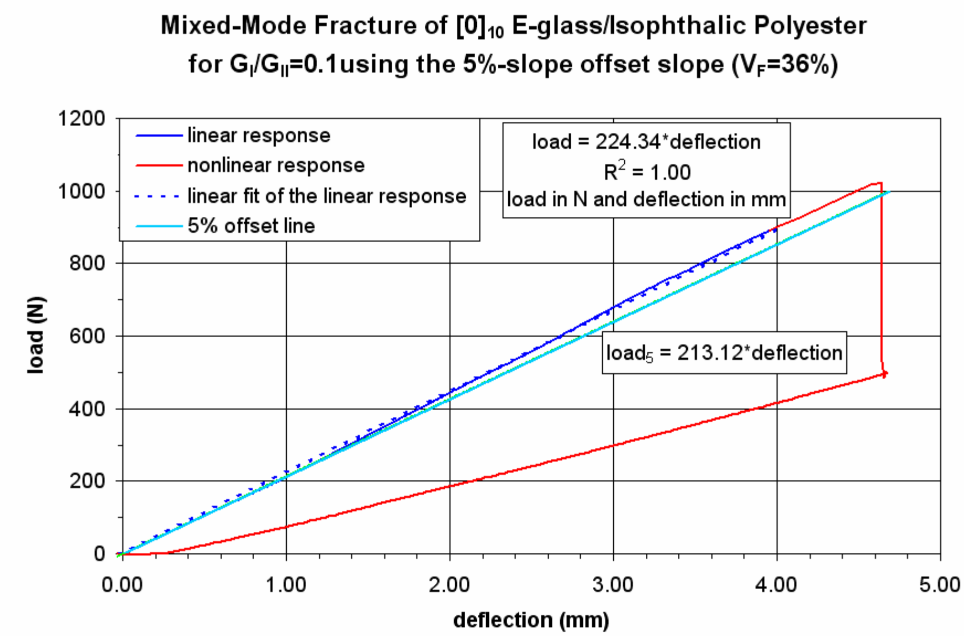

Figure 19 Illustration of a test using the MMB specimen, where the critical load is considered as the actual maximum load

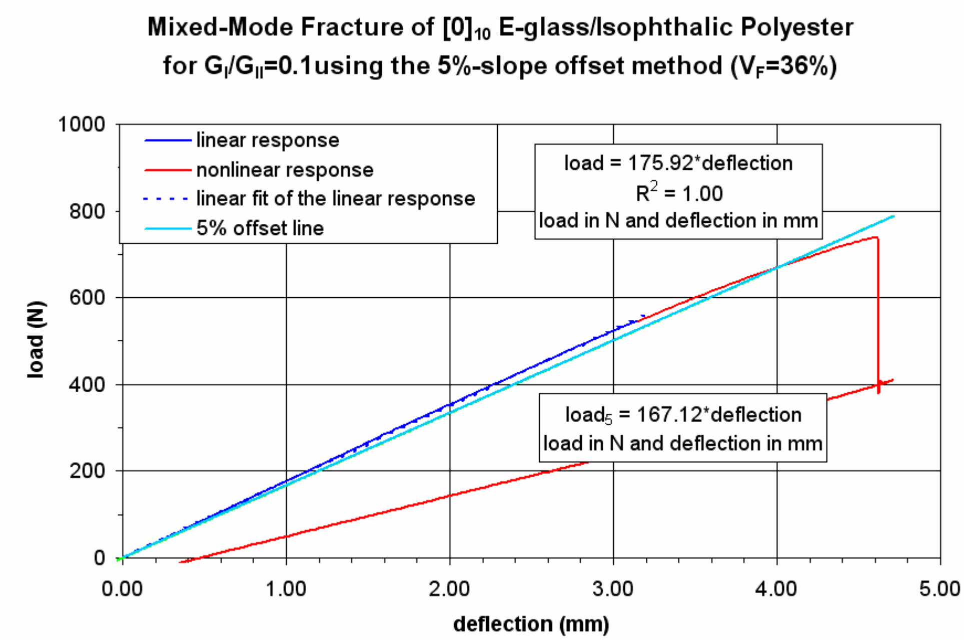

Figure 20 Illustration of a test using the MMB specimen, where the critical load is taken as the intersection of the 5%-slope-offset line with the experimental load-deflection curve.

critical load is taken as the intercept of the load-deflection curve with the 5% offset line (see Figure 20). Unstable cracking is indicated by a sudden drop in the load as the crack propagates. The term stable may refer to crack arrest after a crack growth of only 1~3 mm, as discussed later. Mode-II cracks in this study tended to be more unstable, propagating for long distance once initiated.

Crack Tip Position

Isophthalic polyester and vinyl ester produce the most transparent composites; therefore, the crack fronts are easily seen. Straight crack fronts were observed for all specimens. Composites using the epoxy matrix were less transparent; hence, self-similar crack extension can only be verified by observation of the crack position on the edges of specimen. If the material is opaque, a low power microscope with 60× magnification is sufficient to detect the crack tip positions. The crack length is calculated from the average of the two crack tip positions on each edge, and this average length is used in the SERR calculation.

Crack Initiation

In preliminary tests, the crack was grown a small distance from the Nylon starter strip before data were recorded, following standard test procedures [33]. However, because of fiber bridging effects, the initial crack from the Nylon strip proved to give the lowest SERR value, and so the most conservative results for design purposes.

Fiber bridging

Fiber bridging is evident from the experiment as shown in Figure 21. The toughness is increasing as the crack extended farther from the tip of the Nylon strip as shown in Figure 22. For design purposes, the initiation value should be used, because it is the most conservative value. Fiber bridging is less common in prepreg carbon fiber specimens and is the reason Reeder and Crews original work did not use crack data from the Nylon[2] strip in thesis calculation [18,19]. With a tough matrix, the critical SERR may be artificially high near the Nylon strip due to the associated matrix-rich area. This is not the case with the materials used here.

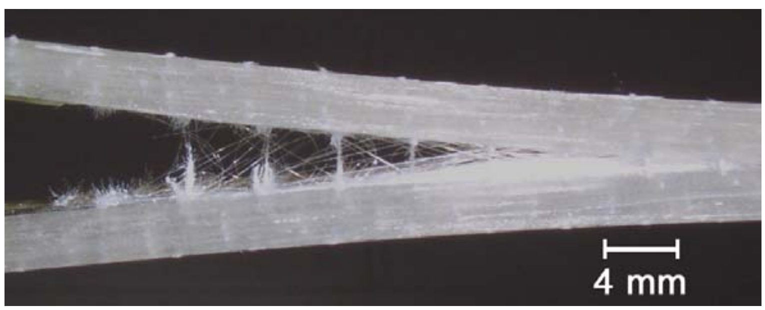

Figure 21 Evidence of fiber bridging as crack extends

Thickness of Nylon strip

Since interest is now focused on cracks staring at the Nylon strip, the dimension of the Nylon strips could well have an effect on the toughness. However, it is also possible that the Nylon is at a thickness irrelevant to the SERR. This will be subjected to further study.

---

[2] In Reeder and Crews original work, Kapton film was used instead of Nylon.

Mode Sequencing Study

Two types of cracking sequences can be used; mode-I and mixed mode were studied. The first sequencing, illustrated in Figure 22, is performing mode-I precrack followed by mode-I crack propagation. This sequencing showed evidence of increasing G_{Ic} as the crack propagates. This R-curve behavior [1,5,6] is typical of fiber glass fabric and because of this effect, the compliance calibration method by ASTM 5528 is not possible. The increase of subsequent G_{Ic} ranged up to 2.0 to 2.5 times the initiation G_{Ic}.

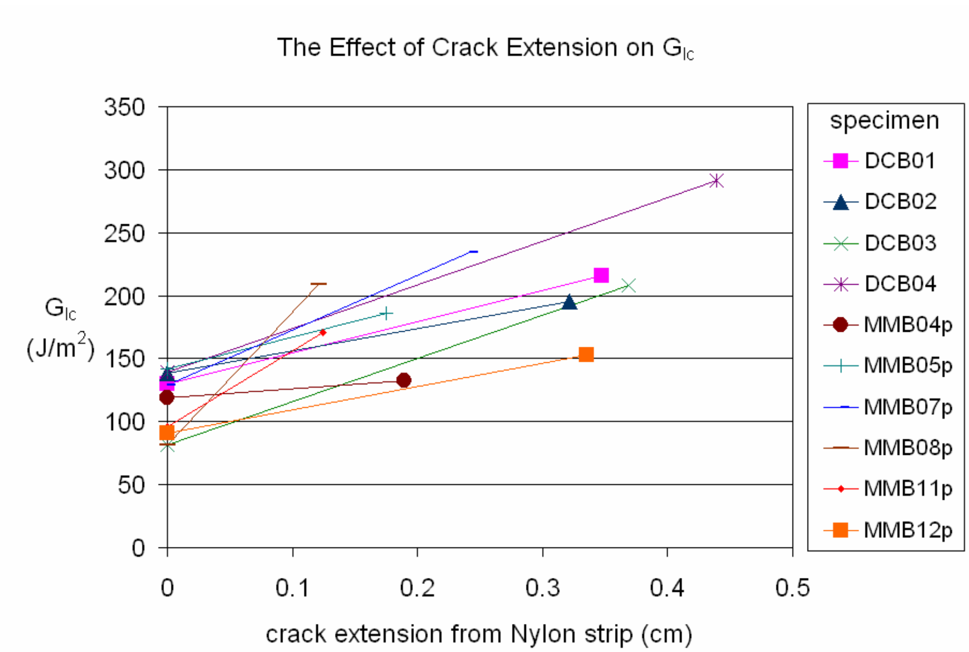

Figure 22 Crack extension affecting G_{Ic} due to fiber bridging

The second sequencing involved mixed mode initial cracking and subsequent mixed mode cracking at R_G=1.7 and 1.1 (Figure 23 and Figure 24), where R_G is defined as the ratio of G_I to G_{II}. The subsequent cracks had G_{Ic} almost double that of the initiation value. The effect of fiber bridging was slightly suppressed with increasing mode-II component.

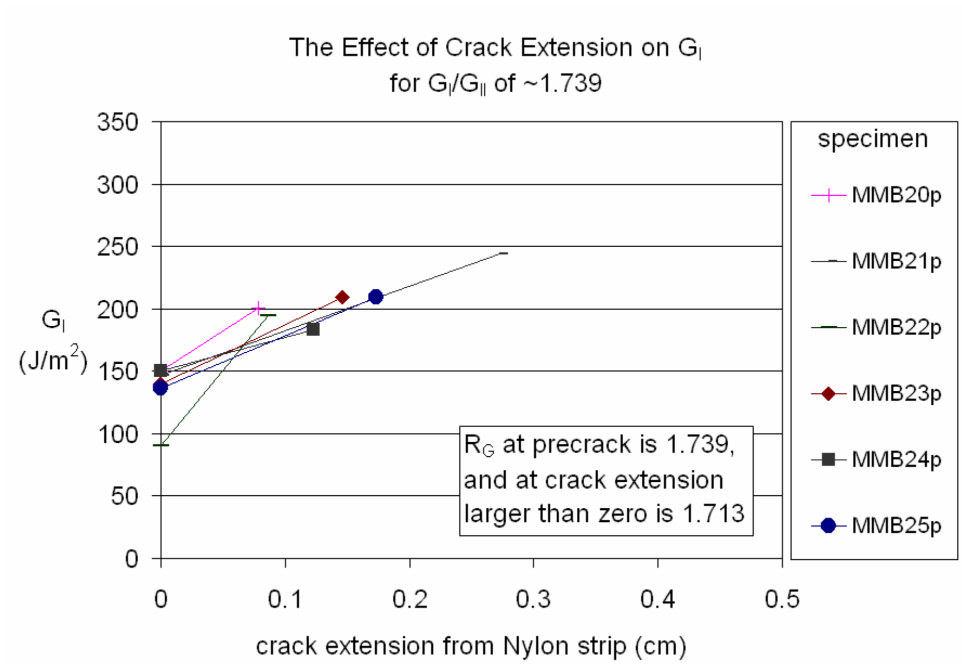

Figure 23 Effect of mixed mode precrack on subsequent mixed mode cracking at R_G~1.7

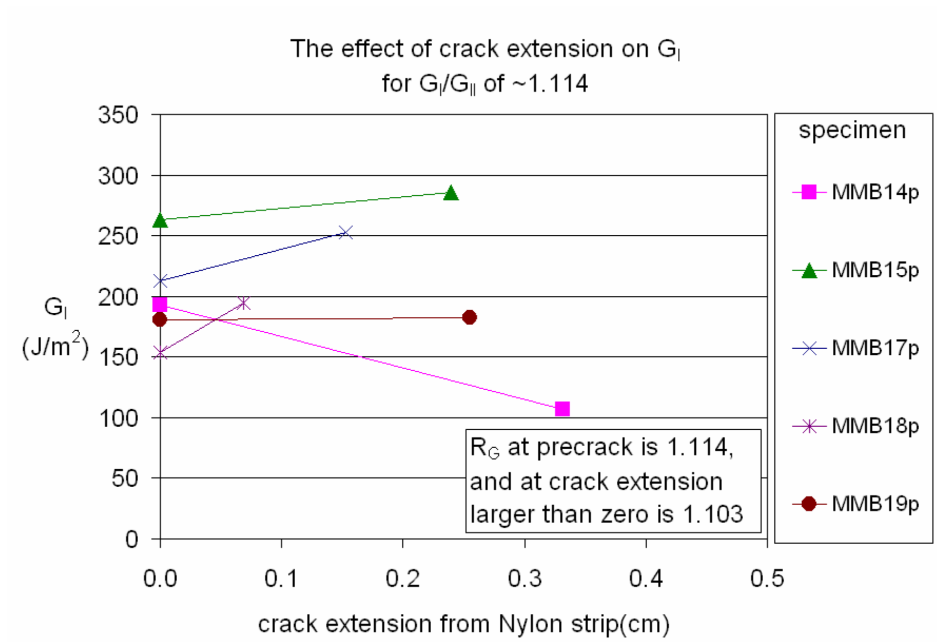

Figure 24 Effect of mode-I precrack on subsequent mixed mode cracking at R_G~1.1

The third case studied the effect of a mode-I initial crack on mixed mode cracking at R_G=0.5. The mode I results are not tabulated here, but available in APPENDIX B. Here, the mode I initial crack still affected the mixed mode propagation significantly; the mixed mode cracking (with no initial crack) averaged a G_I component of 201 J/m^2 while the mixed mode cracking (after a mode-I initial crack) averaged a G_I component of 299 J/m^2 as listed in Table 2.

Table 2 Effect of mode-I initial cracking on subsequent mixed mode crack

specimen	crack extension (cm)	G_I (J/m^2)	G_{II} (J/m^2)	R_G
MMB09	0.232	288	564	0.510
MMB10	0.357	302	593	0.509
MMB11	0.478	278	561	0.495
MMB12	0.637	254	530	0.479
MMB13	0.581	375	759	0.494
	average	299	601	
	std	46	91	

NOTE: These specimens had been initially cracked with mode-I

specimen	crack extension (cm)	G_I (J/m^2)	G_{II} (J/m^2)	R_G
MMB32p	0	244	456	0.536
MMB33p	0	118	221	0.537
MMB34p	0	186	346	0.538
MMB35p	0	209	386	0.541
MMB36p	0	248	473	0.525
	average	201	376	
	std	53	101	

The last sequencing study involved a mode-I initial crack followed by mode-II crack propagation. In this case, the mode-I initial crack does not significantly affect the subsequent mode-II crack. The average G_{II} component for mode II with no initial crack was 1797 J/m^2 and the G_{II} component for mode-II with a mode-I initial crack was 1814 J/m^2 as listed in Table 3. Thus, fiber bridging in mode-II is insignificant, as is frequently reported for other composites [18,19,50].

The mode-II initial crack must be interpreted carefully, because an initial crack implies that further cracking is possible and the extension is assumed small, about 3 mm.

However, the nature of mode-II crack is very unstable; crack extension is sufficiently fast and long that it can pass the mid-loading nose.

Table 3 Effect of mode-I initial crack on subsequent mode-II crack

	crack extension (cm)	G_{II} (J/m^2)
ENF01	0.578	1450
ENF02	0.223	2001
ENF03	0.410	1742
ENF04	0.127	1584
ENF05	0.361	2294
	average	1814
	std	337

NOTE: These specimens had been initially cracked with mode-I

	crack extension (cm)	G_{II} (J/m^2)
ENF07	0	1814
ENF08	0	2232
ENF09	0	1689
ENF10	0	1595
ENF11	0	1655
	average	1797
	std	256

<u>Testing Results for All Modes</u>

Table 4 summarizes MMB results for all matrices. In decreasing order, the toughest material for pure G_I is epoxy (356 J/m^2), vinyl ester (204 J/m^2), and isophthalic polyester (116 J/m^2). This trend is also duplicated for pure G_{II}: epoxy (4054 J/m^2), vinyl ester (3283 J/m^2), and isophthalic polyester (1797 J/m^2). The raw data for each test can be found in APPENDIX C (Experimental Results); the number of test replications for each case varied from 4 to 20.

Table 4 Summary of MMB results for all matrices

Isophthalic Polyester					Vinyl Ester					Epoxy				
R_G	G_I (J/m^2)		G_{II} (J/m^2)		R_G	G_I (J/m^2)		G_{II} (J/m^2)		R_G	G_I (J/m^2)		G_{II} (J/m^2)	
	avg	std	avg	std		avg	std	avg	std		avg	std	avg	std
∞	116	27	0	0	∞	204	59	0	0	∞	356	94	0	0
1.729	136	23	79	13	2.123	383	95	180	46	2.172	761	145	351	68
1.115	201	41	180	36	1.285	539	147	419	111	1.340	895	179	668	133
0.535	201	53	376	101	0.557	587	126	1055	235	0.549	754	106	1374	204
0.219	212	35	968	149	0.133	300	35	2263	243	0.142	442	48	3119	338
0.026	37	10	1412	374	0.016	48	3	2959	217	0.017	63	4	3791	235
0	0	0	1797	256	0	0	0	3283	86	0	0	0	4054	151

Experimental Results for Isophthalic Polyester

Figure 25 gives the initiation values for the isophthalic polyester resin at various R_G. The G_I component reaches a maximum value around R_G of 1.0, with G_I at 201 (41) J/m^2 and 201 (53) J/m^2 for R_G=0.5 and 1.1, respectively. Reeder concluded in his paper that the maximum should be close to R_G~1.0 from his bilinear failure criterion discussed earlier [24]. As R_G decreases from 1.0 (as mode-II increases), the crack becomes increasingly unstable, similar to pure mode-II. On the fracture surface, the hackle features are apparent (Figure 26), which is also found in Reeder's paper with a carbon-fiber/epoxy system [24].

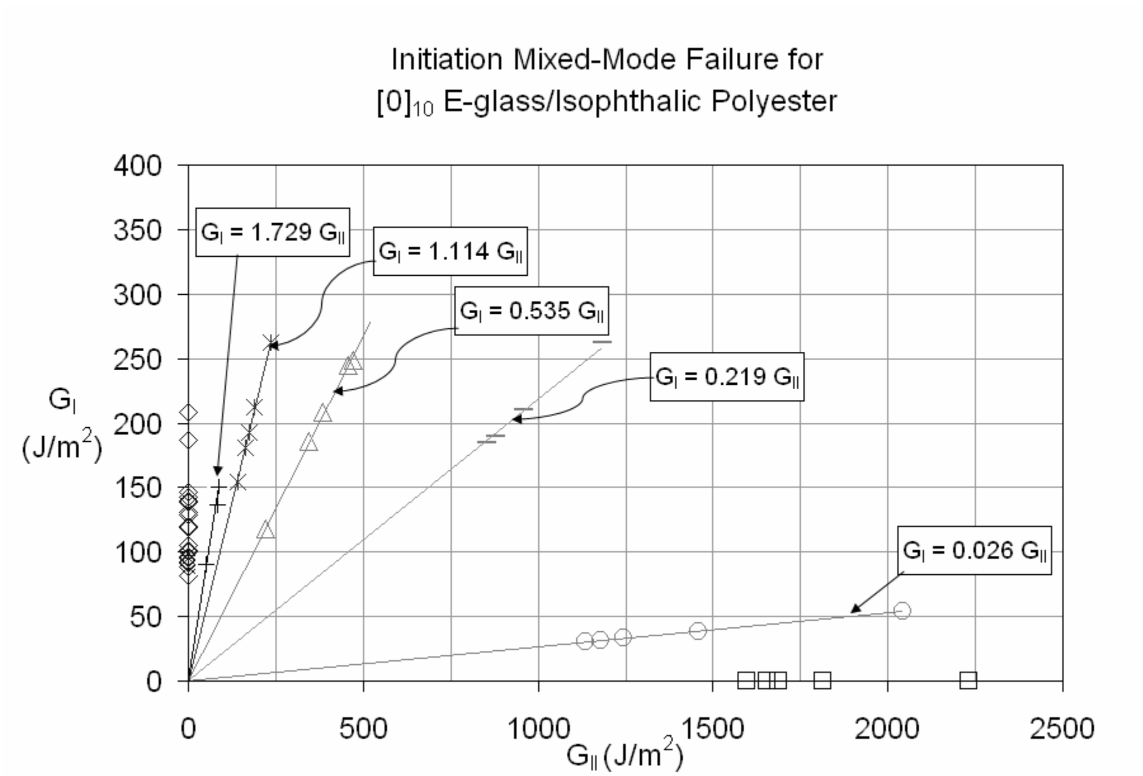

Figure 25 MMB initiation results for isophthalic polyester resin composite

The average value for pure G_{II} is 1797 (256) J/m^2, the lowest among the resins. G_{IIc} is 18 times greater than G_{Ic}. A tremendous amount of energy must be provided to propagate a mode-II crack, which is associated with hackle formation as discussed earlier.

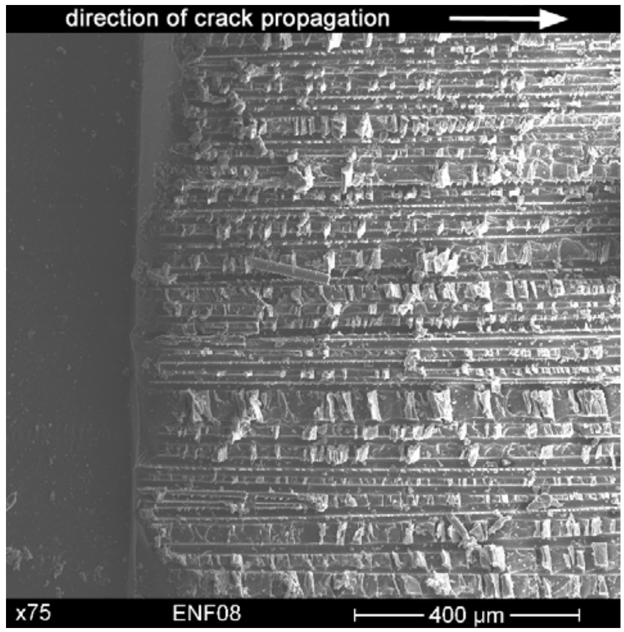

Figure 26 Hackles on fracture surface of an ENF test specimen

Experimental Results for Vinyl Ester

Figure 27 shows the mixed mode results for vinyl ester. For DCB tests, two different initial crack lengths were tested. The increase of G_I at fracture as R_G decreases from ∞ is also obvious with vinyl ester. The increase of G_I is steeper than for the isophthalic polyester, with the maximum value of the G_I component at R_G=0.557, 587 (126) J/m^2, almost triple from pure G_{Ic}, 204 (59) J/m^2. The average value for pure G_{Ic} is 204 (59) J/m^2, 1.8 times that for the Isophthalic polyester. The average value for pure

G_{IIc} is 3283 (86) J/m^2, almost double that for the isophthalic polyester. The results for DCB vinyl ester with two different crack lengths are listed in Table 5.

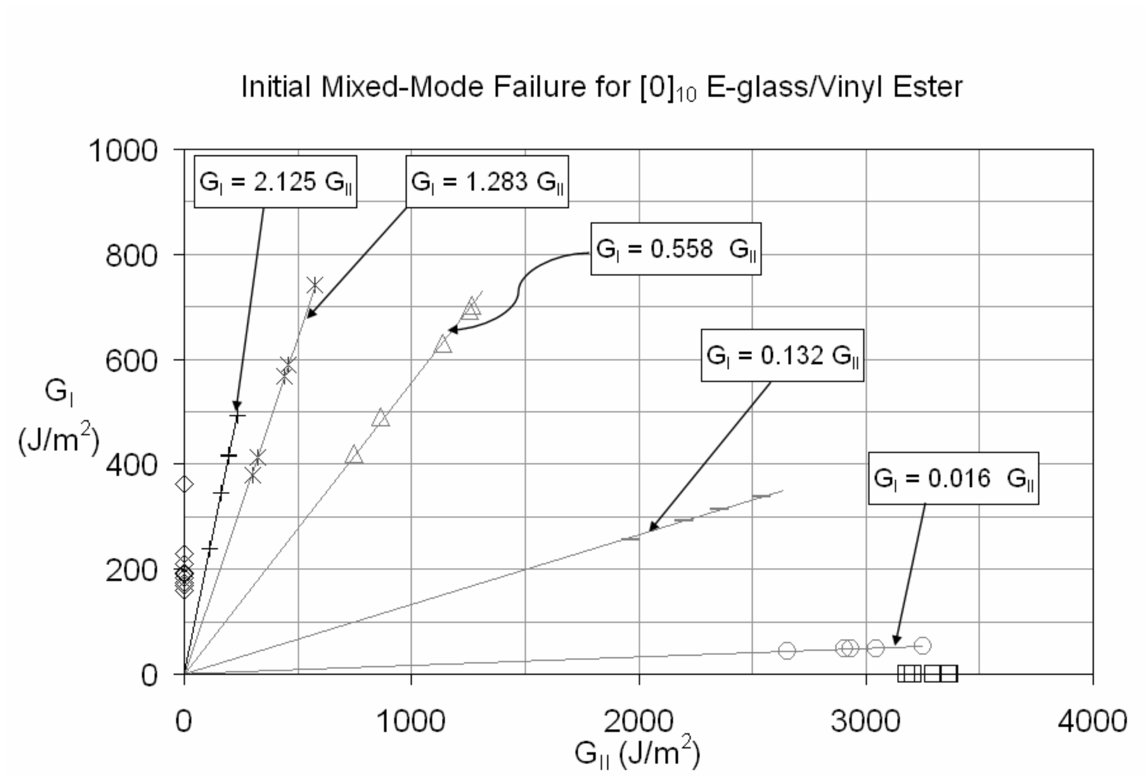

Figure 27 MMB initiation results for vinyl ester resin composites

The two initial crack lengths essentially do not show any significant difference in pure G_{Ic}; the long crack length with an average of 5.9 cm and the short one, 2.8 cm. The averages of pure G_{Ic} for long and short crack initial crack are 223 (81) J/m^2 and 184 (17) J/m^2, respectively. The average might show a noticeable difference, but the scatter in the data sets proved that the difference in the averages is insignificant; removal of the single point at 362 J/m^2 for the long initial crack would bring the averages very close together.

The scatter of data for mixed modes seems to be greater than for pure modes. The standard deviation for the DCB tests of 29% was attributed to the “outlier” of a single data point. After scrutinizing the data, it is found that the scatter was actually small. The level of scatter, as the modes were closer to pure modes, decreased. The reason for this is yet determined and subject to further study. This large scatter might be caused by the different crack tip surface, because of the stacking effect; the crack tip might be wavy through the width as illustrated in Figure 28.

Table 5 DCB results for vinyl ester resin composites with two different crack lengths

Long Initial Crack Length

specimen	initial crack length (cm)	final crack length (cm)	G_{Ic} (J/m^2)
DCB01p	5.870	6.087	192
DCB02p	6.136	6.728	361
DCB03p	5.772	5.836	160
DCB04p	5.797	5.966	229
DCB05p	5.833	5.927	174
average	5.881	6.109	223
std	0.147	0.358	81

Short Initial Crack Length

specimen	initial crack length (cm)	final crack length (cm)	G_{Ic} (J/m^2)
DCB06p	3.104	3.311	189
DCB07p	2.908	3.090	209
DCB08p	2.599	2.753	169
DCB09p	2.717	2.910	168
DCB10p	2.816	2.882	183
average	2.829	2.989	184
std	0.192	0.216	17

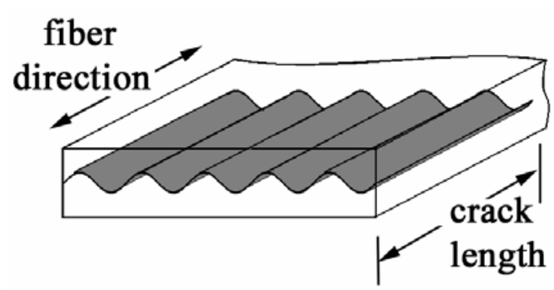

Figure 28 Waviness at the crack tip

<u>Experimental Results for Epoxy</u>

Figure 29 summarizes results for the epoxy resin composites. The increase in G_I component at fracture as R_G decreases from ∞ is even steeper for epoxy than for the other resins. Results for all of the resins show the same trend, with the G_I component at fracture first increasing and then decreasing as the G_{II} component increases. The origins of this trend are explored later in the fracture criterion section.

Despite the different toughness with different resins, the shape of the response is similar. The tougher the materials, the greater the maximum toughening effect due to the mixed mode condition. Certainly, mixed mode conditions can be a toughening mechanism for composite materials, compared to the pure mode I.

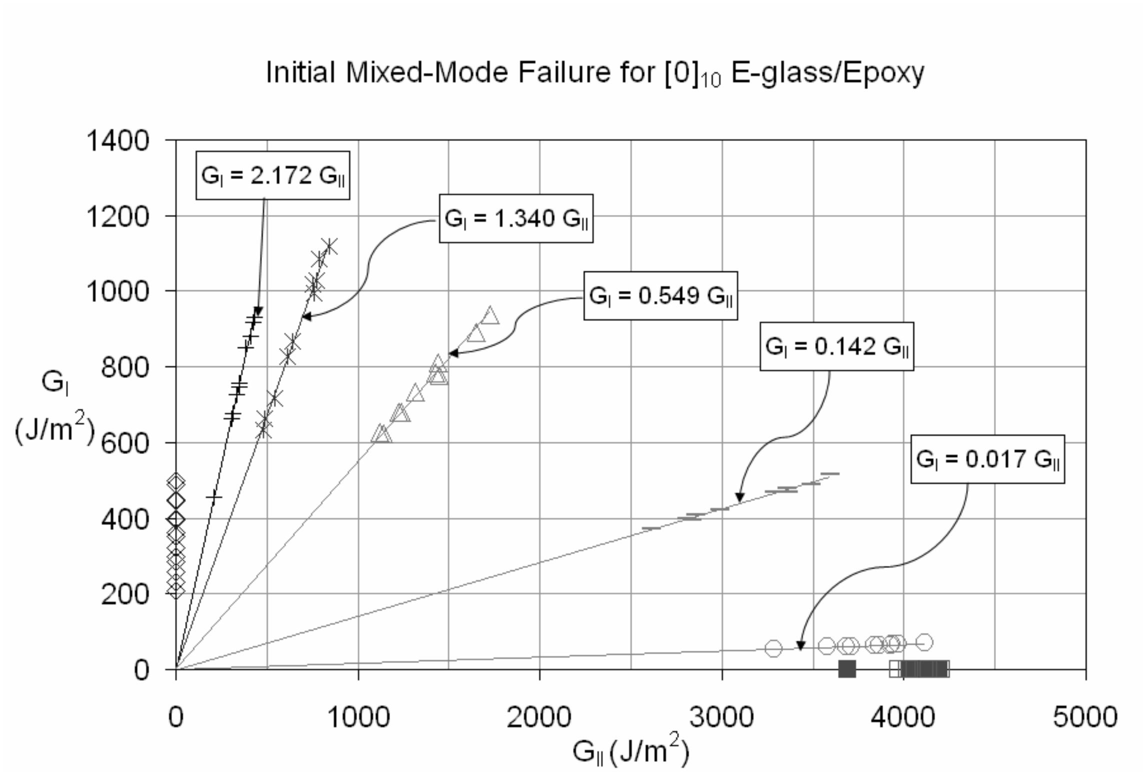

Figure 29 MMB results for epoxy resin composites

<u>Mixed Mode Summary for All Composites</u>

Table 6 gives the maximum average G_I component compared with G_{Ic} and G_{IIc} for each system, and Figure 30 compares the experimental results for the three systems. As illustrated in Figure 30, the toughest to most brittle ordering of epoxy to isophthalic polyester holds for all G_I/G_{II} ratios. Thus, any delamination crack having a combination of modes I and II would be resisted significantly better by epoxy than by vinylester, and isophthalic polyester would give the poorest performance. This is consistent with the finding for skin-stiffener intersection tests reported in References 6 and 17.

Table 6 Maximum average G_I component compared with G_{Ic} and G_{IIc} for each system.

Resin	pure G_{Ic} (J/m^2)		pure G_{IIc} (J/m^2)		maximum G_I component (J/m^2)		R_G at maximum G_I component
	avg	std	avg	std	avg	std	
Isophthalic Polyester	116	27	1797	256	201	41	1.115
Vinyl Ester	204	59	3283	86	587	126	0.557
Epoxy	356	94	4054	151	895	179	1.340

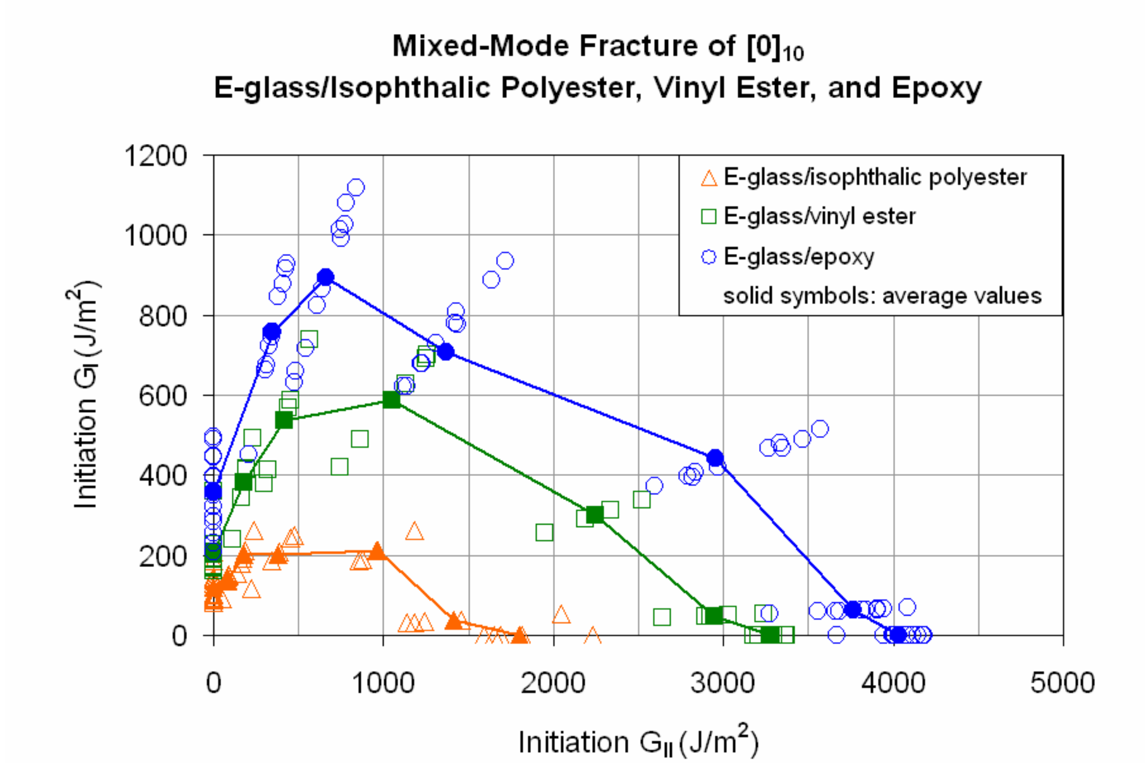

Figure 30 Summary of MMB results of for delamination initiation

NUMERICAL RESULTS

This section first addresses issues related to mesh size in the finite element analysis in ANSYS. The finite element model is then applied to the three specimen types and validated against modified beam-theory for calculation of the strain energy release rates.

Convergence Studies

Through-thickness Convergence Study

The first convergence study was done on the elements through the thickness. At four elements per half-thickness, the change of deflection from three to four elements per half-thickness was only 0.52% and the change of G_{Ic} was only 0.36%. The tolerance for the change is rather arbitrary; the author feels that a change under 1% is sufficient for the analysis. The results of through-thickness convergence study are summarized in Figure 31 and Table 7.

Table 7 Summary of through-thickness convergence study

number of elements per half thickness	element size (mm)	deflection (mm)	deflection percent change	G_{Ic} (J/m^2)	G_{Ic} percent change
8	3.66E-01	6.80E-01	0.05	88.74933	0.03
7	4.19E-01	6.80E-01	0.06	88.72223	0.04
6	4.88E-01	6.80E-01	0.09	88.68580	0.06
5	5.86E-01	6.79E-01	0.13	88.63418	0.09
4	7.33E-01	6.78E-01	0.23	88.55506	0.16
3	9.77E-01	6.77E-01	0.52	88.41787	0.36
2	1.47E+00	6.73E-01	2.64	88.09984	1.85
1	2.93E+00	6.56E-01	---	86.49781	---

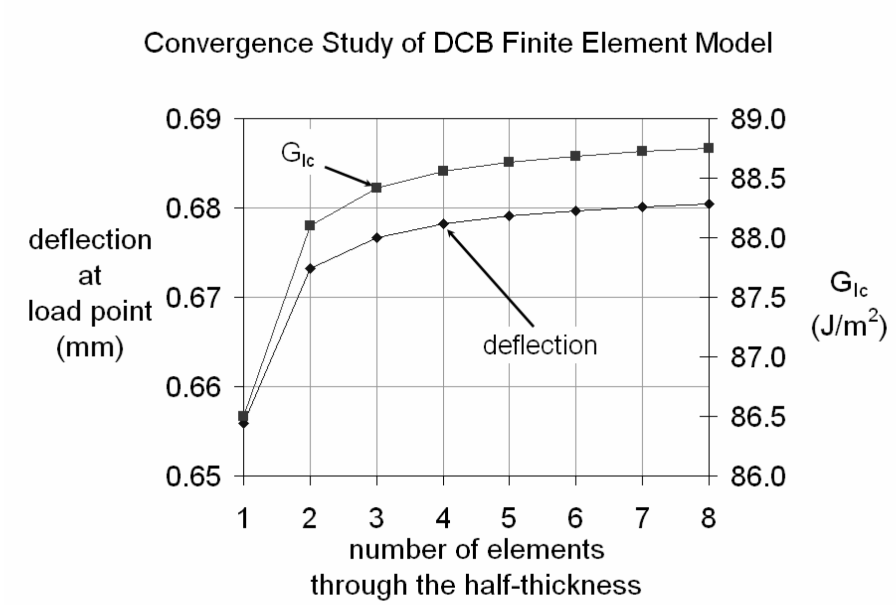

Figure 31 Convergence study on the number of elements through the half-thickness

<u>Crack-Tip Refinement</u>

The through-thickness convergence study was followed by a crack-tip refinement. The line division around the crack tip was found to be 40 elements with spacing ratio of 0.2 as illustrated in Figure 32 (ndiv is the line division around the crack tip). The refinement using spacing ratio produces an element that is not a square, but still four sided. Two studies in comparing different methods of refinement were performed.

One study maintained a square element but does not maintain a smooth size transition. In ANSYS, the command used to implement this method is KREF (for refinement of elements around keypoints) [62]. The other study is exactly the opposite; a smooth transition, but the square shape is not maintained. However, the element is still four sided. The ANSYS method for this is the employment of the parameter spacing ratio in the command RESIZE [61].

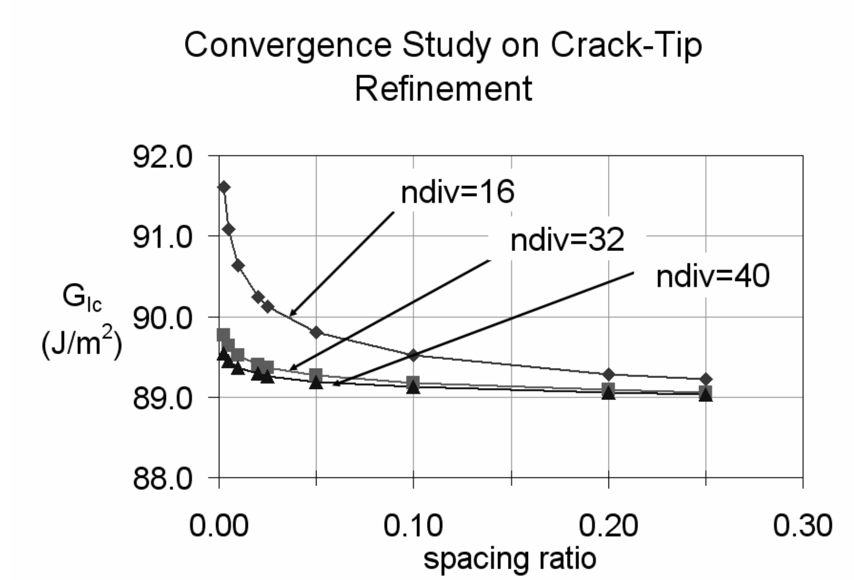

Figure 32 Crack tip refinement using line division and spacing ratio

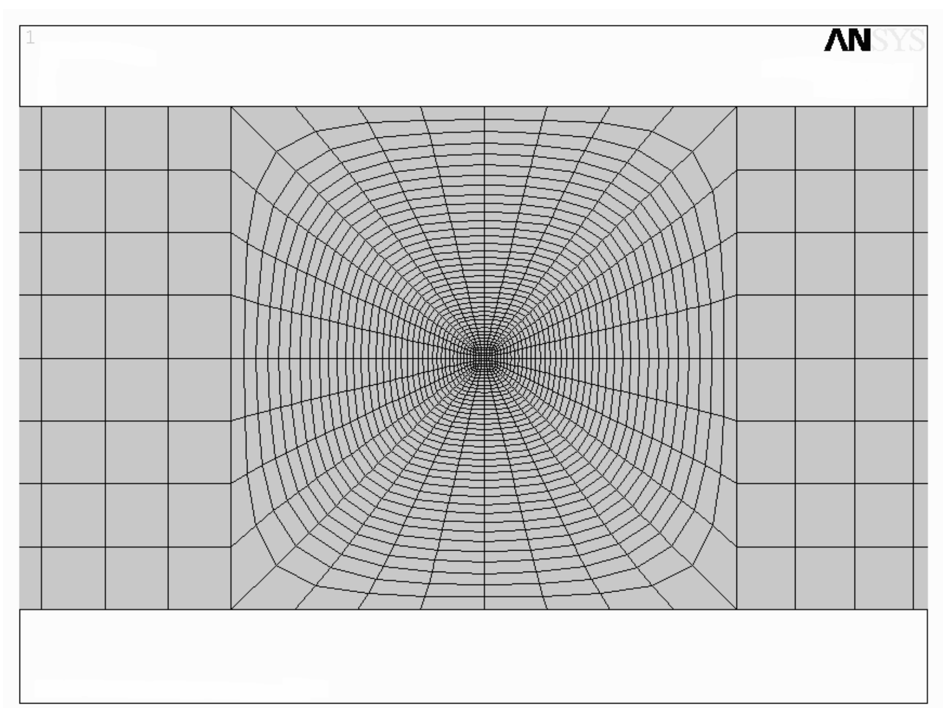

Figure 33 Mesh refinement at the crack tip

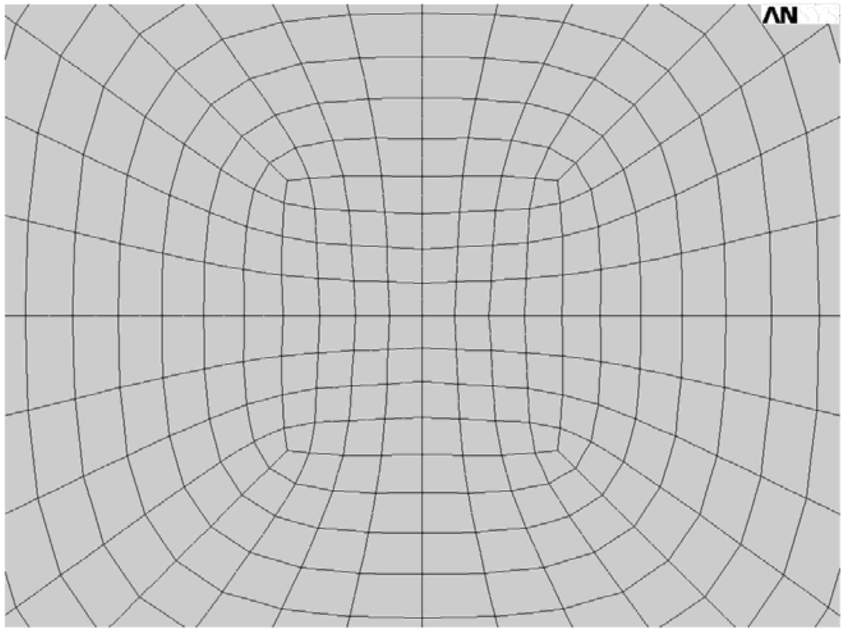

Figure 34 Close-up of mesh refinement at the crack tip

A special element called the quarter point (QP) element is available from Raju [9]. This element is special because at one of the corners a singularity exists, because the mid-node is placed in the quarter point location [55,57] At the time this paper was written, the QP element was still under study by the author. There is a macro by ANSYS that enables automated creation of quarter point elements, but it required a free-mesh (an unstructured method of creating a finite element mesh), a least desired mesh because of aesthetic and consistency reasons. This element will be subject to further study.

Validation of FE Model

Deflection as a First Validation

The element division per half thickness was set to four, with refinement at the crack tip. All dimensions and loads were based on the experimental data. The model deflection was compared with the experimental results to check for first-order verification of validity. Prior to comparing the FE model deflection, the number of elements per thickness was first determined; using a convergence study, four elements per thickness was found sufficient for accuracy.

SERR as A Second Validation

The next step was comparison of G-values between the model and the modified beam theory. Prior to calculating the SERR using VCCT1, the element size around the crack tip was refined using independent optimization procedures. The element size was then compared with a criterion suggested by ANSYS, 0.5 to 2.0% of crack length; as a conservative measure, 0.5% was used as the required scale of element size around the crack tip. This element size is considered as the size of the assumed infinitesimal crack extension.

Online Moduli

Two types of moduli were used, the average and the calculated. The calculated moduli are called the online moduli, because they are the specimen actual moduli, not the average for the batch where the specimen was made. As a part of the sensitivity analysis, these moduli were used as a comparison with the average (batch) moduli.

The moduli were calculated using equations developed by Mandell et. al. [1,2]. The fiber volume percentage is directly related to the average one-ply thickness of the composites by Equation 27, and the moduli are functions of the fiber volume fraction by Equations 28 to 31 as follows:

$$V_f = \frac{1}{1000}\left(\frac{20.666}{t}\right)^{\frac{1}{0.9999}} \tag{27}$$

where t is the average one-ply thickness in m and V_f is the fiber volume percentage.

$$E_L = \frac{E_L^*}{32.71}\left(3.1 + .658\,V_f\right) \tag{28}$$

$$E_T = \frac{E_T^*}{2.206}\left(\frac{1 + .00836\,V_f}{1 - .00836\,V_f}\right) \tag{29}$$

$$G_{LT} = \frac{G_{LT}^*}{2.809}\left(\frac{1 + .01672\,V_f}{1 - 0.00836\,V_f}\right) \tag{30}$$

$$\nu_{LT} = \frac{\nu_{LT}^*}{0.318}\left(0.385 - 0.0015\,V_f\right) \tag{31}$$

Where, E_L, E_L, G_{LT}, and ν_{LT}, are the longitudinal modulus (E_{11}), the transverse modulus (E_{22},E_{33}), the longitudinal-transverse shear modulus (G_{12}, G_{13}), and longitudinal-transverse poison ratio (ν_{12}, ν_{13}), respectively. The asterisks signify the properties at 45% fiber volume content [1]. The online ν_{23} remained as the value obtained from Reference 1. The total thickness t, as a function of half thickness h and number of plies n, is calculated as follows:

$$t = \frac{2h}{n} \tag{32}$$

In this study n is equal to 10 plies. Combining Equations 27 through 32, the moduli as functions of h and n are the following:

$$E_L = 0.03057\,E_L^*\left(3.1 + .00680\left(\frac{n}{h}\right)^{1.0001}\right) \tag{33}$$

$$E_T = 0.45331\, E_T^{*}\left(\frac{1 + 8.64 \times 10^{-5}\left(\frac{n}{h}\right)^{1.0001}}{1 - 8.64 \times 10^{-5}\left(\frac{n}{h}\right)^{1.0001}}\right) \tag{34}$$

$$G_{LT} = 0.35600\, G_{LT}^{*}\left(\frac{1 + 1.72 \times 10^{-4}\left(\frac{n}{h}\right)^{1.0001}}{1 - 8.64 \times 10^{-5}\left(\frac{n}{h}\right)^{1.0001}}\right) \tag{35}$$

$$\nu_{TL} = 3.14465\,\nu_{LT}^{*}\left(0.385 - 1.55 \times 10^{-5}\left(\frac{n}{h}\right)^{1.0001}\right) \tag{36}$$

Equations 33 to 36 were used to calculate the online moduli.

Design Guidelines

Designing the test specimen required the optimization of certain dimensions. The three major variables are the tab dimensions, the pinholes (including the pins), and the crack length.

1. The best designs for tabs are ones with small glue area, while still maintaining a good bonding with specimen. The smallest tab base will reduce the beam stiffening effect.
2. Pinholes that are close to the mid-thickness of specimen will reduce the opposite moment, which arises due to friction at the pins as deflection increases. Small pins imply that the center of rotation is closer to the beams, making the application of moment closer to the desired location, which is directly onto the beam instead of the tabs. Care must be maintained with small pins, because they may increase friction, as

the normal forces increase, and they may deform significantly, because of the low stiffness.

3. Moderate values of crack length will reduce the large deflection effect, a nonlinear behavior. However, too short a crack length may introduce some beam stiffening effect and tab adhesion problems.

Design guidelines number one and two are easily optimized. Item three can be modeled, but for the simplicity of the modeling, the pins were not modeled for the current study. The study of optimum crack length was performed due to differences between experimental and predicted (FEA) displacements. Theoretically, each crack length should correspond to a particular critical load, but in actuality, because of the stochastic nature of the material, two similar crack lengths may yield two different critical loads, therefore, preventing it from being optimized.

DCB Modeling

The DCB models were the simplest to work with, because they do not involve contact elements, which required extra time for convergence during solution. Two comparisons were done, the deflection and the SERR. Three different deflections were obtained for comparison: experimental, modified beam-theory, and finite element analysis. Two SERR were obtained from modified beam-theory and finite element result using VCCT.

The deflections between the MBT and FEA agreed, but not with the experimental result, which triggered a sensitivity analysis on the crack length to investigate the disagreement. The SERR always showed excellent agreement between the FEA and the MBT.

DCB Modeling for Isophthalic Polyester Resin Composites

This modeling is based on the specimen coded DCB05p. DCB modeling of the isophthalic polyester specimen including the tabs is illustrated in Figure 35, shown in terms of Von Mises stresses. Von Mises stress σ_e is computed as follows:

$$\sigma_e = \left(\frac{1}{2}\left[(\sigma_1 - \sigma_2)^2 + (\sigma_2 - \sigma_3)^2 + (\sigma_3 - \sigma_1)^2\right]\right)^{\frac{1}{2}} \tag{37}$$

where σ_1, σ_2, and σ_3 are the principle stresses [64]. The model restricts all displacement on the bottom tab and x-direction on the top tab. DCB results are summarized in Table 8.

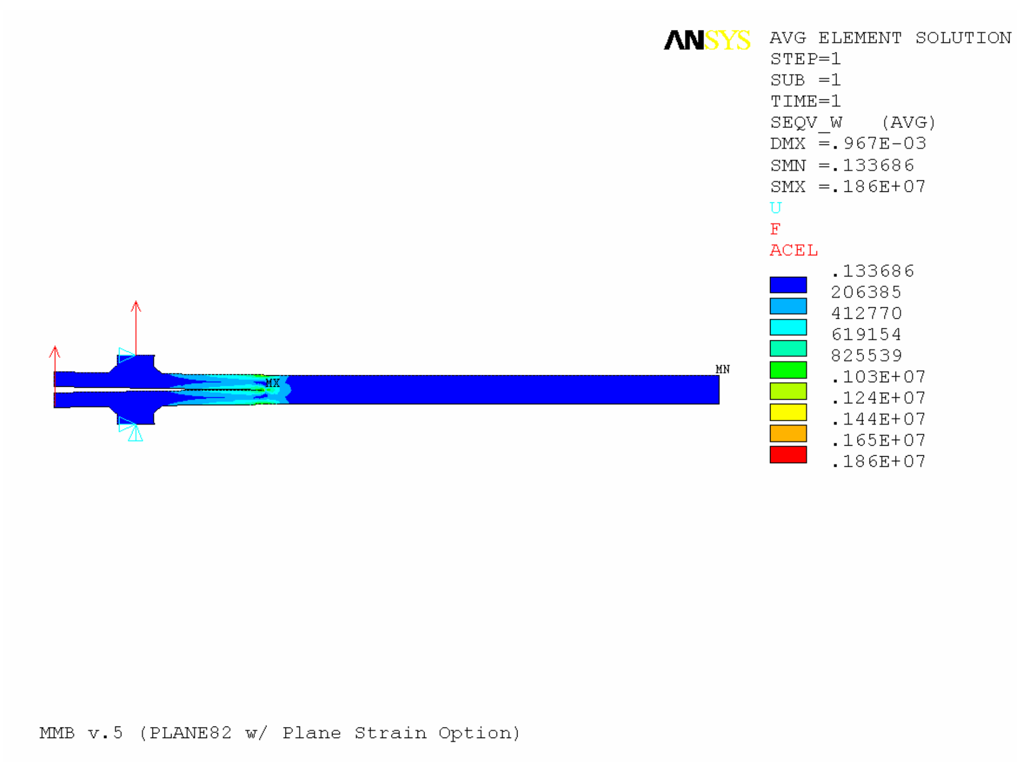

Figure 35 DCB specimen modeling using "T"-tabs

Four different cases were done for each test: linear with tab, nonlinear with tab, linear without tab and nonlinear without tab. Tab vs. no tab models were done to check how much the tab affects the result of beam stiffening due to the tabs. FE results revealed that the tabs do no affect G-values significantly.

Table 8 Results for DCB isophthalic polyester specimen for four different cases

			deflection (mm)	G_{Ic} (J/m^2)	deflection ratio*	G_{Ic} ratio**
Experimental			0.6883		1.000	
MBT			0.6740	88.51	0.979	1.000
FEA	Tab	Linear	0.6823	89.06	0.991	1.006
	Tab	Nonlinear	0.6776	88.55	0.984	1.000
	No Tab	Linear	0.6849	89.11	0.995	1.007
	No Tab	Nonlinear	0.6836	89.01	0.993	1.006

* The ratio with the experimental value if applicable

** The ratio with the MBT value if applicable

Linear vs. nonlinear solutions are required to study the large deflection effect. "When the strains in a material exceed more than a few percent, the changing geometry due to this deformation can no longer be neglected [ANSYS]." For a more elaborate explanation, please see Chapter 3, Structures with Geometric Nonlinearities, of ANSYS Theory Reference.

The results also showed a very good accuracy for the experimental, MBT, and the FE deflections, with the largest difference of 2.1% attributed to the MBT deflection. The MBT deflection for a DCB test specimen is calculated as follows [45-47]:

$$\delta_{DCB} = \frac{12P_I}{E_{11}bh^3}\left(\frac{2}{3}a_o{}^3 + \frac{2}{\lambda}a_o{}^2 + \frac{2}{\lambda^2}a_o + \frac{1}{\lambda^3} + \frac{a_o h^2 E_{11}}{5G_{13}}\right) \tag{38}$$

The FE results showed the largest difference of about 1.6% for the deflection, attributed to the nonlinear tab solution. All four cases showed a consistency in the deflections and the SERR, implying insensitivity to the tab or nonlinear analysis.

The deflection is a function of the crack length to the third power, and the SERR varies with crack length to the second power. Sensitivity analysis is important to check how much the measurement in crack length would affect the calculation of the deflection and the SERR. Two different sets of parameters were used for the analysis, the crack length and the moduli. The modulus of concern is the longitudinal modulus E_{11}, which is inversely proportional to both the deflection and the SERR. Even though E_{11} appears in the elastic foundation terms and the shear terms for G_I, and only in the shear terms for G_{II}, the effect of E_{11} in these terms is very small. The results for sensitivity analysis are shown in Table 9.

Sensitivity Analysis for DCB Isophthalic Polyester Specimen

A 10% change in the crack length caused a 30% change in the deflection and 18% in G_{Ic}. As expected, the crack length affected the deflection more than the SERR, because of the cubic power of crack length in the MBT deflection calculation. The online moduli caused more change in the deflections and the SERR than the crack length. The changes in moduli are not summarized here, because they involved the calculation of four different constants, E_{11}, E_{22}, G_{12}, and ν_{12}. The nonlinear and no-tab solutions were consistently insensitive to the changes in crack length and the moduli.

Table 9 Sensitivity analysis for DCB isophthalic polyester

			deflection (mm)				Ratio with original		
			original*	(a) 10% crack length increase	(b) online moduli**	(c) online moduli and 10% crack length increase	(a)	(b)	(c)
MBT			0.6740	0.8712	0.6341	0.8194	1.293	0.941	1.216
FEA	Tab	Linear	0.6823	0.8807	0.6415	0.8281	1.291	0.940	1.214
	Tab	Nonlinear	0.6776	0.8742	0.6374	0.8223	1.290	0.941	1.214
	No Tab	Linear	0.6849	0.8834	0.6440	0.8306	1.290	0.940	1.213
	No Tab	Nonlinear	0.6836	0.8817	0.6428	0.8290	1.290	0.940	1.213
Experimental			0.6883						
			G_{Ic} (J/m^2)				Ratio with original		
MBT			88.51	105.16	83.18	98.81	1.188	0.940	1.116
FEA with VCCT	Tab	Linear	89.06	105.54	83.72	99.21	1.185	0.940	1.114
	Tab	Nonlinear	88.55	104.88	83.27	98.63	1.185	0.940	1.114
	No Tab	Linear	89.11	105.60	83.77	99.27	1.185	0.940	1.114
	No Tab	Nonlinear	89.01	105.48	83.69	99.16	1.185	0.940	1.114

* Calculation using the measured crack length and average moduli

** Calculation using the moduli equations 33 to 36

If the moduli were changed to the online, the deflection and the SERR would change the same way, because both are a strong function of the (longitudinal) modulus. The other moduli do not affect the calculations much.

DCB Modeling for Vinyl Ester

DCB modeling of the vinyl ester specimen showed similar inaccuracy in the deflection like that for the isophthalic polyester specimen as listed in Table 10. The specimen used for modeling vinyl ester is coded DCB03p.

The errors for the MBT and the FE deflection were approximately 12%. A similar trend is apparent in all FE solutions, showing essentially no difference in the type of solutions, no-tab or nonlinear. The MBT and the FE G_{Ic} always showed a very good agreement, even if the deflections were inaccurate. The error in deflection triggered a sensitivity analysis using the crack length and the moduli as the parameters. The results are shown in Table 11.

Table 10 Results for DCB vinyl ester specimen

			deflection (mm)	G_{Ic} (J/m^2)	deflection ratio*	G_{Ic} ratio**
Experimental			4.2342		1.000	
MBT			3.7382	160.91	0.883	1.000
FEA	Tab	Linear	3.7448	159.40	0.884	0.991
	Tab	Nonlinear	3.7075	157.89	0.876	0.981
	No Tab	Linear	3.7482	159.56	0.885	0.992
	No Tab	Nonlinear	3.7336	158.88	0.882	0.987

* The ratio with the experimental value if applicable

** The ratio with the MBT value if applicable

Sensitivity Analysis for DCB Vinyl Ester Specimen

Table 11 Sensitivity analysis for DCB vinyl ester specimen

			deflection (mm)				Ratio with original		
			original*	(a) 10% crack length increase	(b) online moduli**	(c) online moduli and 10% crack length increase	(a)	(b)	(c)
MBT			3.7382	4.9098	3.9690	5.2134	1.313	1.062	1.395
FEA	Tab	Linear	3.7448	4.9070	3.9540	5.1842	1.310	1.056	1.384
	Tab	Nonlinear	3.7075	4.8527	3.9121	5.1223	1.309	1.055	1.382
	No Tab	Linear	3.7482	4.9109	3.9575	5.1883	1.310	1.056	1.384
	No Tab	Nonlinear	3.7336	4.8889	3.9410	5.1634	1.309	1.056	1.383
Experimental			4.2342						
			G_{Ic} (J/m^2)				Ratio with original		
MBT			160.91	193.06	170.91	205.06	1.200	1.062	1.274
FEA with VCCT	Tab	Linear	159.40	190.87	168.69	202.07	1.197	1.058	1.268
	Tab	Nonlinear	157.89	188.85	166.99	199.74	1.196	1.058	1.265
	No Tab	Linear	159.56	191.05	168.85	202.26	1.197	1.058	1.268
	No Tab	Nonlinear	158.88	190.10	168.08	201.19	1.197	1.058	1.266

* Calculation using the measured crack length and average moduli

** Calculation using the moduli equations 33 to 36

In the vinyl ester specimen, a change of 10% in the crack length changed the deflection 31%, and the SERR, 20%. The changes in moduli caused small changes in both the deflections and the SERR, 6%, implying that the online moduli were close to the average experimental values. If the calculated moduli were taken as the true moduli (instead of the average moduli), the crack length is within a 2% error to get to the experimental deflection. If the average (original) moduli were taken as the true moduli, the crack length is within a 4% error.

DCB Modeling for Epoxy Resin Composites

Epoxy also showed similar trends; the MBT and the FEA deflections were 13 to 14% off from the experimental, and the FEA SERR were consistent with the MBT's. The sensitivity analysis for the deflection is summarized in Table 13. The specimen used in this modeling is DCB03p.

Table 12 Results for DCB epoxy specimen

			deflection (mm)	G_{Ic} (J/m^2)	deflection ratio*	G_{Ic} ratio**
Experimental			1.3106		1.000	
MBT			1.1238	208.52	0.857	1.000
FEA	Tab	Linear	1.1490	211.58	0.877	1.015
	Tab	Nonlinear	1.1392	210.02	0.869	1.007
	No Tab	Linear	1.1518	211.64	0.879	1.015
	No Tab	Nonlinear	1.1473	210.81	0.875	1.011

* The ratio with the experimental value if applicable
** The ratio with the MBT value if applicable

For the epoxy specimen, the 10% change in crack length caused a 29% change in the deflections, and 19% change in the SERR, similar to isophthalic polyester and vinyl ester sensitivity analyses. The online moduli caused a change of about 10% in both the deflection and the SERR, showing that the original moduli were far from average. If the original modulus were used, the crack length is within 6% error, but if the online modulus were used, it is only a 2% error.

Table 13 Sensitivity analysis for DCB epoxy specimen

			deflection (mm) original*	(a) 10% crack length increase	(b) online moduli**	(c) online moduli and 10% crack length increase	Ratio with original (a)	(b)	(c)
MBT			1.1238	1.4535	1.2308	1.5933	1.293	1.095	1.418
FEA	Tab	Linear	1.1490	1.4831	1.2456	1.6100	1.291	1.084	1.401
	Tab	Nonlinear	1.1392	1.4692	1.2341	1.5935	1.290	1.083	1.399
	No Tab	Linear	1.1518	1.4859	1.2485	1.6129	1.290	1.084	1.400
	No Tab	Nonlinear	1.1473	1.4797	1.2432	1.6055	1.290	1.084	1.399
Experimental			1.3106						
			G_{Ic} (J/m^2)				Ratio with original		
MBT			208.52	247.82	229.16	272.47	1.188	1.099	1.307
FEA with VCCT	Tab	Linear	211.58	250.76	230.59	273.54	1.185	1.090	1.293
	Tab	Nonlinear	210.02	248.68	228.75	271.07	1.184	1.089	1.291
	No Tab	Linear	211.64	250.83	230.65	273.61	1.185	1.090	1.293
	No Tab	Nonlinear	210.81	249.76	229.68	272.36	1.185	1.090	1.292

* Calculation using the measured crack length and average moduli
** Calculation using the moduli equations 33 to 36

Summary for DCB modeling

DCB modeling is successful with respect to the SERR consistency between the MBT and the FEA results. Whether the deflections are inaccurate or not, the SERR are always consistent. The crack length and the modulus are certainly the major contributors to the deflection discrepancy. The online moduli are the best elastic constants to use, because they are not the average values. Many of the supposedly intrinsic material properties, i.e., modulus, fiber volume content, etc., vary from batch to batch. The use of the online moduli caused the error of the crack length to be small, which is expected, because they are, once again, not the average values and the crack length can be measured accurately using a microscope. However, the crack visible to the eyes may not be where the material has completely separated, because the crack lengths are only measured from the edges of specimen.

ENF Modeling

Contact Element as a Requirement

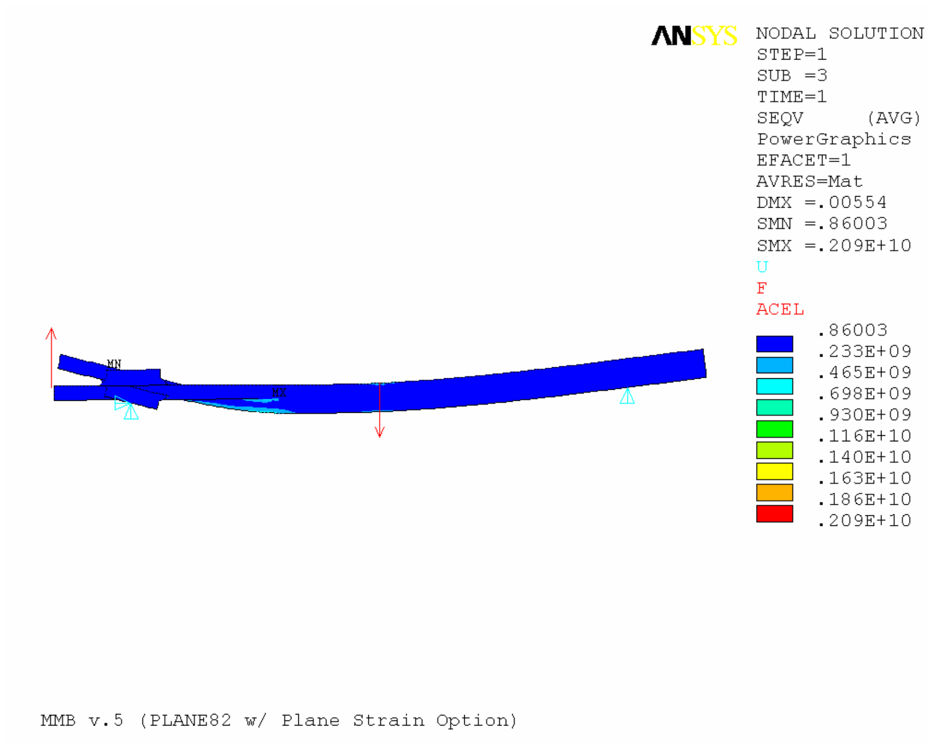

Figure 36 ENF modeling without contact elements resulted in overlapping of beams (the stress contour is Pa/m)

ENF modeling required the use of contact elements to simulate the contact at the crack interface. Without contact elements, the beams would be overlapping. These contact elements replace the elements used in the Gillespie model, in which he used 2D elements with infinite compressive and zero tensile moduli. Contact elements require fine-tuning for the convergence rate to be optimum. A more elaborate explanation of the fine-tuning of contact elements is available in Chapter 10 of The ANSYS Structural Guide [65] and the implementation is in the ANSYS input file in APPENDIX B.

Figure 36 illustrates effects of the absence of contact elements, as the beams overlap.

ENF Deflection Prediction by MBT

The ENF deflection was calculated using the MBT, using the following equation [35]:

$$\delta_{ENF} = \frac{P_{II}}{E_{11}bh^3}\left(\left(\frac{1}{4}L^3 + \frac{3}{8}a_o{}^3\right) + \left(\frac{9}{40}a_o + \frac{3}{10}L\right)\frac{h^2E_{11}}{G_{13}}\right) \tag{39}$$

The MBT deflection is used as a validation for the experimental and the FE values. Similar to the DCB modeling, deflection is the first step in validating the measured dimension, which is the crack length. In ENF deflection, the crack length is not the only variable to the third power, but also the length between supports. This must be noted, because the support length does not contribute to the G_{IIc} calculation.

Friction Modeling in ENF Test Specimen

Linear and nonlinear solutions have been obtained for the ENF specimen. Friction is an issue for pure mode-II, because of the beam contacts. For the sake of simplicity, the initial friction is taken to be small, 0.01, because of the Nylon strip that acts as a lubricant. However, this assumption will be explored later. Gillespie has discussed the calculation of friction in the MBT [35].

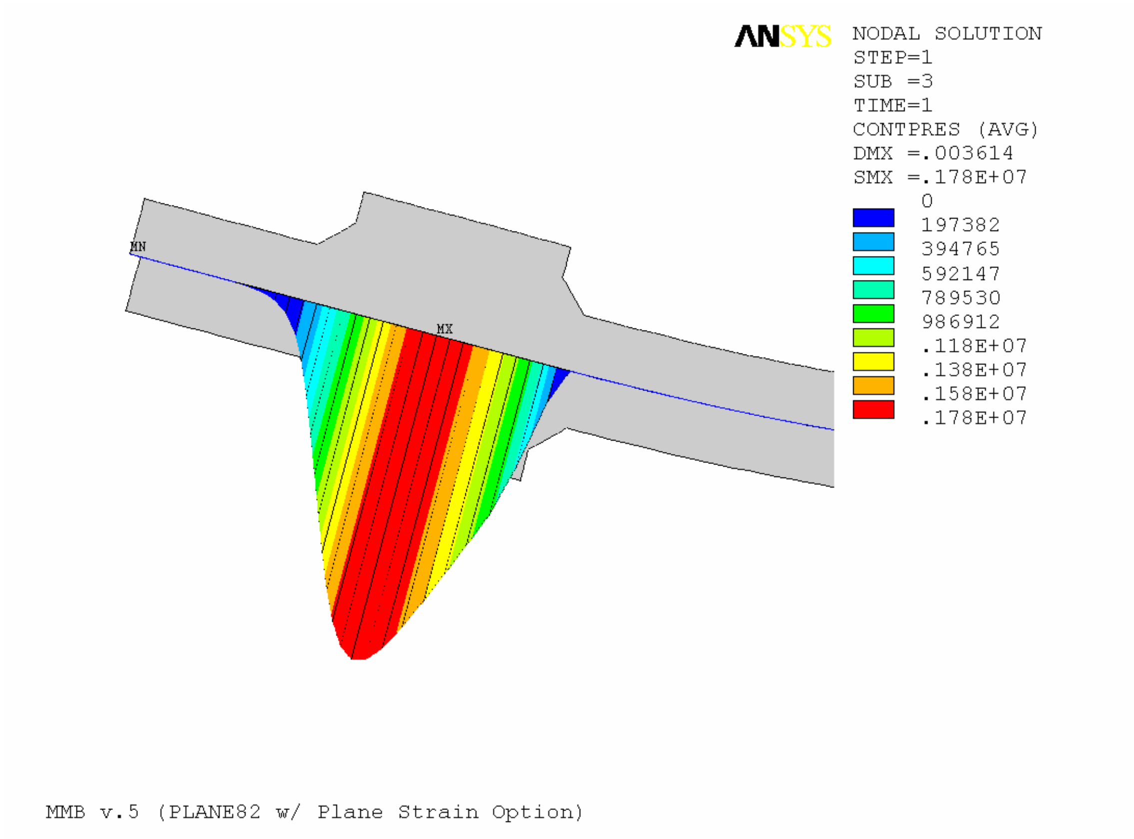

Figure 37 The presence of contact pressure between the beams at the crack interface (contact pressure is in stress per unit width Pa/m)

Contact pressure will be visited briefly to validate Gillespie assumption stating that the pressure distribution is extending only 2h away from the pin. Figure 37 illustrates the results of ANSYS in analyzing the contact between the two beams at the crack interface.

<u>Sensitivity Analysis on Friction in ENF Test Specimen</u>

The changes in deflection and G_{IIc} are linear with respect to the coefficient of friction. The results of the friction study of the ENF test specimen are summarized in Table 14 and Figure 38. Increasing the coefficient of friction from 0.01 to 0.6 only changed the deflection by -1.3% and the SERR by -7.8%. If the Nylon coefficient of friction were taken as 0.4 (matweb.com), the deflection and G_{IIc} only changed by -0.6% and -3.8%, respectively.

Table 14 Result of Sensitivity Analysis on Friction for the ENF Test Specimen

coefficient of friction	absolute deflection (mm)	G_{IIc} (J/m^2)	percent change deflection*	percent change G_{IIc}*
0.01	3.554	2347	---	---
0.10	3.547	2318	-0.2	-1.2
0.20	3.539	2288	-0.4	-2.5
0.30	3.531	2257	-0.6	-3.8
0.40	3.522	2225	-0.9	-5.2
0.50	3.515	2194	-1.1	-6.5
0.60	3.506	2162	-1.3	-7.8

* reference value is at coefficient of friction equal to 0.01

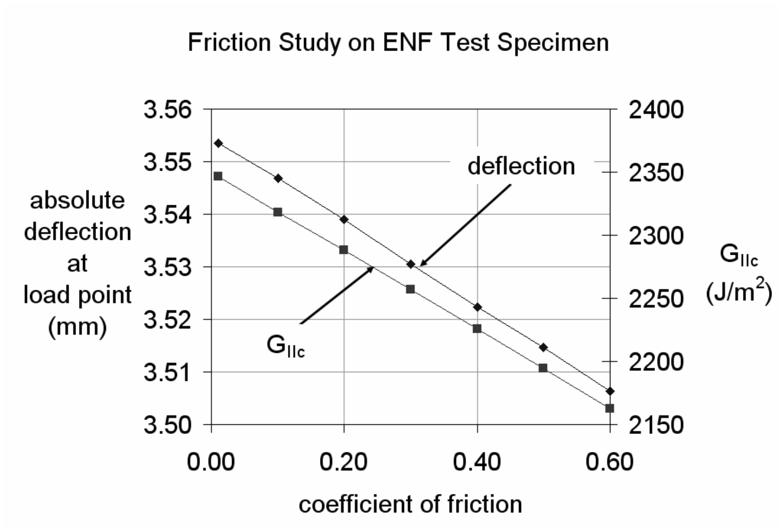

Figure 38 Graphical Summary of Friction Study on ENF Test Specimen

ENF Modeling of Isophthalic Polyester Resin Composite

The ENF test specimen coded ENF05 has been successfully modeled with contact elements as illustrated in Figure 39 with a contour of Von Mises stresses in Pascal. It must be noted that the stresses here are the actual stress, not the stresses per unit width. (This note is to avoid confusion because the original calculation was based on a unit width.) The FE results for ENF isophthalic polyester are summarized in Table 15.

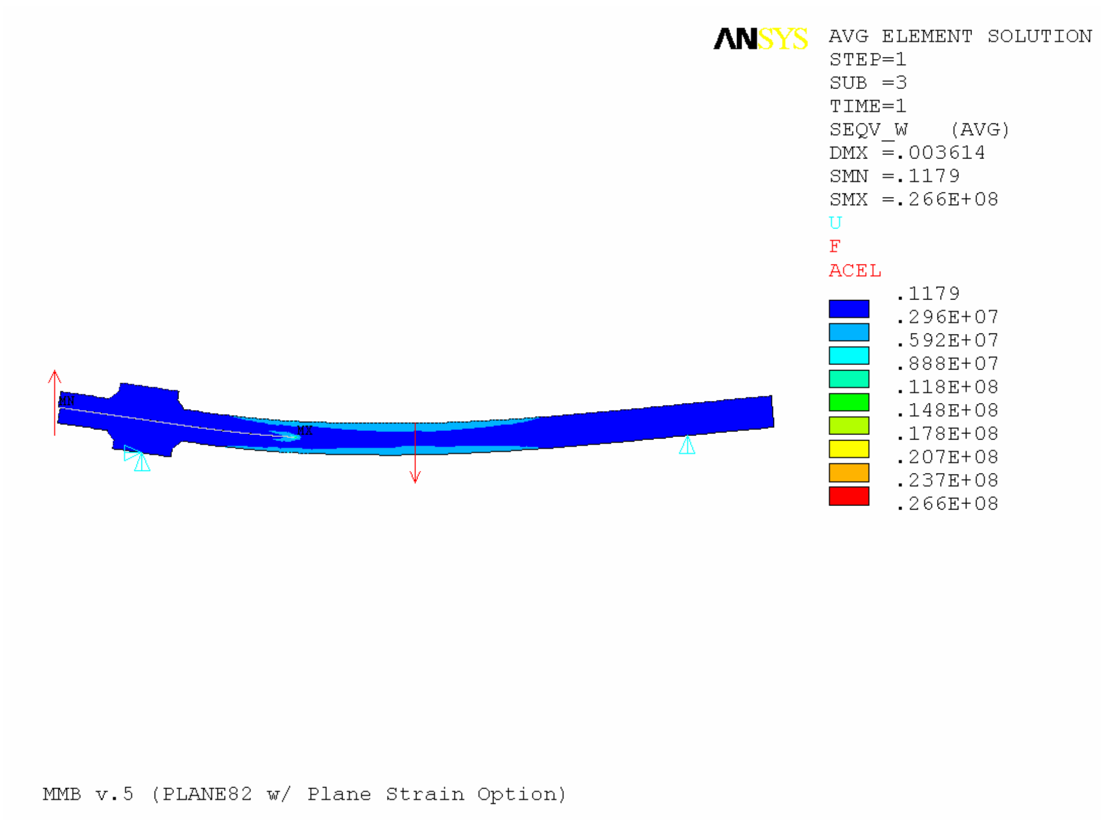

Figure 39 ENF modeling with tabs

The FEA deflections were consistent with the MBT's, and so were the FEA G-values. The FEA deflections were off by 2~5% off with the largest error attributed to the tab linear solution. The FEA G-values were off by 0.1~2.2%, with the largest error attributed to the tab nonlinear. G_I apparently was present in the ENF test specimen, based on the FEA. This topic is discussed in the next subheading.

Table 15 Results for ENF isophthalic polyester specimen

			deflection (mm)	G_{Ic} (J/m^2)	G_{IIc} (J/m^2)	deflection ratio*	G_{IIc} ratio**
Experimental			-3.636			1.000	
MBT			-3.547		2297	0.976	1.000
FEA	Tab	Linear	-3.473	2.73	2335	0.955	1.017
	Tab	Nonlinear	-3.554	25.89	2347	0.977	1.022
	No Tab	Linear	-3.482	2.71	2335	0.957	1.016
	No Tab	Nonlinear	-3.515	25.42	2295	0.967	0.999

* The ratio with the experimental value if applicable

** The ratio with the MBT value if applicable

Tabbed and non-tabbed solutions were determined. This study is to validate the MBT for excluding the tabs and to simplify the finite element modeling. Clearly, the tabs can be excluded from the model with high confidence.

The deflections from linear runs are consistent regardless of the tabs. However, there is large discrepancy between the experimental and both the MBT and the FEA deflections. This discrepancy will be resolved in the later subsection. However, for nonlinear runs, the tabs have a slight effect on SERR. The difference between linear and nonlinear runs is small compared to the (experimental) standard deviation of G_{IIc}.

For linear runs, G_{II} is not affected by the tabs. However, the nonlinear runs give contradictory results. The result with no tabs is actually closer to the experimental value than that with tabs. The 2% error is still contained within the standard deviation of G_{IIc} of 14 % (see Table 4).

Presence of Mode I Component in ENF Test Specimen

Another suspicion was that at longer cracks, the two beams might not deflect equally. It is suspected that the lower beam is bending more than the top beam, causing a small mode-I presence. For less-tough materials, the crack would already be propagating before a "large" deflection were reached. However, for tougher materials, the deflection can be so large that mode I can be present in the magnitude order of G_{Ic}. This suspicion can be verified using the ENF FE model. If mode-I exists in the magnitude order of G_{Ic}, then ENF tests cannot be used as a pure mode-II tests. Ultimately, this means that the MMB test may need revision for very high mode-II. Table 15 summarizes G_I present in the ENF test using specimen coded ENF05.

The prediction based on deflection and SERR is accurate, hence, MBT is valid and the tabs can be excluded from the model. Sensitivity analysis is also done on ENF test specimen, isophthalic polyester result is summarized in Table 16.

Sensitivity Analysis for ENF Isophthalic Polyester Specimen

The crack length was increased by 10% causing 7% and 20% changes in the deflections and the SERR, respectively. Using the original elastic constants, the error in crack length is approximately 3.7%.

Switching to the online moduli changed both the deflections and the SERR changed by 7%, as expected. The longitudinal modulus, the most important variable among the other moduli, is inversely proportional to the deflection and the SERR.

Using the online modulus, the crack length is within 16% error and using the original moduli, only 4%. The 16% percent error is attributed to the crack length and the moduli discrepancy. Another explanation is that the crack propagation was slow, in which the crack has already propagated even before maximum load is reached. The calculation of G_{IIc} even though inaccurate, is still conservative, that is the calculated value is lower than the actual value.

Table 16 Sensitivity analysis for ENF isophthalic polyester specimen

			deflection (mm)				Ratio with original		
			original*	(a) 10% crack length increase	(b) online moduli**	(c) online moduli and 10% crack length increase	(a)	(b)	(c)
MBT			-3.5473	-3.7870	-3.2736	-3.4949	1.068	0.923	0.985
FEA	Tab	Linear	-3.4733	-3.7133	-3.2172	-3.4400	1.069	0.926	0.990
FEA	Tab	Nonlinear	-3.5535	-3.8023	-3.2876	-3.5188	1.070	0.925	0.990
FEA	No Tab	Linear	-3.4815	-3.7214	-3.2248	-3.4473	1.069	0.926	0.990
FEA	No Tab	Nonlinear	-3.5145	-3.7562	-3.2546	-3.4785	1.069	0.926	0.990
Experimental			-3.6363						
			G_{IIc} (J/m^2)				Ratio with original		
MBT			2296.81	2769.87	2120.05	2556.78	1.206	0.923	1.113
FEA with VCCT	Tab	Linear	2334.82	2804.26	2162.88	2598.11	1.201	0.926	1.113
FEA with VCCT	Tab	Nonlinear	2346.54	2814.20	2175.53	2609.60	1.199	0.927	1.112
FEA with VCCT	No Tab	Linear	2334.50	2803.90	2162.65	2597.64	1.201	0.926	1.113
FEA with VCCT	No Tab	Nonlinear	2295.26	2757.00	2131.66	2559.82	1.201	0.929	1.115
			G_{Ic} (J/m^2)				Ratio with original		
FEA with VCCT	Tab	Linear	2.73	2.18	2.12	1.76	0.799	0.777	0.645
FEA with VCCT	Tab	Nonlinear	25.89	27.87	21.08	23.55	1.076	0.814	0.909
FEA with VCCT	No Tab	Linear	2.71	2.25	2.11	1.75	0.828	0.777	0.644
FEA with VCCT	No Tab	Nonlinear	25.42	27.41	20.53	22.06	1.078	0.808	0.868

* Calculation using the measured crack length and average moduli
** Calculation using the moduli equations 33 to 36

The G_I presence is very small, that is on the order of 1% of G_{IIc}. The presence of mode I is inevitable if the beams are not deflecting equally. Since the presence if very small, the G_I can be neglected.

ENF Modeling for Vinyl Ester Specimen

The deflections in vinyl ester are in better agreement than for isophthalic polyester. In the linear solution, the tabs have no effect, but in nonlinear runs, the tab solution is closer to the actual experimental value. The model is based on specimen coded ENF03.

The SERR for linear solutions are the same for the tab and non-tab solutions. The tabs virtually do not cause any nonlinearity as shown by the linear and nonlinear solutions for the tab model. Sensitivity analysis for ENF vinyl ester is tabulated in Table 18.

For the linear runs, the tab solution deflection is expected to be less than for the not-tab. However, the nonlinear solutions reveal the opposite results, implying that the tabs have a geometric effect. This geometric effect is nonetheless small considering the differences among the solutions are also small.

Table 17 Results for ENF vinyl ester specimen

			deflection (mm)	G_{Ic} (J/m^2)	G_{IIc} (J/m^2)	deflection ratio*	G_{IIc} ratio**
Experimental			-4.324			1.000	
MBT			-4.116		3368	0.952	1.000
FEA	Tab	Linear	-4.038	4.99	3426	0.934	1.017
	Tab	Nonlinear	-4.140	54.98	3423	0.957	1.016
	No Tab	Linear	-4.043	4.98	3426	0.935	1.017
	No Tab	Nonlinear	-4.082	53.11	3342	0.944	0.992

* The ratio with the experimental value if applicable
** The ratio with the MBT value if applicable

<u>Sensitivity Analysis for ENF Vinyl Ester Specimen</u>

The measurement of crack length is less accurate than the measurement of the moduli, because a 10% crack length increase changed the deflection by 7% and the G_{IIc} by 20%, whereas the changes of moduli only change both the deflection and the G_{IIc} by 2%. The crack length is 7% off if the original moduli were used and 5% if the online were used. The presence of the G_I is also small, 1%.

Table 18 Sensitivity analysis for ENF vinyl ester

			deflection (mm)			Ratio with original		
		original*	(a) 10% crack length increase	(b) online moduli**	(c) online moduli and 10% crack length increase	(a)	(b)	(c)
MBT		-4.1162	-4.4017	-4.1832	-4.4742	1.069	1.016	1.087
FEA	Tab Linear	-4.0377	-4.3235	-4.1099	-4.4008	1.071	1.018	1.090
FEA	Tab Nonlinear	-4.1398	-4.4355	-4.2156	-4.5167	1.071	1.018	1.091
FEA	No Tab Linear	-4.0429	-4.3283	-4.1149	-4.4055	1.071	1.018	1.090
FEA	No Tab Nonlinear	-4.0816	-4.3671	-4.1547	-4.4452	1.070	1.018	1.089
Experimental		-4.3240						

			G_{IIc} (J/m^2)			Ratio with original		
MBT		3368.15	4060.94	3431.70	4139.18	1.206	1.019	1.229
FEA with VCCT	Tab Linear	3425.63	4113.95	3490.98	4194.06	1.201	1.019	1.224
FEA with VCCT	Tab Nonlinear	3422.65	4103.83	3486.67	4181.67	1.199	1.019	1.222
FEA with VCCT	No Tab Linear	3425.91	4113.67	3491.26	4193.75	1.201	1.019	1.224
FEA with VCCT	No Tab Nonlinear	3341.94	4011.75	3402.51	4085.98	1.200	1.018	1.223

			G_{Ic} (J/m^2)			Ratio with original		
FEA with VCCT	Tab Linear	4.99	4.07	5.27	4.28	0.814	1.054	0.856
FEA with VCCT	Tab Nonlinear	54.98	59.74	54.47	58.18	1.087	0.991	1.058
FEA with VCCT	No Tab Linear	4.98	4.05	5.25	4.26	0.813	1.055	0.856
FEA with VCCT	No Tab Nonlinear	53.11	58.19	52.70	56.65	1.096	0.992	1.067

* Calculation using the measured crack length and average moduli

** Calculation using the moduli equations 33 to 36

ENF Modeling of Epoxy Specimens

The FEA deflection for ENF epoxy is substantially off, 22% from the experimental value as seen in Table 19. This modeling is based on specimen coded ENF04. The G_{IIc} from MBT is always consistent with the FEA; however, this obviously does not guarantee the consistency in the deflection. In addition, the presence of G_I is 2% that of G_{IIc}; greater than that for isophthalic polyester and vinyl ester. The sensitivity analysis is summarized in Table 20.

Table 19 Results for ENF epoxy

			deflection (mm)	G_{Ic} (J/m^2)	G_{IIc} (J/m^2)	deflection ratio*	G_{IIc} ratio**
Experimental			-5.135			1.000	
MBT			-3.999		4022	0.779	1.000
FEA	Tab	Linear	-3.930	7.11	4120	0.765	1.024
FEA	Tab	Nonlinear	-4.040	79.11	4118	0.787	1.024
FEA	No Tab	Linear	-3.937	7.08	4119	0.767	1.024
FEA	No Tab	Nonlinear	-3.983	76.09	4009	0.776	0.997

* The ratio with the experimental value if applicable

** The ratio with the MBT value if applicable

Sensitivity Analysis for ENF Epoxy Specimen

Table 20 Sensitivity analysis results for ENF epoxy specimen

			deflection (mm)				Ratio with original		
			original*	(a) 10% crack length increase	(b) online moduli**	(c) online moduli and 10% crack length increase	(a)	(b)	(c)
MBT			-3.9986	-4.2441	-4.4044	-4.6757	1.061	1.101	1.169
FEA	Tab	Linear	-3.9296	-4.1762	-4.3159	-4.5865	1.063	1.098	1.167
FEA	Tab	Nonlinear	-4.0399	-4.2978	-4.4462	-4.7293	1.064	1.101	1.171
FEA	No Tab	Linear	-3.9366	-4.1831	-4.3234	-4.5939	1.063	1.098	1.167
FEA	No Tab	Nonlinear	-3.9828	-4.2315	-4.3758	-4.6469	1.062	1.099	1.167
Experimental			-5.1350						
			G_{IIc} (J/m^2)				Ratio with original		
MBT			4021.98	4843.59	4443.52	5354.17	1.204	1.105	1.331
FEA with VCCT	Tab	Linear	4119.65	4941.10	4530.96	5437.14	1.199	1.100	1.320
FEA with VCCT	Tab	Nonlinear	4118.45	4928.73	4521.52	5412.36	1.197	1.098	1.314
FEA with VCCT	No Tab	Linear	4119.23	4940.43	4531.09	5436.92	1.199	1.100	1.320
FEA with VCCT	No Tab	Nonlinear	4009.35	4806.74	4389.61	5263.30	1.199	1.095	1.313
			G_{Ic} (J/m^2)				Ratio with original		
FEA with VCCT	Tab	Linear	7.11	6.23	9.77	8.66	0.876	1.374	1.218
FEA with VCCT	Tab	Nonlinear	79.11	89.90	95.59	107.09	1.136	1.208	1.354
FEA with VCCT	No Tab	Linear	7.08	6.29	9.73	8.62	0.889	1.375	1.218
FEA with VCCT	No Tab	Nonlinear	76.09	86.52	91.61	102.87	1.137	1.204	1.352

* Calculation using the measured crack length and average moduli

** Calculation using the moduli equations 33 to 36

The sensitivity did not reveal a match in the deflection values, even though the crack length had been increased and the moduli had been corrected. Both the moduli and the crack length add up to the 22% discrepancy in the deflections. This summation of error is obviated by the 10% increase in crack length and the online moduli, which give changes to the deflection of 6% and 10%, respectively. Another sensitivity analysis specifically for the ENF epoxy specimen was done to investigate the large discrepancy in the deflection, summarized under subheading Deflection Discrepancy in Epoxy ENF Modeling.

Deflection Discrepancy in Epoxy ENF Modeling

The discrepancy prompted another investigation, because the deflection was much higher. The most probable contribution to the high deflection is the crack length, followed by the moduli. Investigation results are summarized in Table 21 and Table 22. This investigation was done using tab and nonlinear solutions for ENF epoxy. Using the online moduli, the average longitudinal modulus, 31.0 GPa, while using the online modulus yielded 28.0 GPa, a difference of approximately 10%. During the test, the only thing that changes the compliance is the crack length.

Table 21 Sensitivity analysis of ENF epoxy with crack increase up to 40% using the average moduli

crack length increase	deflection (mm)	G_{IIc} (J/m^2)	percent change deflection	percent change G_{IIc}
0.00	-4.040	4022	---	---
0.10	-4.298	4844	6.4	20.4
0.20	-4.603	5743	13.9	42.8
0.30	-4.960	6722	22.8	67.1
0.40	-5.372	7778	33.0	93.4

Table 22 Sensitivity analysis of ENF epoxy with crack increase up to 40% using the online moduli

crack length increase	deflection (mm)	G_{IIc} (J/m^2)	percent change deflection	percent change G_{IIc}
0.00	-4.446	4522	---	---
0.10	-4.729	5354	6.4	18.4
0.20	-5.065	6352	13.9	40.5
0.30	-5.456	7436	22.7	64.5
0.40	-5.908	8606	32.9	90.3

In calculating G_{IIc}, the crack length is correct, but the load is wrong, because the load has corresponded to a different crack length. Each load-deflection graph is very distinct to its mechanical properties. Now, since in the test, there is no way for the material properties to change, i.e., moduli, the only contribution to the epoxy ENF discrepancy in deflection is the crack length. This discrepancy is caused by using the recorded crack length with the critical load that could be two types: actual maximum or the 5%-offset slope.

The analysis also concludes that the crack propagation was stable, unlike the usual mode-II on brittle matrix like isophthalic polyester. This kind of propagation may require the standard 5%-offset slope be revised, because the 5% may be too non-conservative for composite materials like E-glass/epoxy system.

MMB Modeling

Surface-to-surface contact is discussed is Section 10.4 of ANSYS Structural Guide [65]. An attempt to model the MMB specimen without the loading lever was done to simplify the model and to verify the modified beam theory.

For MMB without the loading lever, the beams overlapped, P_I was not large enough to overcome the deformation from P_{II}. This phenomenon is not accounted for in Reeder and Crews MMB finite element model. The model was run with the calculated P_I and P_{II} from P_c. Since the crack interface is not accounted for, G_{Ic} can still be calculated if the beams overlap, this overlap would make an opposite G_{Ic}. Considering the beam overlap, a reverse procedure is then performed to find the critical load for each mode. This method was done in using the Optimization Procedure in ANSYS [66]. Figure 40 illustrates the overlaps between beams.

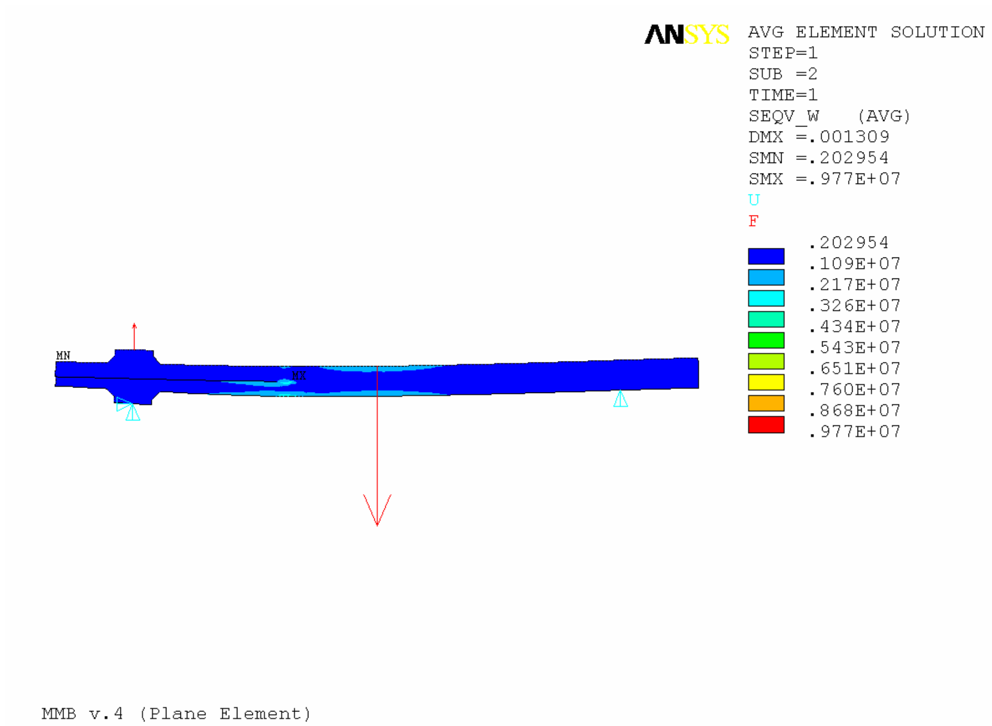

Figure 40 An attempt to model MMB specimen without the loading lever (the load vectors are exaggerated for clarity)

The beam overlap called for the loading lever to be modeled. The loading lever was modeled with contact elements at the fulcrum that is touching the specimen. The rotation at the clevis is simulated by coupling the nodes at the loading lever and the tabs of specimen. The loading roller is omitted and the load is applied at the center of the roller. The deflection is at the point of load application. More results are generated with the new model that includes the loading lever.

Figure 41 illustrates MMB modeling with the loading lever. The results show significant discrepancies, especially as the critical load was increasing, which is evident with the epoxy specimen. The test specimen for the isophthalic polyester MMB model was coded MMB00 with c=31.87 mm, a=32.17 mm, giving an R_G value of 0.496. The results exhibited discrepancies: G_{Ic} is 30% off and G_{IIc} are 16% off. This error triggered another investigation on the loading lever. Maximum stress occurs at the crack tip as illustrated in Figure 42, and a close-up of the crack tip with elemental boundaries is illustrated in Figure 43. .

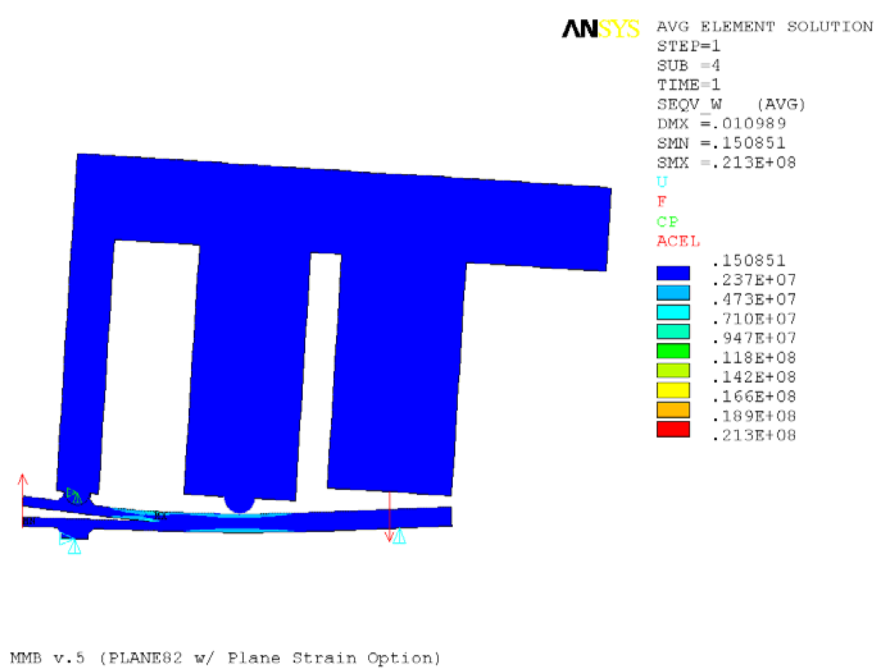

Figure 41 MMB modeling with loading lever

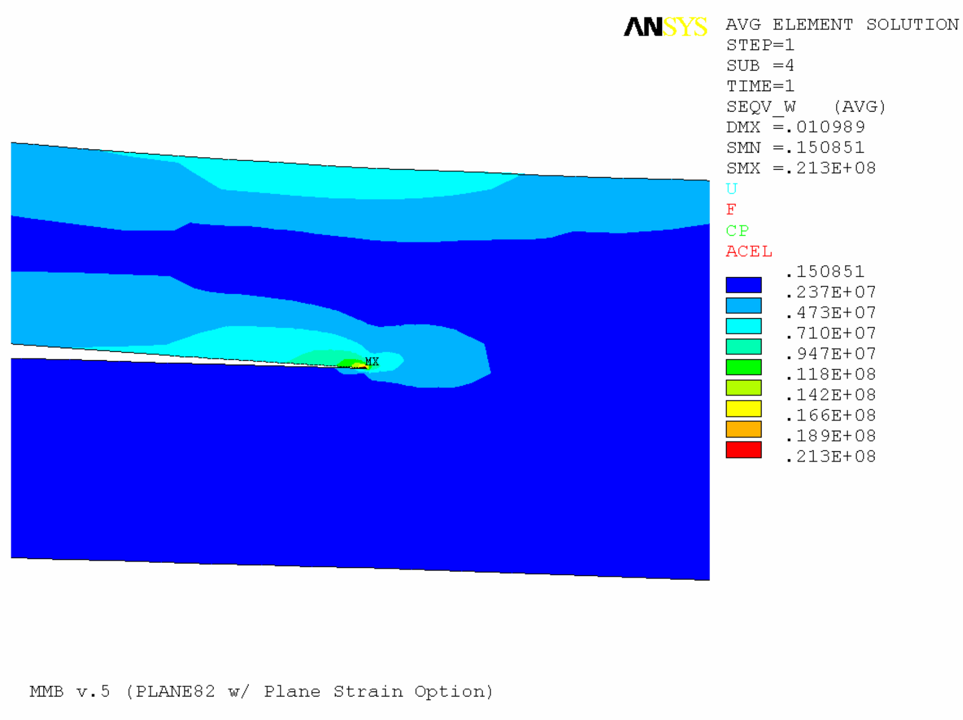

Figure 42 Von Mises stress contour around the crack tip

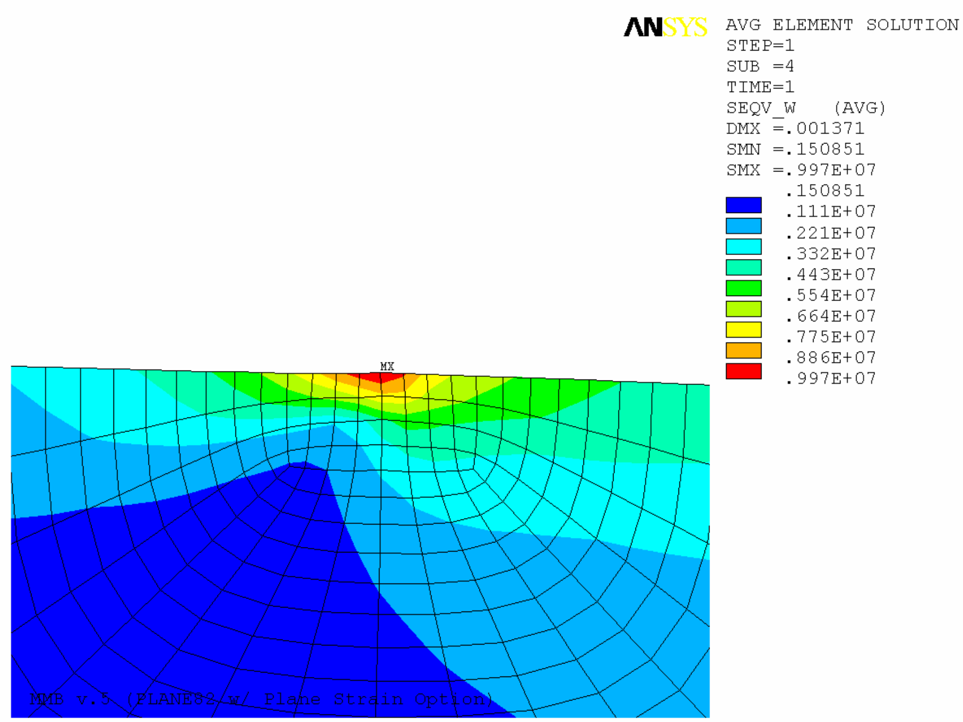

Figure 43 Von Mises contour around a meshed crack-tip at close-up with the lower-half section only.

Table 23 Results for MMB isophthalic polyester

		deflection (mm)	G_I (J/m^2)	G_{II} (J/m^2)	R_G	deflection ratio*	G_I ratio**	G_{II} ratio**	R_G ratio**
Experimental		-3.430				1.000			
MBT			243.3	492.4	0.494		1.000	1.000	1.000
FEA	Tab Linear	-2.742	226.0	503.9	0.448	0.799	0.929	1.023	0.908
FEA	Tab Nonlinear	-2.747	262.6	467.9	0.561	0.801	1.079	0.950	1.136

* The ratio with the experimental value if applicable
** The ratio with the MBT value if applicable

The only available solution for MMB modeling is the tab solution. Removing the tab would certainly change the rotation of the loading lever. For the deflection, the linear and nonlinear solutions essentially give the same results, but for the SERR, the linear solution is more accurate than the nonlinear. The solutions show interesting results as the G_I component and the G_{II} component switched value with respect to the magnitude of the experimental values. The linear solution gives a lower G_I and a higher G_{II}, but the nonlinear shows a higher G_I and a lower G_{II}. Since the linear solution does not take account of geometric effects, the discrepancy is attributed to the geometry of the loading lever. The FEA G_{Ic} and G_{IIc} results are both consistent with the MBT results as shown in the DCB and ENF Modeling.

Sensitivity Analysis for MMB Isophthalic Polyester Specimen

The 10% crack length increase always changed the deflections by 12%, regardless of the moduli used, and the SERR by 21% (both G_I and G_{II}). The moduli always change the deflection and the SERR approximately the same amount. As previously discussed, the most influential modulus is the longitudinal modulus, which is inversely proportional to both the deflection and the SERR. The discrepancy in the deflection prompted another special sensitivity analysis in heading Neglected Dimensions of the Loading Lever.

Table 24 Sensitivity result for MMB isophthalic polyester specimen

		deflection (mm)				Ratio with original		
		original*	(a) 10% crack length increase	(b) online moduli**	(c) online moduli and 10% crack length increase	(a)	(b)	(c)
FEA	Tab Linear	-2.742	-3.066	-2.673	-2.986	1.118	0.975	1.089
	Tab Nonlinear	-2.747	-3.077	-2.677	-2.999	1.120	0.975	1.092
Experimental		-3.430						
		G_{II} (J/m^2)				Ratio with original		
MBT		492.4	594.1	478.7	577.6	1.207	0.972	1.173
FEA with VCCT	Tab Linear	503.9	607.8	491.3	592.0	1.206	0.975	1.175
	Tab Nonlinear	467.9	565.5	456.8	552.3	1.209	0.976	1.180
		G_I (J/m^2)				Ratio with original		
MBT		243.3	289.9	237.0	282.4	1.192	0.974	1.161
FEA with VCCT	Tab Linear	226.0	271.7	220.2	264.2	1.203	0.975	1.169
	Tab Nonlinear	262.6	319.2	255.3	310.5	1.216	0.972	1.182

* Calculation using the measured crack length and average moduli

** Calculation using the moduli equations 33 to 36

MMB Modeling for Vinyl Ester Specimen

The deflection is inaccurate with an error of 23%, for both linear and nonlinear solutions. The linear solution for the G_I component underestimates the experimental value by 3% and the nonlinear solution overestimate by 5%. The linear solution for the G_{II} component overestimates the experimental value by 4% and the nonlinear underestimates by 8%. The SERR results are more accurate than the deflection. Similar to the isophthalic polyester results, the linear solution is more accurate than the nonlinear. The linear solution underestimates the G_I component and overestimates the G_{II} component, whereas the nonlinear solution reverses the results. This modeling is based on the specimen MMB13p.

Table 25 Results for MMB vinyl ester specimen

		deflection (mm)	G_I (J/m^2)	G_{II} (J/m^2)	R_G	deflection ratio*	G_I ratio**	G_{II} ratio**	R_G ratio**
Experimental		-4.069				1.000			
MBT			379.7	298.8	1.271		1.000	1.000	1.000
FEA	Tab Linear	-3.137	366.9	310.7	1.181	0.771	0.966	1.040	0.929
	Tab Nonlinear	-3.123	397.3	275.2	1.444	0.767	1.046	0.921	1.136

* The ratio with the experimental value if applicable

** The ratio with the MBT value if applicable

Sensitivity Analysis for MMB Vinyl Ester Specimen

The online moduli were close to the original; therefore, for both types of moduli, the 10% crack length increase caused essentially the same change in the deflections, 13%, and in the SERR, 21%. The sensitivity analysis reveals an error in the crack length of 23% for both types of moduli.

Table 26 Sensitivity analysis for MMB vinyl ester

		deflection (mm)				Ratio with original		
		original*	(a) 10% crack length increase	(b) online moduli**	(c) online moduli and 10% crack length increase	(a)	(b)	(c)
FEA	Tab Linear	-3.137	-3.542	-3.146	-3.551	1.129	1.003	1.132
	Tab Nonlinear	-3.123	-3.521	-3.130	-3.530	1.128	1.002	1.130
Experimental		-4.069						
		G_{II} (J/m^2)				Ratio with original		
MBT		298.8	360.4	300.3	362.3	1.206	1.005	1.212
FEA with VCCT	Tab Linear	310.7	372.2	312.5	374.3	1.198	1.006	1.205
	Tab Nonlinear	275.2	328.6	277.1	331.1	1.194	1.007	1.203
		G_I (J/m^2)				Ratio with original		
MBT		379.7	452.2	382.4	455.5	1.191	1.007	1.200
FEA with VCCT	Tab Linear	366.9	435.6	367.4	436.3	1.187	1.001	1.189
	Tab Nonlinear	397.3	473.7	397.0	473.5	1.192	0.999	1.192

* Calculation using the measured crack length and average moduli

** Calculation using the moduli equations 33 to 36

MMB Modeling for Epoxy

The specimen coded MMB33 was used to model MMB epoxy. The FEA deflections are substantially off by 16%. The linear solution gives more accurate results than the nonlinear for the SERR. The linear solution underestimates the G_I component by 1% and overestimates the G_{II} component by 2%. The nonlinear solution overestimates the G_I component by 9% and underestimates the G_{II} component by 18%. The results for MMB epoxy specimen are summarized in Table 27.

Table 27 Results for MMB epoxy specimen

		deflection (mm)	G_I (J/m^2)	G_{II} (J/m^2)	R_G	deflection ratio*	G_I ratio**	G_{II} ratio**	R_G ratio**
Experimental		-5.097				1.000			
MBT			844.6	623.9	1.354		1.000	1.000	1.000
FEA	Tab Linear	-4.264	836.2	635.7	1.315	0.837	0.990	1.019	0.972
	Tab Nonlinear	-4.229	922.0	512.4	1.799	0.830	1.092	0.821	1.329

* The ratio with the experimental value if applicable

** The ratio with the MBT value if applicable

Sensitivity Analysis for MMB Epoxy Specimen

The sensitivity analysis for MMB epoxy shed some light on the deflection discrepancy. The accuracy of the deflections is increased by using the online moduli and the 10% crack length increase, which give an error in the deflection down to 6%. The SERR are also affected by the increase of length the change of moduli, causing a change of 25%.

Table 28 Sensitivity analysis for MMB epoxy specimen

		deflection (mm) original*	deflection (mm) (a) 10% crack length increase	deflection (mm) (b) online moduli**	deflection (mm) (c) online moduli and 10% crack length increase	Ratio with original (a)	Ratio with original (b)	Ratio with original (c)
FEA	Tab Linear	-4.264	-4.637	-4.406	-4.792	1.088	1.033	1.124
FEA	Tab Nonlinear	-4.229	-4.594	-4.367	-4.744	1.086	1.033	1.122
Experimental		-5.097						
		G_{II} (J/m^2)				Ratio with original		
MBT		623.9	751.2	647.8	780.3	1.204	1.038	1.251
FEA with VCCT	Tab Linear	635.7	755.4	658.3	783.5	1.188	1.036	1.233
FEA with VCCT	Tab Nonlinear	512.4	607.9	530.5	630.7	1.186	1.035	1.231
		G_I (J/m^2)				Ratio with original		
MBT		844.6	1001.7	876.2	1039.5	1.186	1.037	1.231
FEA with VCCT	Tab Linear	836.2	982.2	861.3	1014.2	1.175	1.030	1.213
FEA with VCCT	Tab Nonlinear	922.0	1091.5	948.3	1125.1	1.184	1.028	1.220

* Calculation using the measured crack length and average moduli

** Calculation using the moduli equations 33 to 36

Neglected Dimensions of the Loading Lever

Several things were not accounted for by the SERR in the MMB test. The equations are only applicable to the specimen without the taking account of the geometry of the loading lever (except for the variable c). Optimizations were done to check on how much the SERR, using the VCCT1, would be affected by the neglected dimensions. The results and discussion follow.

Optimization of MMB Loading Lever

The investigation is started by observing the G-ratio as the experiment is in progress. Since incremental load can be applied in the model, the G-ratio at each incremental load is recorded and graphed in Figure 44. The ratio was found to be increasing due to the rotation of the loading lever.

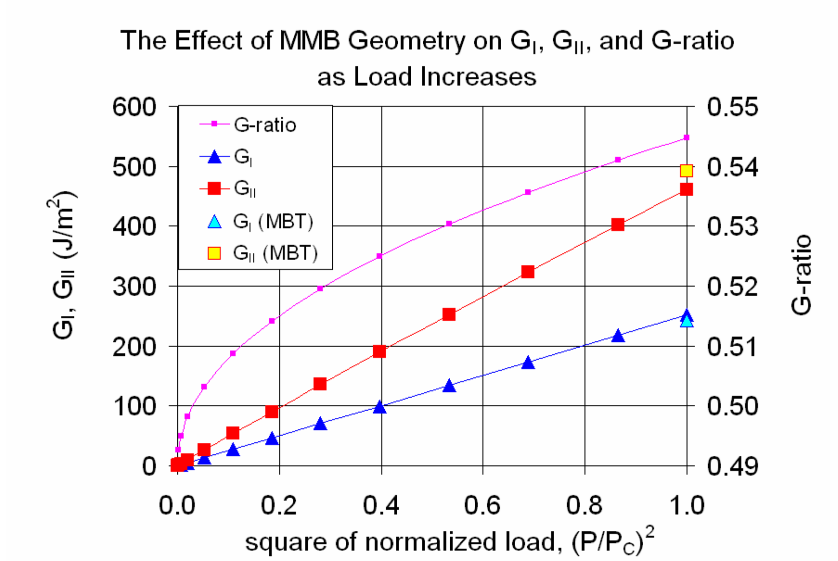

Figure 44 Changes in G-values and ratio as the load increases

The investigation proceeded by an optimization procedure to find the correct loading point vertical position. The optimization is done by minimizing the error between experimental and numerical values by changing the loading point vertical height and the loading lever height. The results of the optimization follow.

<u>Optimization Result for MMB Loading Lever</u>

The height of the loading lever was suspected to give rise to the discrepancy. Using the optimization method in ANSYS, the vertical relative position of the loading point with respect to the specimen was found to be different by 28 mm from the actual apparatus; a significant difference from the Reeder revision on the loading lever [22]. His results showed a loading position above the specimen, whereas in this experiment, the loading lever below the specimen gave a better agreement between the FEA and MBT G-values.

Another aspect is the rotation of the loading lever as the load increases. Variable "c" may have been changed as the fulcrum rotates. This phenomenon is also discussed by Reeder in his redesign of the apparatus.

Optimization was done by choosing variable "c", the height of the loading point, and the height of the loading lever from the specimen as the independent variable and by choosing the sum-squared error of the SERR as the function to be minimized. The variables used are illustrated in Figure 45 and the results for optimizing vertical position of the loading point are summarized in Figure 46.

This investigation proved that the vertical position of the loading point with respect to the specimen matters. An improved agreement is achieved by lowering the loading point further below the specimen.

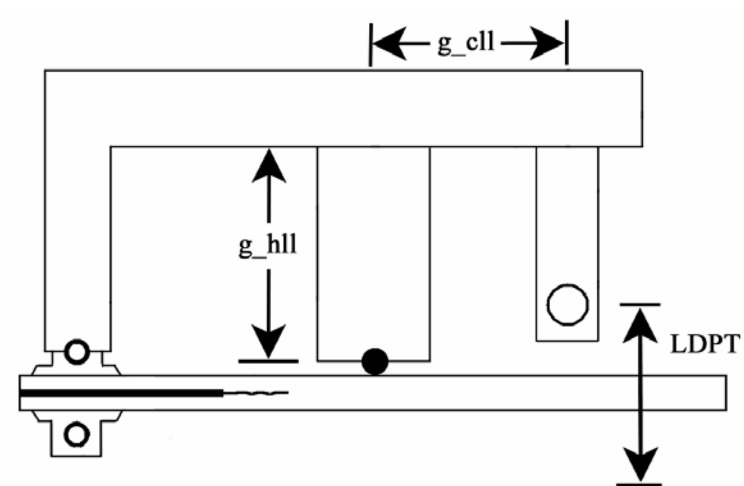

Figure 45 Variables for Loading Lever Optimization

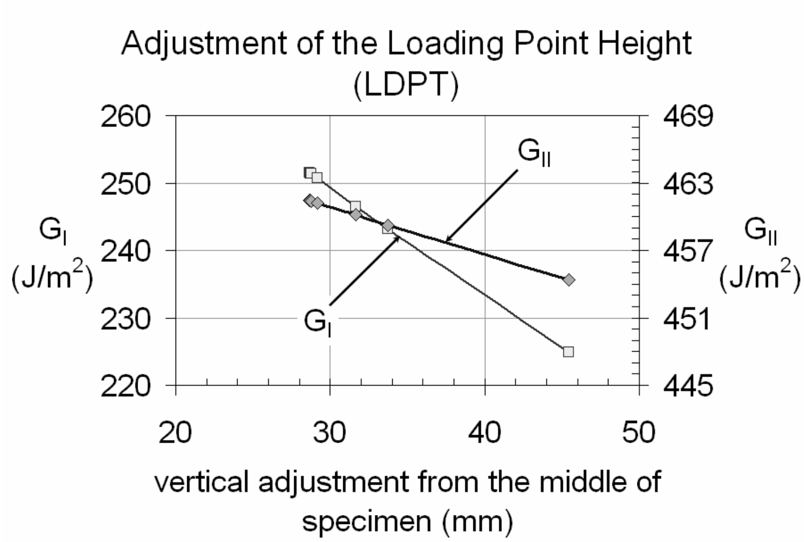

Figure 46 Optimization of Loading Lever Position, LDPT (see Figure 45)

Another improved optimization minimizes the sum squared-error of G's with respect to LDPT, g_hll, and g_cll. The rotation of the loading lever means the variable "c" shortens, and the optimization should confirm this. Results are illustrated in Table 29. A figure is not constructed instead of a table because it may confuse the reader, as the variables used are more than three; a simple surface plot would be insufficient.

This lengthy pursuit of minimizing the sum squared of error of SERR is very important, because four things can be learned:

a) The apparatus may need revisions.

b) The modeling should closely mimic the experiments.

c) The model can validate the modified beam theory.

d) Failure criteria must be correct and based on conservative numbers.

Items a) and b) should converge to the same number if more corrections are applied. Validating MBT is important for understanding its limitations in application. The failure criterion will be based on MBT values not VCCT1 values. After improving both the model and the actual experiments, some confidence can be gained about the failure criterion, because there is some error associated with it. Accuracy and precision of the experimental results will affect the failure criterion.

Table 29 Optimization results using three parameters: LDPT, g_hll, and g_cll (see Figure 45)

LDPT (mm)	g_hll (mm)	variable "c" (mm)	deflection (mm)	G_I (J/m^2)	G_{II} (J/m^2)	SSE_G
25.51	26.56	37.85	-2.294	490.2	513.1	61376
24.44	27.70	37.69	-2.738	485.8	512.3	59200
40.85	23.92	26.95	-2.436	106.6	415.7	24562
45.42	45.60	27.76	-2.708	119.6	420.8	20427
45.44	20.19	29.38	-2.238	157.3	434.1	10801
0.03	41.65	31.54	-3.430	228.8	455.4	1577.3
25.68	55.20	32.26	-3.444	269.2	466	1370.6
25.35	39.17	31.22	-2.683	236.2	457.4	1275.9
29.89	55.64	31.56	-2.673	239.3	458.3	1181.3
35.63	57.50	31.89	-2.790	240.4	458.6	1154.3
29.61	64.39	31.64	-2.739	242.4	459.1	1111.4
46.68	56.05	33.09	-2.733	260.1	463.7	1106.7
47.41	61.51	32.57	-2.699	242.7	459.2	1104.1
24.31	53.58	31.41	-2.710	243.8	459.4	1086.5
36.91	57.94	32.15	-2.706	246.5	460.2	1049.8
37.30	58.19	32.17	-2.737	246.5	460.2	1048.9
37.26	58.18	32.17	-2.733	246.7	460.2	1047.4
38.15	58.61	32.22	-2.732	246.7	460.2	1047.3
46.44	67.12	32.95	-2.733	256	462.6	1046.7
40.77	50.10	32.36	-2.734	246.8	460.3	1046.3
41.08	66.36	32.39	-2.789	247.2	460.4	1042.2
37.88	59.73	32.24	-2.775	247.6	460.5	1038.7
43.46	62.38	32.73	-2.757	254.1	462.1	1031.6
41.73	61.44	32.63	-2.762	253.6	462	1029.3
41.68	61.44	32.61	-2.765	253.3	461.9	1027.6
41.49	61.30	32.60	-2.760	253.2	461.9	1027.3
41.44	61.28	32.60	-2.759	253.1	461.9	1027
40.93	61.30	32.56	-2.760	252.7	461.8	1025.6
40.93	61.30	32.51	-2.753	251.3	461.4	1023.7
40.93	61.30	32.51	-2.753	251.3	461.4	1023.7
40.93	61.30	32.51	-2.753	251.2	461.4	1023.7

The modeling of the loading lever allows several studies to be done.

1. The height of the loading point
2. The change of variable “c” as the beam deflects.
3. The source of error has been investigated and found to be the relative position of the loading point to specimen mid-thickness.

Optimization Discussions

According to the optimization results, the variable changed by 0.6 mm, and the thickness of the loading lever g_hll, 14 mm, and the position of the loading point LDPT, 41 mm. With the lowest position of the loading point, the deflection stabilizes at 2.8 mm, approximately 25% off from the experiment.

The large discrepancy in the FEA deflection can only be explained by the fact that the modeling is in 2D, which is stiffer than 3D. The apparatus has 3D features on the loading lever, which have to be simplified in the 2D modeling. The 3D modeling is a lot more involved than 2D, therefore will be subject to further study.

Another explanation is that the MMB modeling is very simplified; many details were not included. Since some of the parts on the left side of the fulcrum are omitted, this makes the deflection less compliant; hence, the FEA deflection is smaller than the experimental. The omitted parts would have added some mass to the loading lever and made the deflection more compliant.

It is understood that there is still discrepancy between the FEA model and the experimental values. The limitation will be acknowledged as a topic of further study.

The failure criterion will be deduced from the MBT analysis, despite of the discrepancy with the numerical results.

MIXED MODE FAILURE CRITERIA

Experimental Trends

Pure mode II G_{IIc} values are much larger than pure mode I G_{Ic} values. This is related to the formation of hackle in mode II, which consumes the entire volume of matrix material between plies, compared with the relatively small plastic zone in mode I [18]. The presence of mode-II complicates simple crack propagation in mode-I, because the crack forms at 45º angles (normal to the direction of maximum tensile stress) with respect to the crack direction (the interlaminar direction), hence the hackles (Figure 26) [37]. Reeder showed the hackles using scanning electron microscopy (SEM) in his paper [24]. The mixed mode results show that the mode I component at fracture increases with increasing mode-II component at high R_G ratio. Below some R_G, the mode-I component decreases as mode-II increases (Fig. 25, 27, and 29). The maximum value of the mode-I component is near where R_G is equal to one.

Thus, the failure envelopes have two distinct parts:

1. increasing G_I with increasing G_{II}, above the critical R_G.
2. decreasing G_I with increasing G_{II}, below the critical R_G.

In the first part, a small presence of mode-II significantly increases G_I, by a factor of two or more. Mode II distorts the simple crack propagation of mode-I, by blunting the main crack, and causing much more surface formation and energy absorption. Since G_{II} does not have an apex, it is considered here as the independent variable.

In the second part, as the G_I component decreases, mode-II dominates the crack propagation. The increase of G_I as mode-II increases in the first part means that mixed mode loading can be used to toughen the material. This toughening occurs because the crack no longer grows in a self-similar mode-I fashion, with minimum surface formation and energy absorption.

Summary of Failure Criterion Search

Failure Criterion for Isophthalic Polyester

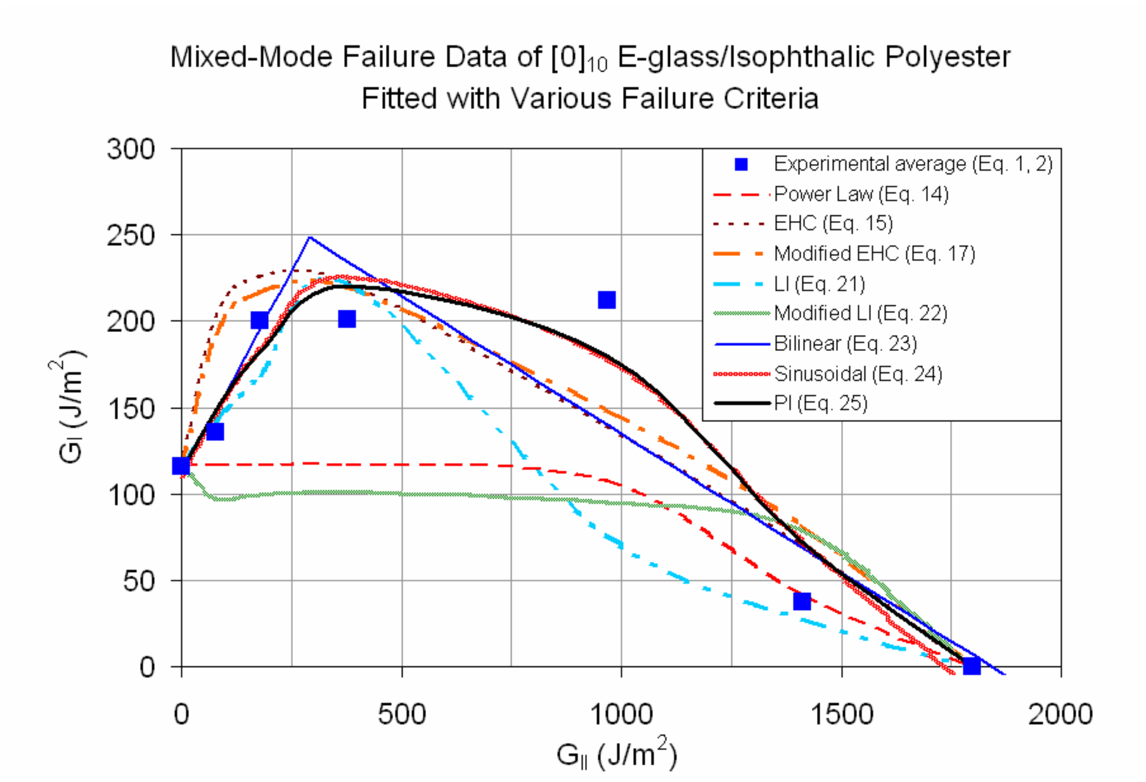

Figure 47 MMB results for isophthalic polyester matrix fitted with various failure criteria

The isophthalic polyester composite is the least tough matrix, with G_{Ic} and G_{IIc} of 116 (27) J/m^2 and 1797 (256) J/m^2, respectively. The mixed mode toughening increased the G_I component up to 212 (35) J/m^2, an 83% increase at R_G=0.219. However, if toughening is assumed to increase at R_G~1, G_I is increased up to 201 (41) J/m^2, a 73% increase. Either increase is high, compared to the pure mode-I toughness and to literature trends for carbon/epoxy prepreg [18,19].

Failure Criterion for Vinyl Ester

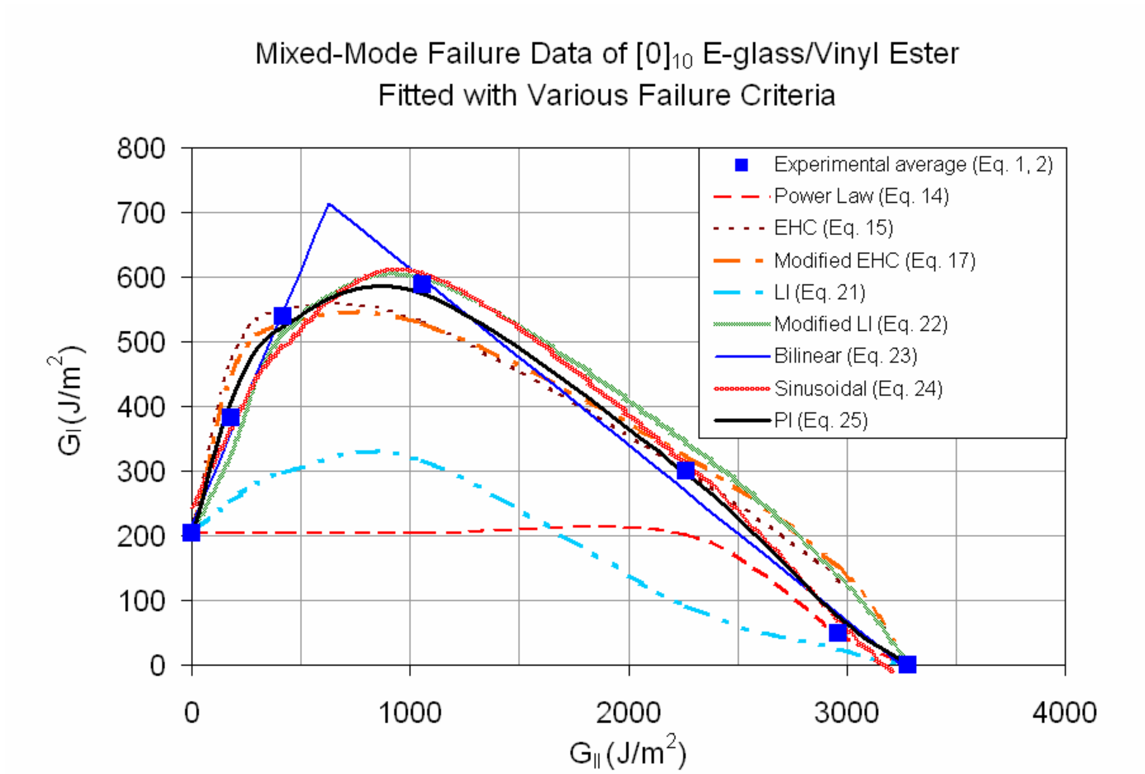

Figure 48 MMB results for vinyl ester matrix fitted with various failure criteria

The vinyl ester composite has G_{Ic} and G_{IIc} of 204 (59) J/m^2 and 3283 (86) J/m^2, respectively. Mixed mode toughening increased the G_I component by 188%, at 587 (126) J/m^2 and R_G=0.557. This toughening effect is much larger for the vinyl ester matrix than for the isophthalic polyester matrix. Vinyl ester is tougher in any mode, but it retains the same shape of curve, with a maximum at R_G=0.557. The decrease of G_I

after the maximum is rather linear and this is why the bilinear criterion is included. The only problem with the bilinear criterion is the mixed mode at R_G around 1.0, because there is no smooth transition between the linear fit for the increasing and the decreasing G_I component.

The vinyl ester resin composite is 76% percent tougher in G_{Ic} and 83% in G_{IIc} compared with the isophthalic polyester resin. The increase in toughness is evident at all R_G ratios. The increase in the G_I component is more sensitive for vinyl ester than for isophthalic polyester; the increase in G_I is steeper for vinyl ester than for isophthalic polyester. The sensitivity is evident in the bilinear criterion as indicated by the slope of the first part (R_G>1).

<u>Failure Criterion for Epoxy</u>

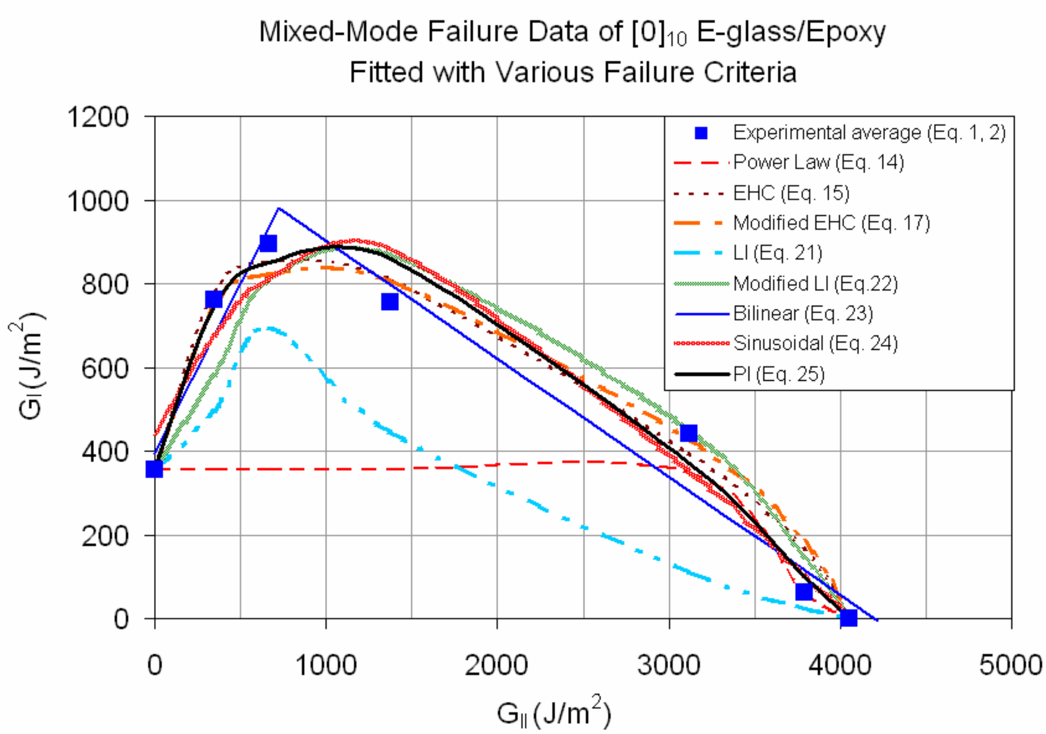

Figure 49 MMB results for epoxy matrix fitted with various failure criteria

The epoxy matrix is the toughest among all of the matrices tested, with G_{Ic} and G_{IIc} values of 356 (94) J/m^2 and 4054 (151) J/m^2, respectively. Mixed mode toughening increased the G_I component by a maximum of 151% at 895 (179) J/m^2 and R_G=1.340. The increase in the G_I component in epoxy is also the highest among the matrices.

Finally, the epoxy matrix composite is 207% tougher than isophthalic polyester composite and 75% tougher than vinyl ester composite in the G_{Ic} component, and 126% tougher than isophthalic polyester and 23% tougher than vinyl ester in the G_{IIc} component. The failure criterion fitting of epoxy is illustrated in Figure 49.

Discussion of Failure Criterion Fitting

It may seem that the quest for the best model is a mere curve fitting exercise. However, this is not the case, because the curve fit has to be optimized for the number of parameters, which is related to the meaning of the parameters—parameters should not be arbitrary but something insightful to trend, goodness of fit, and form. All models seem to fit the experimental data pretty well. Some models are less conservative than others, but may have very meaningful parameters. Discussion of each model follows.

The best criterion is explicit and has sufficient parameters to describe the relationship between G_I and G_{II}. Too few parameters will deem the model too simplified, hence, reducing the flexibility of the model to include any nonlinear behavior. To determine the critical load using the failure criterion, two variables are required for implicit models and for explicit models one is required, G_{II} or R_G. The goodness of fit of the model is based on the R^2 value.

Table 30 Summary of fitting various failure criteria

	Isophthalic Polyester		Vinyl Ester		Epoxy	
Failure Criterion	Constants	R^2	Constants	R^2	Constants	R^2
Power Law (Eq. 14)	m= 0.171 n= 7.639	0.498	0.136 16.746	0.385	0.141 22.626	0.418
Exponential Hackle (Eq. 15)	γ= 0.313	0.786	0.488	0.936	0.631	0.974
Modified Exponential Hackle (Eq. 17)	γ_m= 0.521	0.803	0.814	0.929	1.062	0.963
Linear Interaction (Eq. 21)	κ= -1.024 φ= 7.942	0.670	-0.826 7.178	0.524	-0.874 6.558	0.657
Quartic Interaction (Modified Linear Interaction) (Eq. 22)	κ_m= 0.509 φ_m= 1.653	0.384	0.432 1.805	0.950	0.402 1.635	0.912
Bilinear (Eq. 23)	ξ= 0.478 ζ= -0.160	0.951 0.797	0.791 -0.272	0.986 0.990	0.813 -0.282	0.937 0.932
Sinusoidal (Eq. 24)	α= 2.022 β= 0.503 χ= 4.644	0.915	2.989 0.516 4.609	0.980	2.506 0.484 4.773	0.936
Power Interaction (Eq. 25)	δ= 0.091 ε= 0.863 ϕ= 1.567	0.933	0.014 0.492 1.316	0.994	0.012 0.388 1.093	0.974

For the isophthalic polyester composite, the highest R^2 is achieved by two criteria: the power interaction and the increasing part of the bilinear criterion, at 0.933 and 0.951, respectively. Even though the bilinear criterion achieved a higher R^2, it is problematic at predicting the toughness at R_G~1. The best criterion is then the power interaction criterion.

The most unsuitable criteria are the quartic interaction criterion and the power law, at R^2 of 0.384 and 0.498, respectively. The other implicit criteria do not fit the data well, with R^2 around 0.7. The sine is the best fit next to the bilinear criterion at R^2=0.915.

For the vinyl ester composite, the power interaction and the bilinear criterion yielded excellent curve fits, at R^2 of 0.994, and 0.986 for the increasing and 0.990 for the decreasing part of the bilinear criterion, respectively. The other implicit criterion fitted the data quite well, at R^2 around 0.9: the exponential hackle, the modified exponential hackle. The unfit models are the power law and the linear interaction criterion with R^2 of 0.385 and 0.524, respectively.

For the epoxy composite, all but the power law (R^2=0.481) and the linear interaction criteria (R^2=0.657) fit the data well, with R^2 of around 0.9. The best fits are the power interaction and the exponential hackle criteria, both with R^2 of 0.974.

CONCLUSIONS AND RECOMMENDATIONS

Application of Mixed Mode Results for the Wind Turbine Blade Design

The availability of mixed mode results can improve the design of wind turbine blades in two ways: (1) through using a tough resin such as epoxy, which performed well in our test, and (2) through improved designs based on finite element delamination analysis with an improved delamination failure criterion. Additionally, designing a structural detail to include a mode II component where mode I is dominant should improve the delamination resistance.

Experimental Methods Validation

The MMB test method is superior for determining the mixed mode G-values; the mathematics seems to be simple and easily applicable to a known geometry. In the actual experiment, however, there are many variables in the loading lever that needed to be optimized. Another complication seems to arise from the loading lever that creates an extra load (because of gravity). Reeder has tried to account for the loading lever in an analysis that requires the relationship between the center of gravity of the loading lever and the variable “c”. Measuring “c” is easy with the current apparatus, but finding the center of gravity would be very difficult. Furthermore, the constant weight of the loading lever adds one more load to the applied load by the machine, which is always increasing.

The weight of the loading lever might be insignificant in the testing of carbon fiber, because the modulus of carbon is high. However, for the fiberglass application, MMB may require more correction for the weight of the loading lever.

Since G-values of interest focus on the initial crack, other mixed mode fracture test methods such as fixed-ratio mixed mode, FRMM [21], should be reviewed, because it is a simple fracture test that is essentially unaffected by gravity.

One of the important requirements of the MMB test is the need to maintain a constant G-ratio during the test. This implies that the crack cannot extend very far during the test. Therefore, if the crack is extends, a constant G-ratio during the test is not possible. If only initial crack growth is of interest, as in this study, then this problem does not occur.

Experimental, MBT, and FEA Values

In the DCB and ENF modeling of all resin systems, the SERR from MBT and VCCT1 always agree, but the experimental deflections do not always agree, because deflections are more sensitive to crack length variation (crack length to the cubic power) than the SERR (critical load and crack length to second power).

In the MMB modeling, there were too many details to model, which means the test is not practical for modeling, unless if it were done in 3D, because of the various dimensions. The discrepancy in the deflections is inherited in the geometry of the loading lever.

Nonetheless, the deflection is a good verification of the material properties as well as the measured dimensions. The obvious dimensions, i.e., thickness, length, width, can be measured with great accuracy. The crack length is more challenging because it is only measured from the edges; hence, the crack length is taken as the average between the two edges.

Using MBT and VCCT for Other Geometries, i.e. Ply Drops

The use of MBT is, unfortunately, not available for ply drops. There is no distinct crack length, and, even if crack were to exist, only stable cracks can be measured [67,68], while unstable cracks would propagate at an instantaneous rate. However, if the crack is stable, only the FEA model can be used to calculate the SERR, and MBT will greatly oversimplify the case.

Resin Response under Mixed Mode Conditions

All the resins responded with increased G_I component at fracture under the mixed mode conditions; the epoxy resin produced the toughest material, isophthalic polyester the least tough, and vinyl ester in the middle. Epoxy gave the greatest increase in G_I component with a 151% increase over the pure G_{Ic} value.

The Failure Criterion

The conventional mixed mode criterion (Eq. 14) is incapable of accounting the increase of G_I component at fracture due to G_{II}. Several models have been fitted to the data; explicit models with the least parameters are desired. The model behavior is related to the number of parameters. More parameters in models will increase the flexibility of the models in fitting the experimental data. The number of parameters dictates how the model would behave.

The mixed mode response is nonlinear, implying it cannot be represented by a simple linear model, unless if responses are separated into two parts like the bilinear criterion, $R_G<1$ and $R_G>1$.

If attempting to include all variables as parameters, then the model would be implicit with respect to G_I, meaning G_I cannot be explicitly expressed as a function of G_{II}. Implicit forms are more cumbersome to work with than explicit, because implicit forms require two iterative calculations.

The most intuitive step is to fit the response using an explicit model, $G_I=f(G_{II})$; as a result, R_G and G_T cannot be included. Explicit or implicit, a model must maintain a minimum number of parameters for simplicity, yet retain accuracy. As a conclusion, the most desirable model has to have a minimum number of parameters and an explicit form. The power interaction criterion is the best fit for the data, hence, the best failure criterion. The power interaction can be programmed in the FEA model to predict the critical load based on the G_{Ic} and G_{IIc} values for the material.

For relatively brittle resins such as the ones under consideration here, there is a difference in the fracture surface with respect to the mode of loading. The plastic zone is much smaller than the resin rich area. However, in tough resin such as PEEK (a thermoplastic), the plastic zone (in the neat resin) is much larger, so yielding completely consumes the resin rich area. Hence, there is no distinction in the fracture surface with respect to the loading condition. If this were the case, the failure criterion would be simple, such as a linear relation[3] (Eq. 14).

Future work

This research has triggered some more questions about mixed mode fractures. All data were reduced using the 5%-slope-offset method, which is adopted from the metal industry. For composites, the scatter might be reduced if the slope-offset is reduced to 2%.

The resin rich area at the edge of the nylon film is the origin for crack propagation. The thickness of Nylon film may have an effect on the G-values. This should be the subject to further study.

Most material properties are easy to determine, i.e. E_{11} and E_{22}, however, others such as G_{23} and ν_{23} are not. Sensitivity analysis must be done to see how much these material properties affect G-values, especially those values that are not easily measured, i.e., G_{23} and ν_{23}.

The MMB test is cumbersome for fatigue and must be modified to the point where the weight of the loading lever is negligible to the SERR calculations.

---

[3] This is not to be confused with the Linear Interaction Criterion.

SERR prediction for complex structure is certainly possible using the VCCT method in FEA. The most crucial detail in calculating the SERR is the rotation of the material properties where the composite geometry is rotated. VCCT is available in both 2D and 3D elements with midside nodes. The only experimental requirement is the introduction of an artificial crack at the stress concentration, in ply drops for example. This would mean that the artificial crack has to be introduced at the tip of the resin rich area in the ply drop geometry.

REFERENCES

1. Mandell, J. F., and Samborsky, D. D., "DOE/MSU Composite Material Fatigue Database: Test Methods, Materials, and Analysis," Contractor Report, SAND97-3002, December 1997.

2. Mandell, J. F., Samborsky, D. D., and Cairns, D. S., "Fatigue of Composite Materials and Substructures for Wind Turbine Blades," Sand Report SAND2002-0771, March 2002.

3. California Energy Markets, May 17, 1996, p. 12

4. Kam, C. Y. and Walker, J. V., "Toughened Composites Selection Criteria," Toughened Composites, ASTM STP 937, Norman J. Johnston, Ed., American Society for Testing and Materials, Philadelphia, 1987, pp. 9-22.

5. Haugen, D. J., "Fracture of Skin-Stiffener Intersections in Composite Wind Turbine Blade Structures," Master's Thesis in Mechanical Engineering, Montana State University—Bozeman, Bozeman, MT, August 1998.

6. Morehead, R. B., III, "Fatigue of Skin-Stiffener Intersections in Composite Wind Turbine Blade Structures," Master's Thesis in Mechanical Engineering, Montana State University—Bozeman, Bozeman, MT, July 2000.

7. "Standard Test Method for Mixed Mode-I-Mode-II Interlaminar Fracture Toughness of Unidirectional Fiber Reinforced Polymer Matrix Composites, D6671-01," Annual Book of ASTM Standards 2001, Vol. 15.3, ASTM International, 2001, pp. 392-403.

8. Rybicki, E. F and M. F. Kanninen, "A Finite Element Calculation of Stress Intensity Factors by a Modified Crack Closure Integral," Eng. Fracture Mechanics, Vol. 9, 1977, pp. 931-938.

9. Raju, I. S., "Simple Formulas for Strain-Energy Release Rates with Higher Order and Singular Finite Elements," NASA Contractor Report 178186, December 1986.

10. Raju, I. S.,"Calculation of Strain-Energy Release Rates with Higher Order and Singular Finite Elements," Engineering Fracture Mechanics, Vol. 28, No. 3, 1987, pp. 251-274.

11. Wang, J. T., and Raju, I. S., "Strain Energy Release Rate Formulae for Skin-Stiffener Debond Modeled with Plate Elements," Engineering Fracture Mechanics, Vol. 54, No. 2, 1996, pp. 211-228.

12. Broek, D., "Elementary Engineering Fracture Mechanics," 4th Ed., Kluwer Academic Publishers, 1986.

13. J. R. Rice, “A Path-Independent Integral and the Approximate Analysis of Strain Concentrations by Notches and Cracks,” Journal of Applied Mechanics, 35, 1968, pp. 379-386.

14. “Standard Test Method for Plane-Strain Fracture Toughness to Interlaminar Fracture Toughness, E399-90,” 1996 Annual Book of ASTM Standards, Vol. 3.01, 1996, pp. 407-437.

15. Barbero, Ever J., “Introduction to Composite Materials Design,” Taylor & Francis, Philadelphia, PA, 1999.

16. Timoshenko, S. P., and Gere, S. M., “Strength of Materials,” Brooks and Cole, 4th ed., October 1996.

17. Mandell, J. F., Cairns, D. S., Samborsky, D. D., Morehead, R. B., and Haugen, D. H., “Prediction of Delamination in Wind Turbine Blade Structural Details,” 2003 ASME Wind Energy Symposium, ASME/AIAA, AIAA-2003-0697, 2003, pp. 202-213.

18. Crews, J. H., Jr., and Reeder, J. R., “A Mixed Mode Bending Apparatus for Delamination Testing,” NASA TM-100662, August 1988.

19. Reeder, J. R., and Crews, J. H., Jr., “The Mixed Mode Bending Method for Delamination Testing,” AIAA Journal, Vol. 28, No. 7, July 1990, pp. 1270-1276.

20. Reeder, J. R., and Crews, J. H., Jr., “Nonlinear Analysis and Redesign of the Mixed Mode Bending Delamination Test,” NASA TM-102777, January 1991.

21. Hashemi, S., Kinloch, A. J., and Williams, G., “Mixed Mode Fracture in Fiber-Polymer Composite Laminates,” Composite Materials: Fatigue and Fracture (Third Volume), ASTM STP 1110, T. K. O’Brien, Ed., American Society for Testing and Materials, Philadelphia, 1991, pp. 143-168.

22. Reeder, J. R., and Crews, J. H., Jr., “Redesign of the Mixed Mode Bending Delamination Test to Reduce Nonlinear Effects,” Journal of Composites Technology & Research, JCTRER, Vol. 14, No. 1, Spring 1992, pp. 12-19.

23. Reeder, J. R., “An Evaluation of Mixed Mode Delamination Failure Criteria,” NASA TM-104210, February 1992.

24. Reeder, J. R., “A Bilinear Failure Criterion for Mixed Mode Delamination,” Composite Materials: Testing and Design (Eleventh Volume), ASTM STP 1206, E. T. Camponeschi, Jr., American Society for Testing and Materials, Philadelphia, 1993, pp. 303-322.

25. Benzeggagh, M. L., and Kenane, M., “Measurement of Mixed Mode Delamination Fracture Toughness of Unidirectional Glass/Epoxy Composites with Mixed Mode Bending Apparatus,” Composites Science and Technology, 56, 1996, pp. 439-449.

26. Ducept, F., Davies, P., and Gamby, D., “An Experimental Study to Validate Tests used to Determine Mixed Mode Failure Criteria of Glass/Epoxy Composites,” Composites Part A, 28A, 1997, pp. 719-729.

27. Bhashyam, S., and Davidson, B. D., “Evaluation of Data Reduction Methods for the Mixed Mode Bending Test,” AIAA Journal, Vol. 35, No. 3, March 1997, pp. 546-552.

28. Martin, R. H., and Hansen, P. L., “Experimental Compliance Calibration for the Mixed Mode Bending (MMB) Specimen,” Composite Materials: Fatigue and Fracture (Sixth Volume), ASTM STP 1285, E. A. Armanios, Ed., American Society for Testing and Materials, 1997, pp. 305-323.

29. Shivakumar, K. N., Crews, J. H., Jr., and Avva, V. S., “Modified Mixed Mode Bending Test Apparatus for Measuring Delamination Fracture Toughness of Laminated Composites,” Journal of Composite Materials, Vol. 32, No. 9, 1998, pp. 804-828.

30. Reeder, J. R., “Refinements to the Mixed Mode Bending Test for Delamination Toughness,” Proceedings of The American Society for Composites-Fifteenth Technical Conference, College Station, TX, 2000.

31. Reeder, J. R., “A Criterion to Control Nonlinear Error in the Mixed Mode Bending Test,” Composite Materials: Testing and Design Fourteenth Volume, ASTM STP 1436, C. E. Bakis, Ed., ASTM International, West Conshohocken, PA, 2003.

32. Russell, A. J. and Street, K. N., “Moisture and Temperature Effects on the Mixed Mode Delamination Fracture of Unidirectional Graphite/Epoxy,” Delamination and Debonding of Materials, ASTM STP 876, W. S. Johnson, Ed., American Society for Testing and Materials, Philadelphia, 1985, pp. 349-370.

33. “Standard Test Method for Mode I Interlaminar Fracture Toughness of Unidirectional Fiber-Reinforced Polymer Matrix Composites, D5528-94a,” Annual Book of ASTM Standards 1997, Vol. 15.03, 1997, pp. 271-279.

34. Gillespie, J. W., Jr., Carlsson, L. A., and Pipes, R. B., ”Finite Element Analysis of the End-Notched Flexure Specimen for Measuring Mode-II Fracture Toughness,” Composites Science and Technology, Vol. 27, 1986, pp. 177-197.

35. Carlsson, L. A., and Gillespie, J. W., and Pipes, R. B., “On the Analysis and Design of the End Notched Flexure (ENF) Specimen for Mode II Testing,” Journal of Composite Materials, Vol. 20, November 1986, pp. 594-604.

36. Carlsson, L. A., and Gillespie, J. W., Jr., “Chapter 4 Mode-II Interlaminar Fracture of Composites,” Application of Fracture Mechanics to Composite Materials, K. Friederich, 1989, pp. 113-157.

37. Carleto, C. R., and Bradley, W. L., “Mode II Delamination Fracture Toughness of Unidirectional Graphite/Epoxy Composites,” Composite Materials, Fatigue and Fracture, Second Volume, ASTM STP 1012, Paul A. Lagace, Ed., American Society for Testing and Materials, Philadelphia, 1989, pp. 201-221.

38. Russell, A. J., “Initiation and Growth of Mode II Delamination in Toughened Composites,” Composite Materials: Fatigue and Fracture (Third Volume), ASTM STP 1110, T. K. O’Brien, Ed., American Society for Testing and Materials, Philadelphia, 1991, pp. 226-242.

39. Cairns, D. S., “Static and Dynamic Mode-II Strain Energy Release Rates in Toughened Thermosetting Composite Laminates,” Journal of Composite Technology & Research, JCTRER, Vol. 14, No. 1, Spring 1992, pp. 37-42.

40. Williams, J. G., “On the Calculation of Energy Release Rates for Cracked Laminates,” International Journal of Fracture, 36, 1988, pp. 101-119.

41. Davies, P., and Benzeggagh, M. L., “Part IIA. Interlaminar Fracture Studies, Chapter 3, Interlaminar Mode-I Fracture Testing,” Application of Fracture Mechanics to Composite Materials, K. Friedrich, Ed., 1989, pp. 81-112.

42. “Failure Analysis of Industrial Composite Materials,” E. E. Gdoutos, K. Pilakoutas, C. A. Rodopoulos, Ed.’s, McGraw-Hill, New York, 2000, pp. 147-226.

43. “Failure Analysis of Industrial Composite Materials,” E. E. Gdoutos, K. Pilakoutas, C. A. Rodopoulos, Ed.’s, McGraw-Hill, New York, 2000, pp. 109-126.

44. Cairns, D. S., Mandell, J. F., Scott, M. E., Maccagnano, J. Z., "Design Considerations for Ply Drops in Composite Wind Turbine Blades," 1997 ASME Wind Energy Symposium, ASME/AIAA, AIAA-97-0953, 1997, pp. 197 – 208.

45. Timoshenko, S., “Strength of Materials: Part I Elementary Theory and Problems,” 3rd Ed., New York, 1963, pp. 170-175.

46. Timoshenko, S., “Strength of Materials: Part I Elementary Theory and Problems,” 3rd Ed., New York, 1963, pp. 316-320.

47. Kanninen, M. F., "An Augmented Double Cantilever Beam Model for Studying Crack Propagation and Arrest," International Journal of Fracture, Vol. 9, No. 1, March 1973, pp. 83-92.

48. Williams, J. G., "Chapter 1. Fracture Mechanics of Anisotropic Materials," Application of Fracture Mechanics to Composite Materials, K. Friedrich, Ed., Elsevier Science, 1989, pp. 3-38.

49. Williams, J. G., "End Corrections for Orthotropic DCB Specimens," Composite Science and Technology, 35, 1989, pp. 367-376.

50. Hashemi, S., Kinloch, A. J., Williams, J. G., "The Effect of Geometry, Rate and Temperature on the Mode-I, Mode-II and Mixed Mode I/II Interlaminar Fracture of Carbon-Fibre/Poly(ether-ether ketone) Composite," Journal of Composite Materials, Vol. 24, September 1990, pp. 918-957.

51. Hashemi, S., Kinloch, A. J., and Williams, J. G., "Mechanics and Mechanism of Delamination in a Poly(ether Sulphone)-Fibre Composite," Composites Science and Technology, 37, 1990, pp. 429-462.

52. Wang, Y., and Williams, J. G., "Corrections for Mode-II Fracture Toughness Specimens of Composite Materials," Composite Science and Technology, 43, 1992, pp. 251-256.

53. Kinloch, A. J., Wang, Y., Williams, J. G., and Yayla, P., "The Mixed Mode Delamination of Fibre Composite Materials," Composite Science and Technology, 47, 1993, pp. 225-237.

54. Riddle, R. A., "The Application of the J Integral to Fracture in Mixed Mode Loading," PhD Thesis, Lawrence Livermore National Laboratory, June 1981.

55. Bathe, Klaus-Jürgen, "Finite Element Procedures," Prentice Hall, Upper Saddle River, New Jersey, 1996.

56. Huebner, K. H., Thorton E. A., and Byrom, T. G., "The Finite Element Method for Engineers," 3rd Ed., John Wiley & Sons, 1995.

57. Burnett, D. S., "Finite Element Analysis: from Concepts to Applications," Addison-Wesley Publishing Company, Reading, MA, 1987.

58. Naik, R. A., Crews, J. H., Jr., and Shivakumar, K. N., "Effect of T-tabs and Large Deflections in Double Cantilever Beam Specimen Tests," Composite Materials: Fatigue and Fracture (Third Volume), ASTM STP 1110, T. K. O'Brien, Ed., American Society for Testing and Materials, Philadelphia, 1991, pp. 169-186.

59. "Standard Test Method for Ignition Loss of Cured Reinforced Resins, D2584," ASTM Standards.

60. http://www1.ansys.com/customer/content/documentation/70/Hlp_E_PLANE82.html, "Part I. Element Library," ANSYS Element Reference.

61. http://www1.ansys.com/customer/content/documentation/70/Hlp_C_LESIZE.html, "LESIZE," ANSYS Commands Reference.

62. http://www1.ansys.com/customer/content/documentation/70/Hlp_C_KREFINE.html, "KREFINE," ANSYS Commands Reference.

63. http://www1.ansys.com/customer/content/documentation/70/Hlp_G_STR9.html, "Chapter 9. Contact," ANSYS Structural Analysis Guide.

64. ANSYS Theory Reference, Chapter 2.4. Combined Stresses and Strains.

65. ANSYS Structural Guide, Chapter 10.4. Performing a Surface-to-Surface Contact Analysis

66. ANSYS Advanced Guide, Chapter 1. Design Optimization

67. Scott, M. E., "Effects of Ply Drops on The Fatigue Resistance of Composite Materials and Structures," Master's Thesis in Chemical Engineering, Montana State University—Bozeman, Bozeman, MT, August 1997.

68. Cairns, D. S., Mandell, J. F., Scott, M. E., Maccagnano, J. Z., "Design Considerations for Ply Drops in Composite Wind Turbine Blades," 1997 ASME Wind Energy Symposium, ASME/AIAA, AIAA-97-0953, 1997, pp. 197 – 208.

APPENDICES

APPENDIX A: LABORATORY PROCEDURE FOR INSTRON MACHINE

1. Turn on slowly the power switch, which is located left-hand side, behind the INSTRON machine and let machine warm-up for one hour.
2. Simultaneously, turn on Data Acquisition Unit and then open the HP data logger, open existing setup, *MMB_Miles*, push F5 to start downloading.
3. Make sure there is tension in hydraulic ramp cross cylinders.
4. Loosen the bolts using the wrench one side at a time.
5. Remove grips and check the size limits. If size is already correct, then reposition the grips.
6. IF using 500-lb load cell: IF NOT then go to 9)
7. Pump the crosshead so the load cell can be placed on the grip
8. Tighten the upper grip using the grip controller (final grip pressure ~2000 psi)
9. Remove lower grip and replace with ½' grip.
10. Put the test fixture on the grip (make sure the lower grip control is on **CLAMP**, and the higher grip control is on **HOLD**). IF using a flat plate for the apparatus to sit on, make sure the welding joint is out of the way by placing metal spacers between stiffeners and grip body.
11. Calibrate the load cell. Make sure that all system/cable is connected. Make sure actuator is **OFF** and control panel is in **POSITION** mode.
12. Calibrate each mode **STRAIN**, **LOAD**, and **POSITION**. (for **LOAD**, calibration is required whenever the load cell is changed). Calibration is deemed necessary when the calibration LED is blinking. Push Setup and followed by **AUTO**.

13. If in **POSITION** mode, make sure that **nothing** is clamped in the grips and the set position to zero. (**POSITION—ACTUATOR ON—GOTO 0 in**.)
14. Lower the upper-grip by releasing pressure until close enough to the test.
15. Calibrate the load to get closer to zero. **LOAD CALIBRATION—BALANCE** (must be turned on first). **LED** “calibrated” will stop blinking once zeroing is done.
16. **IMPORTANT**: Set the **MAXIMUM/MINIMUM LIMITS** on LOAD and **POSITION**. The **MAX/MIN LIMITS LED** will light up once the limits have been set.
17. Load Limit

Type of Load Cell	Max	Min
2.22 kN	2 kN	-2 kN
100 kN	5 kN	-5 kN

18. Tighten the crosshead bolts.
19. Move the load nose closer to the test apparatus using the micro movement until there is a small load showing on the control panel.
20. Use **Function/Unit/Time** to check or change the units.
21. Record the initial position.
22. Use **WAVEFORM** to control displacement and displacement rate.
23. S-Ramp-single ramp
24. Compression in inches must be “**-1**”. In mechanical testing, “+” means tension, even if the hydraulic wedge-grip moves downward.
25. Compression rate in **in/min** is 0.05.

26. Set Display #1 to **LOAD**, and Display #2 to **POSITION** by hitting the button **OUTPUT**.

27. Check the **OUTPUT** of **CONTROL PANEL** to the desired quantity.

digital	A	B
lines	LOAD	POSITION

28. Download the channel from Data Logger.

APPENDIX B: DESIGN OF MMB APPARATUS

The Clevis

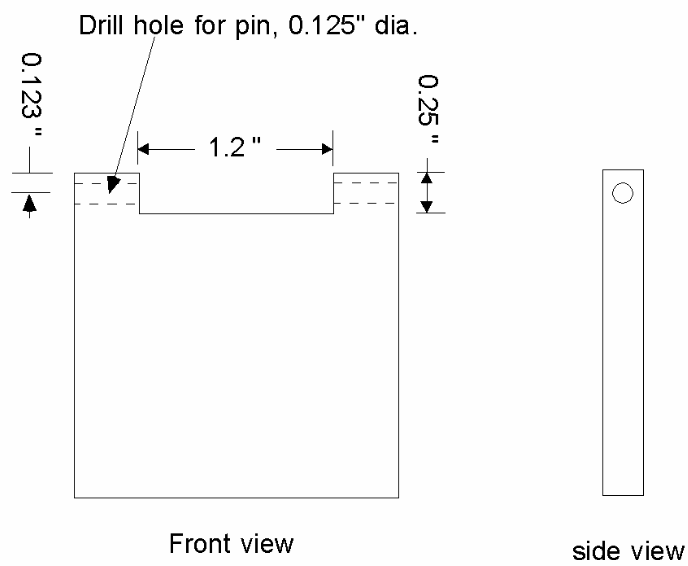

The Clevis Adapter

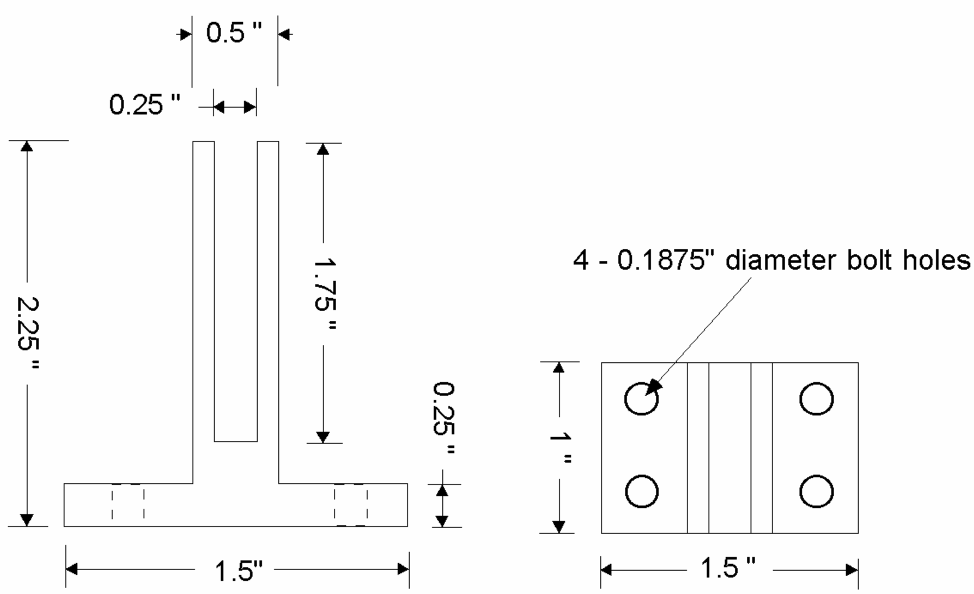

Need two clamping fixtures (clevis)

Also need two 2" x 2" x 0.25" bar stock to stick into clevis

The Saddle

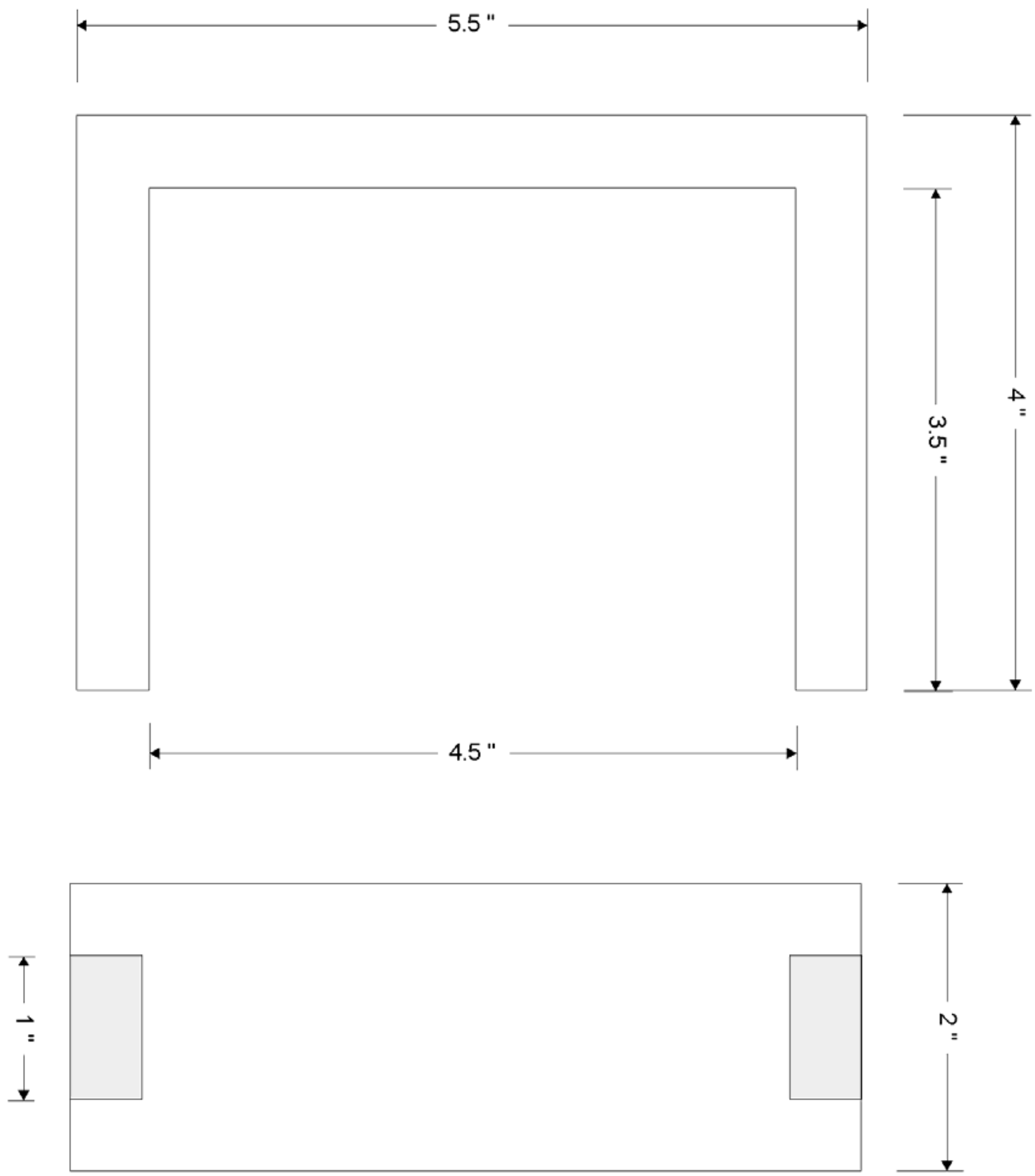

Materials (aluminum) - 5.5" x 2" x 0.5" (1 piece)
- 3.5" x 1" x 0.5" (two pieces)

The Yoke

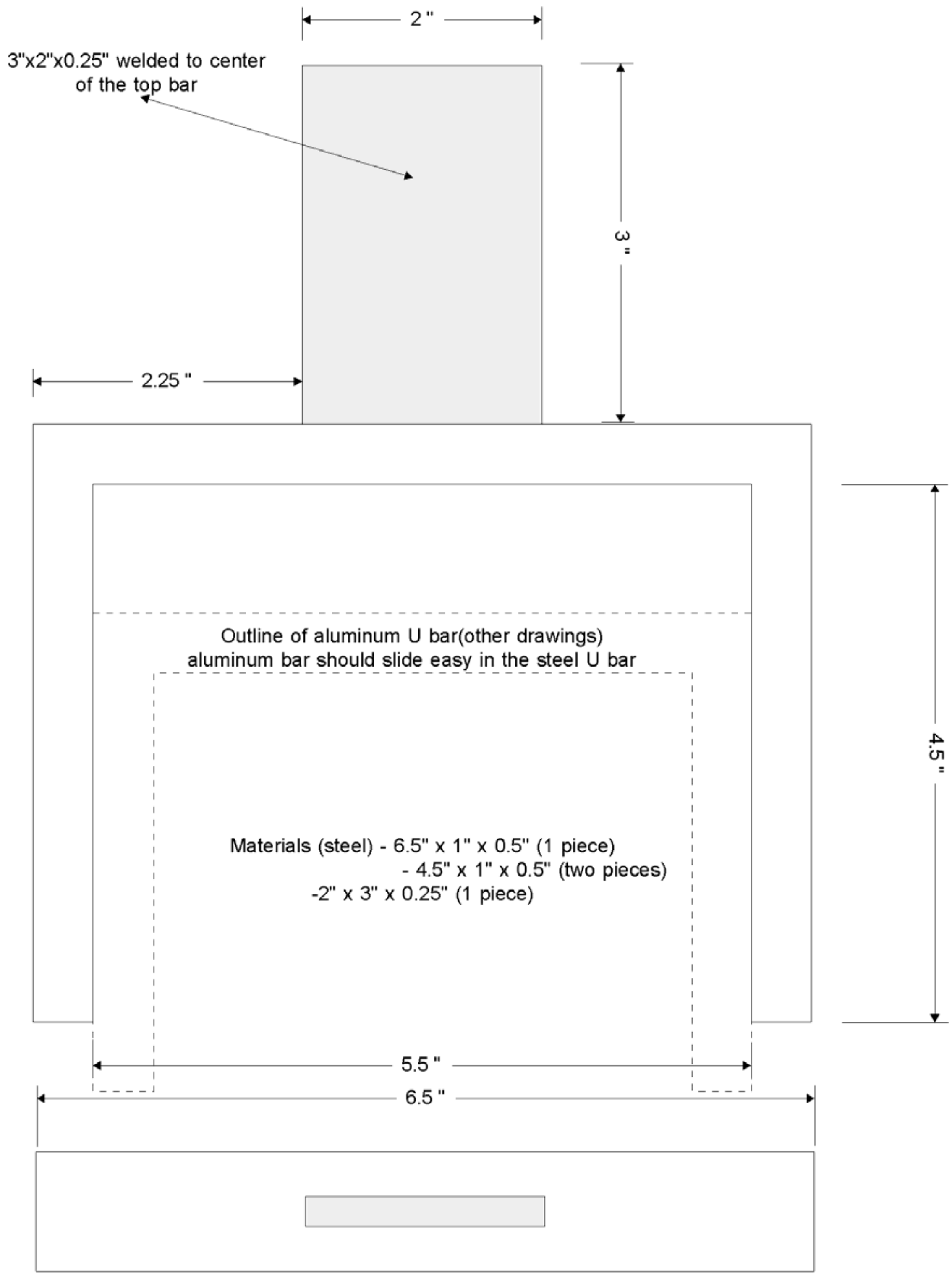
2 "
3"x2"x0.25" welded to center
of the top bar
3 "
2.25 "
4.5 "
Outline of aluminum U bar(other drawings)
aluminum bar should slide easy in the steel U bar
Materials (steel) - 6.5" x 1" x 0.5" (1 piece)
- 4.5" x 1" x 0.5" (two pieces)
-2" x 3" x 0.25" (1 piece)
5.5 "
6.5 "

The Fulcrum

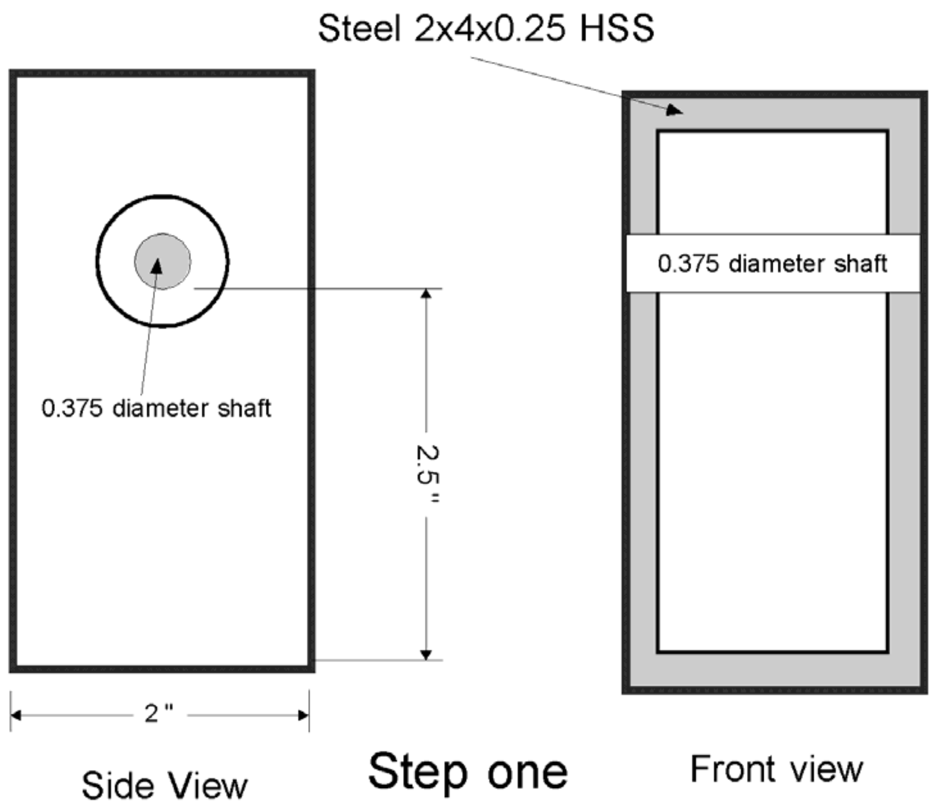
Steel 2x4x0.25 HSS
0.375 diameter shaft
0.375 diameter shaft
2.5 "
2 "
Side View
Step one
Front view

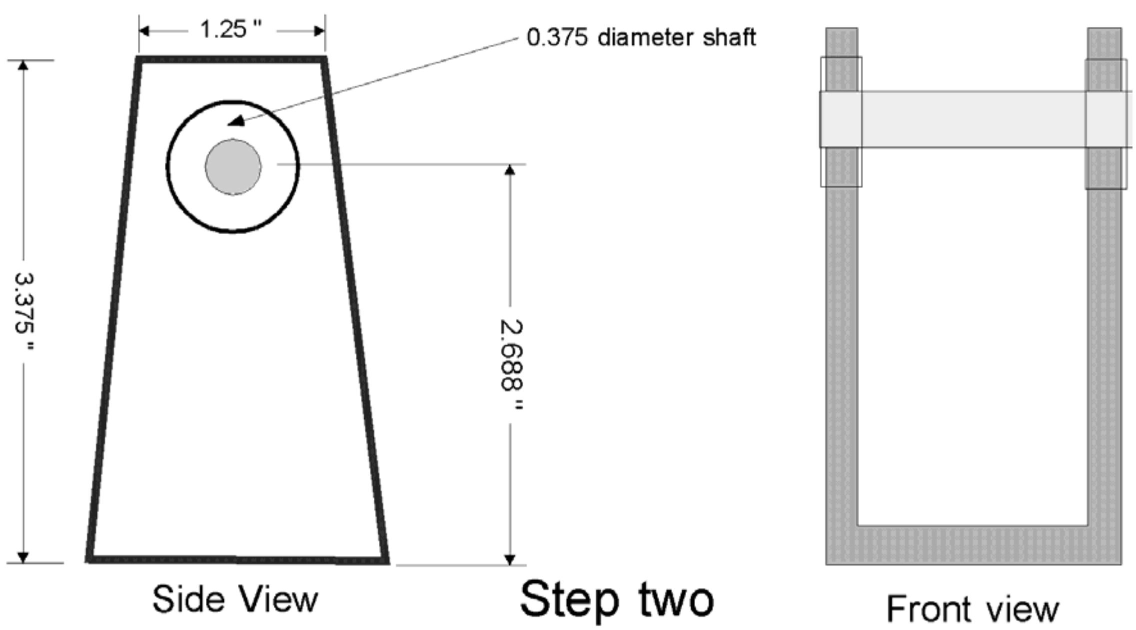
1.25 "
0.375 diameter shaft
3.375 "
2.688 "
Side View
Step two
Front view

APPENDIX C: EXPERIMENTAL RESULTS

Isophthalic Polyester (all data)

h (m)	half-thickness
b (m)	width
λ (m^{-1})	elastic foundation correction
t (m)	Tab height (from arm midpoint to tab hole's midpoint)
L' (m)	Tab length into the crack from tab hole's midpoint
precracking	type of precracking
da_0 (cm)	crack extension from tip of Nylon strip
a_0 (cm)	initial crack length after or at precrack
a_r (cm)	crack arrest
da (cm)	crack extension from a_0 to a_r
P_c (N)	critical load
G_I (J/m^2)	mode-I SERR
G_{II} (J/m^2)	mode-II SERR
R_G	ratio of G_I to G_{II}

Isophthalic Polyester (all data)

specimen	h (m)	b (m)	λ (m^{-1})	t (m)	L' (m)	precracking	da_0 (cm)	a_0 (cm)	a_r (cm)	da (cm)	P_c (N)	G_I (J/m^2)	G_{II} (J/m^2)	R_G
Double Cantilever Beam														
DCB01	3.06E-03	2.53E-02	368.0	5.00E-03	4.76E-03	mode I	0.347	3.043	3.306	0.263	91.12	216	0	
DCB02	3.07E-03	2.49E-02	366.8	4.44E-03	5.23E-03	mode I	0.322	2.940	3.220	0.280	88.16	195	0	
DCB03	3.05E-03	2.53E-02	368.6	4.67E-03	5.16E-03	mode I	0.369	2.779	3.265	0.486	96.82	208	0	
DCB04	3.00E-03	2.54E-02	374.8	5.14E-03	5.26E-03	mode I	0.439	2.871	3.360	0.489	108.97	291	0	
DCB05	2.93E-03	2.49E-02	383.7	5.09E-03	5.21E-03	mode I	0.509	3.084	3.509	0.425	101.62	320	0	
MMB04p2	2.90E-03	2.53E-02	387.7	4.49E-03	5.60E-03	mode I	0.190	2.475	2.921	0.446	79.78	132	0	
MMB05p2	3.29E-03	2.49E-02	342.2	5.35E-03	5.86E-03	mode I	0.175	3.278	3.483	0.205	85.84	186	0	
MMB07p2	3.08E-03	2.49E-02	365.6	5.72E-03	5.77E-03	mode I	0.242	2.806	3.239	0.433	101.39	235	0	
MMB08p2	2.93E-03	2.48E-02	384.4	5.39E-03	5.27E-03	mode I	0.121	2.586	3.014	0.429	95.66	209	0	
MMB11p2	3.10E-03	2.49E-02	363.3	4.49E-03	5.60E-03	mode I	0.125	2.770	3.147	0.378	88.21	171	0	
MMB12p2	3.27E-03	2.50E-02	343.8	5.39E-03	5.27E-03	mode I	0.335	3.934	4.328	0.394	65.72	153	0	
											avg	211		
											std	56		
MODE-I PRECRACK														
DCB01p	3.06E-03	2.53E-02	368.0	5.00E-03	4.76E-03	no	0	2.696	3.043	0.347	79.03	130	0	
DCB02p	3.07E-03	2.49E-02	366.8	4.44E-03	5.23E-03	no	0	2.618	2.940	0.322	82.56	139	0	
DCB03p	3.05E-03	2.53E-02	368.6	4.67E-03	5.16E-03	no	0	2.410	2.779	0.369	68.92	82	0	
DCB04p	3.00E-03	2.54E-02	374.8	5.14E-03	5.26E-03	no	0	2.432	2.871	0.439	87.62	140	0	
DCB05p	2.93E-03	2.49E-02	383.7	5.09E-03	5.21E-03	no	0	2.575	3.084	0.509	62.92	88	0	
ENF01p	3.24E-03	2.49E-02	347.5	4.14E-03	7.68E-03	no	0	3.492	4.069	0.578	58.71	101	0	
ENF02p	3.17E-03	2.52E-02	354.7	5.07E-03	7.84E-03	no	0	2.651	2.874	0.223	70.94	93	0	
ENF03p	3.02E-03	2.49E-02	372.3	4.11E-02	8.30E-03	no	0	3.373	3.782	0.410	55.91	105	0	
ENF04p	3.16E-03	2.49E-02	355.8	5.05E-03	8.31E-03	no	0	2.604	2.730	0.127	106.13	209	0	
ENF05p	2.88E-03	2.49E-02	390.4	4.60E-03	6.95E-03	no	0	2.421	2.782	0.361	94.38	187	0	
MMB04p1	2.90E-03	2.53E-02	387.7	4.49E-03	5.60E-03	no	0	2.286	2.475	0.190	81.19	119	0	
MMB05p1	3.29E-03	2.49E-02	342.2	5.35E-03	5.86E-03	no	0	3.103	3.278	0.175	78.95	142	0	
MMB06p	3.23E-03	2.47E-02	348.6	4.65E-03	5.88E-03	no	0	2.322	2.666	0.344	80.80	95	0	
MMB07p1	3.08E-03	2.49E-02	365.6	5.72E-03	5.77E-03	no	0	2.564	2.806	0.242	81.60	129	0	
MMB08p1	2.93E-03	2.48E-02	384.4	5.27E-03	5.79E-03	no	0	2.465	2.586	0.121	62.28	81	0	
MMB09p	3.01E-03	2.51E-02	373.5	4.78E-03	6.87E-03	no	0	2.248	2.510	0.262	86.30	120	0	
MMB10p	2.98E-03	2.54E-02	377.3	5.00E-03	7.28E-03	no	0	2.155	2.527	0.372	99.27	147	0	
MMB11p1	3.10E-03	2.49E-02	363.3	4.49E-03	5.60E-03	no	0	2.645	2.770	0.125	68.87	96	0	
MMB12p1	3.27E-03	2.50E-02	343.8	5.39E-03	5.27E-03	no	0	3.599	3.934	0.335	55.19	91	0	
MMB13p	2.94E-03	2.51E-02	383.1	4.57E-03	5.20E-03	no	0	2.434	3.015	0.581	71.34	101	0	
											avg	120		
											std	34		

MIXED-MODE PRECRACK c=42.05														
MMB14p	3.08E-03	2.54E-02	365.0	4.84E-03	6.44E-03	no	0	2.663	2.995	0.332	255.90	193	174	1.111
MMB15p	3.21E-03	2.54E-02	350.2	4.85E-03	5.60E-03	no	0	2.655	2.895	0.240	317.03	263	235	1.119
MMB16p						NOT USED								
MMB17p	3.15E-03	2.52E-02	356.9	4.61E-03	4.78E-03	no	0	2.554	2.707	0.153	285.31	212	189	1.123
MMB18p	2.99E-03	2.51E-02	376.0	4.75E-03	5.54E-03	no	0	2.748	2.817	0.069	211.18	154	140	1.101
MMB19p	3.20E-03	2.49E-02	351.3	4.71E-03	5.33E-03	no	0	2.721	2.976	0.255	251.25	181	162	1.114
											avg	201	180	1.114
											std	41	36	0.008
MIXED-MODE PRECRACK c=51.36														
MMB20p	2.89E-03	2.50E-02	389.0	4.85E-03	5.43E-03	no	0	2.376	2.455	0.079	165.20	151	88	1.721
MMB21p	3.09E-03	2.52E-02	364.4	4.92E-03	4.47E-03	no	0	2.400	2.673	0.273	178.20	147	84	1.737
MMB22p	3.07E-03	2.53E-02	366.2	4.73E-03	6.35E-03	no	0	2.360	2.446	0.087	141.76	91	52	1.740
MMB23p	2.95E-03	2.51E-02	381.8	4.66E-03	5.83E-03	no	0	2.117	2.264	0.147	182.21	140	80	1.760
MMB24p	3.26E-03	2.50E-02	344.9	4.92E-03	7.08E-03	no	0	2.413	2.536	0.123	192.07	150	86	1.751
MMB25p	3.00E-03	2.52E-02	374.8	4.92E-03	6.89E-03	no	0	3.042	3.215	0.173	133.59	137	82	1.667
											avg	136	79	1.729
											std	23	13	0.033
End-Notched Flexure														
ENF01	3.24E-03	2.49E-02	347.5	4.14E-03	7.68E-03	mode I	0.578	4.069	5.542	1.473	950.17	0	1450	
ENF02	3.17E-03	2.52E-02	354.7	5.07E-03	7.84E-03	mode I	0.223	2.874	5.735	2.861	1545.70	0	2001	
ENF03	3.02E-03	2.49E-02	372.3	4.11E-02	8.30E-03	mode I	0.410	3.782	5.448	1.666	1010.81	0	1742	
ENF04	3.16E-03	2.49E-02	355.8	5.05E-03	8.31E-03	mode I	0.127	2.730	5.361	2.631	1417.66	0	1584	
ENF05	2.88E-03	2.49E-02	390.4	4.60E-03	6.95E-03	mode I	0.361	2.782	6.286	3.504	1464.01	0	2294	
												avg	1814	
End-Notched Flexure												std	337	
ENF06						no								
ENF07	2.92E-03	2.50E-02	385.7	5.10E-03	5.13E-03	no	0.000	2.621	5.629	2.861	1407.17	0	1814	
ENF08	3.15E-03	2.53E-02	356.9	4.94E-03	4.82E-03	no	0.000	2.656	6.494	1.666	1753.21	0	2232	
ENF09	2.99E-03	2.44E-02	376.6	5.27E-03	4.77E-03	no	0.000	2.895	5.329	2.631	1248.87	0	1689	
ENF10	2.96E-03	2.52E-02	380.5	4.58E-03	5.21E-03	no	0.000	2.768	5.230	1.666	1289.04	0	1595	
ENF11	3.02E-03	2.53E-02	372.3	6.17E-03	6.01E-03	no	0.000	2.528	6.263	2.631	1483.64	0	1655	
												avg	1797	
												std	256	

c=22.74													
MMB01	2.99E-03	2.51E-02	376.0	5.17E-03	4.89E-03	mixed mode	0.495	3.254	3.722	0.468	699.15	135	1334	0.101
MMB03	3.21E-03	2.39E-02	350.8	5.10E-03	6.06E-03	mixed mode	0.431	3.242	5.248	2.006	765.91	146	1428	0.102
MMB05	3.29E-03	2.49E-02	342.2	5.35E-03	5.86E-03	mode I	0.380	3.483	5.030	1.547	740.67	134	1322	0.102
MMB06	3.23E-03	2.47E-02	348.6	4.65E-03	5.88E-03	mode I	0.330	2.666	5.388	2.722	1021.65	169	1598	0.106
MMB07	3.08E-03	2.49E-02	365.6	5.72E-03	5.77E-03	mode I	0.737	3.239	5.219	1.980	767.27	152	1491	0.102
MMB08	2.93E-03	2.48E-02	384.4	5.27E-03	5.79E-03	mode I	0.639	3.014	3.940	0.926	785.67	162	1588	0.102
											avg	150	1460	0.102
											std	14	120	0.002
c=31.87														
MMB09	3.01E-03	2.51E-02	373.5	4.78E-03	6.87E-03	mode I	0.232	2.510	4.552	2.042	525.32	288	564	0.510
MMB10	2.98E-03	2.54E-02	377.3	5.00E-03	7.28E-03	mode I	0.357	2.527	4.457	1.930	534.77	302	593	0.509
MMB11	3.10E-03	2.49E-02	363.3	5.32E-03	4.97E-03	mode I	0.478	3.147	4.312	1.165	433.41	278	561	0.495
MMB12	3.27E-03	2.50E-02	343.8	5.39E-03	5.27E-03	mode I	0.637	4.328	4.842	0.514	335.61	254	530	0.479
MMB13	2.94E-03	2.51E-02	383.1	4.57E-03	5.20E-03	mode I	0.581	3.015	4.760	1.745	491.40	375	759	0.494
MMB04	2.90E-03	2.53E-02	387.7	4.49E-03	5.60E-03	mixed mode	0.907	3.148	5.086	1.938	473.37	385	785	0.491
MMB00	3.06E-03	2.42E-02	368.0	4.31E-03	5.42E-03	mixed mode	0.815	3.217	4.100	0.883	378.35	242	491	0.493
											avg	303	612	0.496
											std	56	114	0.011
c=42.05														
MMB14						NOT USED								
MMB15	3.21E-03	2.54E-02	350.2	4.85E-03	5.60E-03	mixed mode	0.240	2.895	3.331	0.436	305.86	286	259	1.104
MMB16	3.29E-03	2.50E-02	341.7	4.77E-03	5.92E-03	mixed mode	n/a	2.787	3.467	0.680	300.89	247	222	1.115
MMB17	3.15E-03	2.52E-02	356.9	4.61E-03	4.78E-03	mixed mode	0.153	2.707	3.055	0.349	295.25	253	227	1.112
MMB18	2.99E-03	2.51E-02	376.0	4.75E-03	5.54E-03	mixed mode	0.069	2.817	2.951	0.135	232.06	194	177	1.097
MMB19	3.20E-03	2.49E-02	351.3	4.71E-03	5.33E-03	mixed mode	0.255	2.976	3.397	0.422	232.56	182	166	1.099
											avg	232	210	1.105
											std	43	38	0.008
c=51.36														
MMB20	2.89E-03	2.50E-02	389.0	4.85E-03	5.43E-03	mixed mode	0.079	2.455	2.913	0.459	185.14	201	117	1.712
MMB21	3.09E-03	2.52E-02	364.4	4.92E-03	4.47E-03	mixed mode	0.273	2.673	3.132	0.458	208.66	244	143	1.706
MMB22	3.07E-03	2.53E-02	366.2	4.73E-03	6.35E-03	mixed mode	0.087	2.446	2.809	0.363	201.00	194	112	1.730
MMB23	2.95E-03	2.51E-02	381.8	4.66E-03	5.83E-03	mixed mode	0.147	2.264	2.592	0.328	209.97	209	120	1.740
MMB24	3.26E-03	2.50E-02	344.9	4.92E-03	7.08E-03	mixed mode	0.123	2.536	2.934	0.398	203.23	183	105	1.737
MMB25	3.00E-03	2.52E-02	374.8	4.92E-03	6.89E-03	mixed mode	0.173	3.215	3.930	0.716	157.07	209	126	1.655
											avg	207	121	1.713
											std	21	13	0.032

MIXED-MODE PRECRACK c=19.51														
MMB26p	3.06E-03	2.51E-02	358.6	4.52E-03	6.02E-03	no	0.000	2.714	5.183	2.469	859.94	31	1180	0.026
MMB27p	3.03E-03	2.50E-02	361.6	4.73E-03	5.66E-03	no	0.000	2.463	5.624	3.161	954.82	33	1245	0.027
MMB28p	2.91E-03	2.52E-02	376.5	4.97E-03	4.94E-03	no	0.000	2.463	5.624	3.161	865.43	30	1135	0.026
MMB30p	2.90E-03	2.51E-02	377.8	4.65E-03	5.18E-03	no	0.000	2.467	5.194	2.727	969.99	39	1459	0.026
MMB31p	3.09E-03	2.51E-02	355.1	6.22E-03	5.50E-03	no	0.000	2.581	5.807	3.226	1204.92	54	2043	0.027
											avg	37	1412	0.026
											std	10	374	0.000
MIXED-MODE PRECRACK c=32.14														
MMB32p	3.02E-03	2.53E-02	362.8	4.76E-03	6.02E-03	no	0.000	2.346	3.202	0.856	514.84	244	456	0.536
MMB33p	3.00E-03	2.48E-02	365.8	4.55E-03	5.32E-03	no	0.000	2.313	2.507	0.195	353.04	118	221	0.537
MMB34p	3.05E-03	2.50E-02	359.8	5.13E-03	5.87E-03	no	0.000	2.313	2.507	0.195	456.45	186	346	0.538
MMB35p	3.00E-03	2.50E-02	365.8	4.80E-03	6.05E-03	no	0.000	2.217	2.585	0.369	489.42	209	386	0.541
MMB36p	3.00E-03	2.52E-02	365.8	6.31E-03	5.52E-03	no	0.000	2.620	3.687	1.067	464.48	248	473	0.525
											avg	201	376	0.535
											std	53	101	0.006
MIXED-MODE PRECRACK c=25.835														
MMB40	2.93E-03	2.51E-02	374.6	5.11E-03	5.80E-03	no	0.000	2.714	4.747	2.033	628.60	185	854	0.216
MMB41	2.98E-03	2.52E-02	368.3	5.20E-03	4.19E-03	no	0.000	2.376	5.463	3.087	864.62	262	1181	0.222
MMB42	3.08E-03	2.49E-02	356.3	5.55E-03	4.68E-03	no	0.000	2.847	4.889	2.042	647.39	190	877	0.216
MMB43	2.91E-03	2.49E-02	376.5	6.21E-03	4.69E-03	no	0.000	2.478	4.652	2.174	716.61	210	958	0.219
											avg	212	968	0.219
											std	35	149	0.003

Isophthalic Polyester (crack extension from Nylon strip)

specimen	h (m)	b (m)	λ (m^{-1})	t (m)	L' (m)	precracking	da_0 (cm)	a_0 (cm)	a_r (cm)	da (cm)	P_c (N)	G_I (J/m^2)	G_{II} (J/m^2)	R_G
Double Cantilever Beam														
DCB01p	3.06E-03	2.53E-02	368.0	5.00E-03	4.76E-03	no	0.000	2.696	3.043	0.347	79.03	130		
DCB02p	3.07E-03	2.49E-02	366.8	4.44E-03	5.23E-03	no	0.000	2.618	2.940	0.322	82.56	139		
DCB03p	3.05E-03	2.53E-02	368.6	4.67E-03	5.16E-03	no	0.000	2.410	2.779	0.369	68.92	82		
DCB04p	3.00E-03	2.54E-02	374.8	5.14E-03	5.26E-03	no	0.000	2.432	2.871	0.439	87.62	140		
DCB05p	2.93E-03	2.49E-02	383.7	5.09E-03	5.21E-03	no	0.000	2.575	3.084	0.509	62.92	88		
ENF01p	3.24E-03	2.49E-02	347.5	4.14E-03	7.68E-03	no	0.000	3.492	4.069	0.578	58.71	101		
ENF02p	3.17E-03	2.52E-02	354.7	5.07E-03	7.84E-03	no	0.000	2.651	2.874	0.223	75.88	106		
ENF03p	3.02E-03	2.49E-02	372.3	4.11E-02	8.30E-03	no	0.000	3.373	3.782	0.410	55.69	104		
ENF04p	3.16E-03	2.49E-02	355.8	5.05E-03	8.31E-03	no	0.000	2.604	2.730	0.127	80.56	120		
ENF05p	2.88E-03	2.49E-02	390.4	4.60E-03	6.95E-03	no	0.000	2.421	2.782	0.361	94.38	187		
MMB04p1	2.90E-03	2.53E-02	387.7	4.49E-03	5.60E-03	no	0.000	2.286	2.475	0.190	81.19	119		
MMB05p1	3.29E-03	2.49E-02	342.2	5.35E-03	5.86E-03	no	0.000	3.103	3.278	0.175	78.95	142		
MMB06p	3.23E-03	2.47E-02	348.6	4.65E-03	5.88E-03	no	0.000	2.322	2.666	0.344	80.80	95		
MMB07p1	3.08E-03	2.49E-02	365.6	5.72E-03	5.77E-03	no	0.000	2.564	2.806	0.242	81.60	129		
MMB08p1	2.93E-03	2.48E-02	384.4	5.27E-03	5.79E-03	no	0.000	2.465	2.586	0.121	62.28	81		
MMB09p	3.01E-03	2.51E-02	373.5	4.78E-03	6.87E-03	no	0.000	2.248	2.510	0.262	86.30	120		
MMB10p	2.98E-03	2.54E-02	377.3	5.00E-03	7.28E-03	no	0.000	2.155	2.527	0.372	99.27	147		
MMB11p1	3.10E-03	2.49E-02	363.3	4.49E-03	5.60E-03	no	0.000	2.645	2.770	0.125	68.87	96		
MMB12p1	3.27E-03	2.50E-02	343.8	5.39E-03	5.27E-03	no	0.000	3.599	3.934	0.335	55.19	91		
MMB13p	2.94E-03	2.51E-02	383.1	4.57E-03	5.20E-03	no	0.000	2.434	3.015	0.581	71.34	101		
											average	116		
											stdev	27		
MIXED-MODE PRECRACK c=51.36 mm														
MMB20p	2.89E-03	2.50E-02	389.0	4.85E-03	5.43E-03	no	0.000	2.376	2.455	0.079	165.20	151	88	1.721
MMB21p	3.09E-03	2.52E-02	364.4	4.92E-03	4.47E-03	no	0.000	2.400	2.673	0.273	178.20	147	84	1.737
MMB22p	3.07E-03	2.53E-02	366.2	4.73E-03	6.35E-03	no	0.000	2.360	2.446	0.087	141.76	91	52	1.740
MMB23p	2.95E-03	2.51E-02	381.8	4.66E-03	5.83E-03	no	0.000	2.117	2.264	0.147	182.21	140	80	1.760
MMB24p	3.26E-03	2.50E-02	344.9	4.92E-03	7.08E-03	no	0.000	2.413	2.536	0.123	192.07	150	86	1.751
MMB25p	3.00E-03	2.52E-02	374.8	4.92E-03	6.89E-03	no	0.000	3.042	3.215	0.173	133.59	137	82	1.667
											average	136	79	1.729
											stdev	23	13	0.033

MIXED-MODE PRECRACK c=42.05 mm														
MMB14p	3.08E-03	2.54E-02	365.0	4.84E-03	6.44E-03	no	0.000	2.663	2.995	0.332	255.90	193	174	1.111
MMB15p	3.21E-03	2.54E-02	350.2	4.85E-03	5.60E-03	no	0.000	2.655	2.895	0.240	317.03	263	235	1.119
MMB16p						NOT USED								
MMB17p	3.15E-03	2.52E-02	356.9	4.61E-03	4.78E-03	no	0.000	2.554	2.707	0.153	285.31	212	189	1.123
MMB18p	2.99E-03	2.51E-02	376.0	4.75E-03	5.54E-03	no	0.000	2.748	2.817	0.069	211.18	154	140	1.101
MMB19p	3.20E-03	2.49E-02	351.3	4.71E-03	5.33E-03	no	0.000	2.721	2.976	0.255	251.25	181	162	1.114
											average	201	180	1.114
											stdev	41	36	0.008
MIXED-MODE PRECRACK c=32.14 mm														
MMB32p	3.02E-03	2.53E-02	362.8	4.76E-03	6.02E-03	no	0.000	2.346	3.202	0.856	514.84	244	456	0.536
MMB33p	3.00E-03	2.48E-02	365.8	4.55E-03	5.32E-03	no	0.000	2.313	2.507	0.195	353.04	118	221	0.537
MMB34p	3.05E-03	2.50E-02	359.8	5.13E-03	5.87E-03	no	0.000	2.313	2.507	0.195	456.45	186	346	0.538
MMB35p	3.00E-03	2.50E-02	365.8	4.80E-03	6.05E-03	no	0.000	2.217	2.585	0.369	489.42	209	386	0.541
MMB36p	3.00E-03	2.52E-02	365.8	6.31E-03	5.52E-03	no	0.000	2.620	3.687	1.067	464.48	248	473	0.525
											average	201	376	0.535
											stdev	53	101	0.006
MIXED-MODE PRECRACK c=25.835 mm														
MMB40	2.93E-03	2.51E-02	374.6	5.11E-03	5.80E-03	no	0.000	2.714	4.747	2.033	628.60	185	854	0.216
MMB41	2.98E-03	2.52E-02	368.3	5.20E-03	4.19E-03	no	0.000	2.376	5.463	3.087	864.62	262	1181	0.222
MMB42	3.08E-03	2.49E-02	356.3	5.55E-03	4.68E-03	no	0.000	2.847	4.889	2.042	647.39	190	877	0.216
MMB43	2.91E-03	2.49E-02	376.5	6.21E-03	4.69E-03	no	0.000	2.478	4.652	2.174	716.61	210	958	0.219
											average	212	968	0.219
											stdev	35	149	0.095
MIXED-MODE PRECRACK c=19.51 m														
MMB26p	3.06E-03	2.51E-02	358.6	4.52E-03	6.02E-03	no	0.000	2.714	5.1825	2.4685	859.94	31	1180	0.026
MMB27p	3.03E-03	2.50E-02	361.6	4.73E-03	5.66E-03	no	0.000	2.463	5.624	3.161	954.82	33	1245	0.027
MMB28p	2.91E-03	2.52E-02	376.5	4.97E-03	4.94E-03	no	0.000	2.463	5.624	3.161	865.43	30	1135	0.026
MMB30p	2.90E-03	2.51E-02	377.8	4.65E-03	5.18E-03	no	0.000	2.467	5.194	2.727	969.99	39	1459	0.026
MMB31p	3.09E-03	2.51E-02	355.1	6.22E-03	5.50E-03	no	0.000	2.581	5.8065	3.2255	1204.92	54	2043	0.027
											average	37	1412	0.026
											stdev	10	374	0.000

End-Notched Flexure

ENF06						NOT USED						
ENF07	2.92E-03	2.50E-02	385.7	5.10E-03	5.13E-03	no	0.000	2.621	5.629	2.861	1407.17	1814
ENF08	3.15E-03	2.53E-02	356.9	4.94E-03	4.82E-03	no	0.000	2.656	6.494	1.666	1753.21	2232
ENF09	2.99E-03	2.44E-02	376.6	5.27E-03	4.77E-03	no	0.000	2.895	5.329	2.631	1248.87	1689
ENF10	2.96E-03	2.52E-02	380.5	4.58E-03	5.21E-03	no	0.000	2.768	5.230	1.666	1289.04	1595
ENF11	3.02E-03	2.53E-02	372.3	6.17E-03	6.01E-03	no	0.000	2.528	6.263	2.631	1483.64	1655
											average	1797
											stdev	256

Vinyl Ester

specimen	h (m)	b (m)	λ (m^{-1})	t (m)	L' (m)	precracking	da_0 (cm)	a_0 (cm)	a_r (cm)	da (cm)	P_c (N)	G_I (J/m^2)	G_{II} (J/m^2)	R_G
DCB01p	2.98E-03	2.63E-02	374.2	5.00E-03	5.07E-03	no	0.000	5.870	6.087	0.218	49.00	192	0	
DCB02p	2.78E-03	2.62E-02	401.2	4.46E-03	4.66E-03	no	0.000	6.136	6.728	0.593	57.98	362	0	
DCB03p	2.99E-03	2.61E-02	372.9	5.36E-03	5.92E-03	no	0.000	5.772	5.836	0.064	45.37	161	0	
DCB04p	2.79E-03	2.61E-02	399.7	4.57E-03	4.83E-03	no	0.000	5.797	5.966	0.085	48.87	229	0	
DCB05p	2.99E-03	2.61E-02	372.3	4.79E-03	4.68E-03	no	0.000	5.833	5.927	0.094	46.84	174	0	
DCB06p	2.93E-03	2.58E-02	379.9	4.71E-03	4.67E-03	no	0.000	3.104	3.311	0.207	84.73	190	0	
DCB07p	2.90E-03	2.62E-02	383.9	4.68E-03	4.63E-03	no	0.000	2.908	3.090	0.181	94.90	210	0	
DCB08p	2.95E-03	2.59E-02	377.4	4.73E-03	5.91E-03	no	0.000	2.599	2.753	0.154	95.45	170	0	
DCB09p	2.85E-03	2.62E-02	391.3	4.79E-03	5.11E-03	no	0.000	2.717	2.910	0.085	87.78	168	0	
DCB10p	2.83E-03	2.60E-02	393.4	4.52E-03	5.55E-03	no	0.000	2.816	2.882	0.065	87.68	183	0	
											avg	204		
											std	59		
End-Notched Flexure, MODE-II PRECRACK														
ENF01	2.91E-03	2.63E-02	383.2	4.32E-03	4.76E-03	no	0.000	2.761	5.524	1.473	1953.85	0	3180	
ENF02	2.86E-03	2.58E-02	389.9	4.54E-03	4.57E-03	no	0.000	2.839	3.398	2.861	1870.69	0	3361	
ENF03	2.86E-03	2.63E-02	389.9	4.43E-03	4.83E-03	no	0.000	2.816	3.429	1.666	1922.71	0	3367	
ENF04	2.97E-03	2.63E-02	374.8	4.82E-03	5.29E-03	no	0.000	2.716	3.399	2.631	2091.68	0	3295	
ENF05	2.83E-03	2.62E-02	394.1	4.59E-03	4.75E-03	no	0.000	2.688	3.680	1.666	1930.51	0	3209	
											avg		3283	
											std		86	
MIXED-MODE PRECRACK c=23.54														
MMB01	2.94E-03	2.63E-02	379.3	4.54E-03	4.54E-03	no	0.000	2.733	5.191	2.458	1130.49	292	2201	0.133
MMB02	3.05E-03	2.64E-02	365.6	4.42E-03	4.79E-03	no	0.000	2.753	5.423	2.671	1232.28	313	2352	0.133
MMB04	2.82E-03	2.64E-02	395.5	4.48E-03	4.84E-03	no	0.000	2.864	4.822	1.958	961.06	257	1963	0.131
MMB05	3.00E-03	2.64E-02	371.7	4.45E-03	4.66E-03	no	0.000	2.674	4.209	1.535	1281.62	338	2537	0.133
											avg	300	2263	0.132
											std	35	243	0.001
MIXED-MODE PRECRACK c=32.93														
MMB06	3.02E-03	2.62E-02	369.2	4.90E-03	5.27E-03	no	0.000	2.592	4.757	2.166	688.07	490	867	0.566
MMB07	2.81E-03	2.61E-02	396.2	4.78E-03	5.58E-03	no	0.000	2.699	5.338	2.639	715.33	703	1264	0.556
MMB08	2.97E-03	2.60E-02	374.8	4.72E-03	5.40E-03	no	0.000	2.664	2.971	0.307	603.92	420	748	0.562
MMB09	2.83E-03	2.62E-02	394.1	4.60E-03	6.07E-03	no	0.000	2.850	4.491	1.641	651.65	629	1139	0.553
MMB10	2.83E-03	2.61E-02	393.4	4.74E-03	6.09E-03	no	0.000	2.851	4.492	1.642	684.54	694	1256	0.553
											avg	587	1055	0.558
											std	126	235	0.006

MIXED-MODE PRECRACK c=45.09														
MMB11p	2.99E-03	2.62E-02	372.3	4.61E-03	5.60E-03	no	0.000	2.696	4.238	1.542	463.42	742	573	1.296
MMB12p	2.86E-03	2.63E-02	389.2	5.18E-03	5.49E-03	no	0.000	2.805	3.053	0.248	314.23	414	323	1.280
MMB13p	2.81E-03	2.63E-02	396.2	4.79E-03	5.09E-03	no	0.000	2.941	3.138	0.197	280.94	379	299	1.268
MMB14p	2.85E-03	2.62E-02	390.6	4.68E-03	4.37E-03	no	0.000	2.737	3.320	0.583	374.41	569	443	1.284
MMB15p	2.83E-03	2.62E-02	393.4	4.80E-03	4.92E-03	no	0.000	2.662	3.573	0.911	386.79	590	458	1.288
											avg	539	419	1.283
											std	147	111	0.010
MIXED-MODE PRECRACK c=58.49														
MMB16p	2.83E-03	2.63E-02	394.1	4.51E-03	4.96E-03	no	0.000	2.600	2.734	0.134	171.39	240	112	2.142
MMB17p	2.89E-03	2.62E-02	385.2	5.17E-03	4.99E-03	no	0.000	2.857	3.032	0.175	194.26	346	163	2.120
MMB18p	2.87E-03	2.59E-02	387.9	4.58E-03	5.34E-03	no	0.000	3.003	3.683	0.680	217.18	494	235	2.103
MMB19p	2.86E-03	2.64E-02	389.9	4.79E-03	5.58E-03	no	0.000	2.685	3.072	0.387	224.20	418	196	2.135
MMB20p	2.88E-03	2.62E-02	386.5	4.59E-03	5.10E-03	no	0.000	2.797	3.155	0.358	216.13	416	196	2.125
											avg	383	180	2.125
											std	95	46	0.015
MIXED-MODE PRECRACK c=18.89														
MMB16p	2.99E-03	2.62E-02	372.3	4.18E-03	5.30E-03	no	0.000	2.652	3.686	1.035	1401.02	44	2655	0.017
MMB17p	2.80E-03	2.62E-02	398.3	4.68E-03	4.51E-03	no	0.000	2.942	3.886	0.944	1201.44	47	2935	0.016
MMB18p	2.86E-03	2.62E-02	389.9	5.02E-03	5.35E-03	no	0.000	2.694	3.330	0.637	1423.63	53	3253	0.016
MMB19p	2.81E-03	2.61E-02	396.2	4.65E-03	5.14E-03	no	0.000	2.980	4.504	1.524	1217.39	49	3044	0.016
MMB20p	2.76E-03	2.63E-02	403.3	5.18E-03	4.74E-03	no	0.000	2.731	3.715	0.984	1269.60	47	2909	0.016
											avg	48	2959	0.016
											std	3	217	0.000

Epoxy

specimen	h (m)	b (m)	λ (m^{-1})	t (m)	L' (m)	precracking	da_0 (cm)	a_0 (cm)	a_r (cm)	da (cm)	P_c (N)	G_I (J/m^2)	G_{II} (J/m^2)	R_G
DCB01p	2.97E-03	2.60E-02	368.1	4.53E-03	4.39E-03	no	0.000	3.033	3.100	0.068	108.93	285	0	
DCB02p	2.88E-03	2.64E-02	380.3	4.49E-03	4.74E-03	no	0.000	2.427	2.533	0.107	115.82	230	0	
DCB03p	3.13E-03	2.62E-02	349.3	4.61E-03	4.62E-03	no	0.000	2.902	2.952	0.049	104.89	208	0	
DCB04p	2.81E-03	2.61E-02	389.7	4.77E-03	5.37E-03	no	0.000	2.967	3.253	0.085	120.76	394	0	
DCB05p	2.82E-03	2.56E-02	388.4	4.47E-03	4.49E-03	no	0.000	3.001	3.286	0.285	118.76	399	0	
											avg	303		
											std	90		
											n	5		
DCB-long crack														
DCB06p	2.88E-03	2.55E-02	379.6	4.80E-03	5.45E-03	no	0.000	5.551	6.132	0.581	76.17	490	0	
DCB07p	2.89E-03	2.29E-02	378.3	4.62E-03	5.79E-03	no	0.000	5.569	5.902	0.333	55.55	321	0	
DCB08p	2.87E-03	2.56E-02	381.6	4.67E-03	5.40E-03	no	0.000	5.274	5.934	0.660	80.21	498	0	
DCB09p	3.06E-03	2.58E-02	357.9	4.79E-03	6.14E-03	no	0.000	5.366	6.092	0.726	73.35	350	0	
DCB10p						NOT USED								
											avg	415		
											std	92		
											n	4		
DCB-short crack														
DCB11p	2.93E-03	2.59E-02	373.1	4.91E-03	4.93E-03	no	0.000	2.924	3.183	0.259	137.73	448	0	
DCB12p	2.93E-03	2.60E-02	373.1	4.76E-03	5.71E-03	no	0.000	2.879	2.900	0.022	114.58	298	0	
DCB13p	3.13E-03	2.60E-02	349.3	5.12E-03	5.49E-03	no	0.000	2.818	2.860	0.041	119.02	258	0	
DCB14p	3.11E-03	2.64E-02	351.5	4.75E-03	5.33E-03	no	0.000	2.653	2.924	0.085	150.13	362	0	
DCB15p	2.88E-03	2.56E-02	380.3	4.80E-03	5.72E-03	no	0.000	2.642	2.819	0.177	144.76	445	0	
											avg	362		
											std	86		
											n	5		
											avg ALL DCB	356		
											std ALL DCB	94		
											n ALL DCB	14		

ENF, no mode-I precrack														
ENF01	2.97E-03	2.59E-02	368.1	4.42E-03	6.18E-03	no	0.000	2.836	4.427	1.591	2225.99	0	4208	
ENF02	2.97E-03	2.65E-02	368.7	4.64E-03	5.34E-03	no	0.000	2.911	3.621	0.710	2168.93	0	4031	
ENF03	2.90E-03	2.62E-02	377.0	4.20E-03	4.88E-03	no	0.000	2.727	3.767	1.040	2193.85	0	3968	
ENF04	3.15E-03	2.53E-02	347.6	4.88E-03	5.51E-03	no	0.000	2.680	2.959	0.280	2442.05	0	4020	
ENF05	3.13E-03	2.57E-02	349.8	4.65E-03	6.20E-03	no	0.000	2.729	3.831	1.102	2447.65	0	4139	
											avg		4073	
											std		98	
											n		5	
ENF, mode-I precrack														
ENF06	2.97E-03	2.60E-02	368.1	4.53E-03	4.39E-03	mode I	0.068	3.100	3.999	0.899	2022.48	0	4096	
ENF07	2.88E-03	2.64E-02	380.3	4.49E-03	4.74E-03	mode I	0.107	2.533	4.678	2.145	2360.26	0	4030	
ENF08	3.13E-03	2.62E-02	349.3	4.61E-03	4.62E-03	mode I	0.050	2.952	4.694	1.743	2188.16	0	3691	
ENF09	2.81E-03	2.61E-02	389.7	4.77E-03	5.37E-03	mode I	0.286	3.253	4.310	1.057	1795.45	0	4190	
ENF10	2.82E-03	2.56E-02	388.4	4.47E-03	4.49E-03	mode I	0.285	3.286	4.531	1.245	1749.87	0	4161	
											avg		4034	
											std		201	
											n		5	
											avg ALL ENF		4054	
											std ALL ENF		151	
											n ALL ENF		10	
c=18.89														
MMB01	3.04E-03	2.64E-02	360.2	4.86E-03	5.46E-03	no	0.000	2.540	5.646	3.107	1868.80	69	4114	0.017
MMB02	2.99E-03	2.54E-02	365.6	4.68E-03	5.55E-03	no	0.000	2.642	3.310	0.668	1657.80	65	3932	0.017
MMB03	3.07E-03	2.62E-02	356.1	4.63E-03	5.20E-03	no	0.000	2.801	4.423	1.622	1624.98	61	3685	0.017
MMB04	2.87E-03	2.57E-02	380.9	4.60E-03	5.06E-03	no	0.000	2.441	5.728	3.287	1712.20	66	3972	0.017
MMB05	2.91E-03	2.56E-02	375.7	4.53E-03	5.48E-03	no	0.000	2.852	4.658	1.806	1470.07	63	3839	0.016
MMB06	2.86E-03	2.58E-02	382.3	4.37E-03	6.25E-03	no	0.000	2.631	3.221	0.591	1580.74	65	3927	0.017
MMB07	3.12E-03	2.61E-02	350.4	5.14E-03	5.05E-03	no	0.000	2.669	3.546	0.877	1709.56	60	3580	0.017
MMB08	2.80E-03	2.56E-02	391.1	4.60E-03	5.42E-03	no	0.000	2.950	3.931	0.982	1237.64	53	3290	0.016
MMB09	3.02E-03	2.58E-02	362.6	4.52E-03	6.90E-03	no	0.000	2.528	3.964	1.436	1760.24	65	3866	0.017
MMB10	3.04E-03	2.47E-02	359.6	4.54E-03	5.34E-03	no	0.000	2.714	3.893	1.179	1559.1847	62	3709	0.017
											average	63	3791	0.017
											stdev	4	235	0.000
											n			10

c=23.885														
MMB11	2.97E-03	2.58E-02	368.1	4.81E-03	5.13E-03	no	0.000	2.542	3.570	1.028	1374.03	410	2858	0.143
MMB12	2.87E-03	2.56E-02	380.9	4.35E-03	4.98E-03	no	0.000	2.502	3.440	0.938	1428.32	480	3359	0.143
MMB13	2.90E-03	2.56E-02	377.0	4.73E-03	4.66E-03	no	0.000	2.710	3.548	0.838	1264.32	422	2985	0.141
MMB14	2.92E-03	2.57E-02	375.0	4.85E-03	5.03E-03	no	0.000	2.962	3.401	0.439	1143.46	396	2835	0.140
MMB15	2.92E-03	2.60E-02	374.4	4.27E-03	5.23E-03	no	0.000	2.691	3.510	0.820	1265.29	398	2807	0.142
MMB16	2.96E-03	2.49E-02	370.0	4.30E-03	5.27E-03	no	0.000	2.932	3.850	0.918	1266.19	489	3487	0.140
MMB17	3.06E-03	2.57E-02	357.3	4.94E-03	4.92E-03	no	0.000	2.749	3.588	0.839	1419.37	468	3289	0.142
MMB18	3.06E-03	2.55E-02	357.9	4.75E-03	5.48E-03	no	0.000	2.684	3.649	0.965	1281.46	373	2613	0.143
MMB19	3.11E-03	2.60E-02	352.1	4.78E-03	4.59E-03	no	0.000	2.674	4.490	1.816	1576.88	515	3594	0.143
MMB20	2.80E-03	2.58E-02	390.8	5.13E-03	5.18E-03	no	0.000	2.973	5.500	2.527	1170.50	468	3367	0.139
											avg	442	3119	0.142
											std	48	338	0.002
											n			10
c=32.695														
MMB21	2.83E-03	2.59E-02	387.0	4.91E-03	5.38E-03	no	0.000	2.994	5.042	2.048	693.63	777	1445	0.538
MMB22	3.00E-03	2.58E-02	365.0	4.76E-03	4.99E-03	no	0.000	2.916	4.609	1.693	686.86	623	1144	0.544
MMB23	3.08E-03	2.58E-02	354.9	5.16E-03	5.03E-03	no	0.000	2.879	4.951	2.073	811.04	783	1430	0.548
MMB24	3.05E-03	2.60E-02	358.4	4.99E-03	5.59E-03	no	0.000	2.743	4.795	2.052	785.83	681	1237	0.551
MMB25	3.17E-03	2.58E-02	344.9	4.58E-03	5.38E-03	no	0.000	2.753	4.126	1.373	817.21	680	1227	0.554
MMB26	3.01E-03	2.57E-02	363.2	5.14E-03	4.89E-03	no	0.000	2.532	4.971	2.439	849.46	733	1317	0.557
MMB27	2.96E-03	2.59E-02	370.0	4.77E-03	5.38E-03	no	0.000	2.336	3.390	1.054	941.56	812	1444	0.562
MMB28	2.82E-03	2.61E-02	387.7	4.43E-03	5.23E-03	no	0.000	2.908	4.007	1.100	766.07	890	1648	0.540
MMB29	2.84E-03	2.64E-02	384.9	4.63E-03	6.27E-03	no	0.000	2.843	3.075	0.232	818.43	938	1730	0.542
MMB30	2.99E-03	2.58E-02	365.6	4.67E-03	5.57E-03	no	0.000	2.498	3.625	1.127	789.35	625	1122	0.557
											avg	754	1374	0.549
											std	106	204	0.008
											n			10

c=45.60															
MMB31	2.87E-03	2.59E-02	381.6	4.47E-03	4.73E-03	no	0.000	2.673	3.666	0.993	500.40	1029	776	1.326
MMB32	2.97E-03	2.61E-02	368.7	4.55E-03	5.31E-03	no	0.000	2.436	2.875	0.439	516.24	827	611	1.353
MMB33	3.14E-03	2.56E-02	348.2	4.49E-03	6.15E-03	no	0.000	2.663	3.187	0.525	517.46	867	644	1.346
MMB34	2.93E-03	2.63E-02	373.1	4.62E-03	5.64E-03	no	0.000	2.424	3.025	0.601	568.53	1017	752	1.351
MMB35	2.90E-03	2.61E-02	377.0	4.69E-03	5.78E-03	no	0.000	2.698	3.152	0.454	530.28	1119	844	1.327
MMB36	3.11E-03	2.63E-02	351.5	4.87E-03	5.70E-03	no	0.000	2.535	2.846	0.311	479.22	662	489	1.355
MMB37	2.97E-03	2.53E-02	368.1	4.61E-03	5.23E-03	no	0.000	2.737	3.669	0.933	394.92	634	477	1.329
MMB38	2.79E-03	2.58E-02	391.8	4.52E-03	5.83E-03	no	0.000	2.054	3.678	1.625	623.96	1085	788	1.378
MMB39	2.87E-03	2.63E-02	380.9	4.28E-03	4.75E-03	no	0.000	2.799	3.447	0.649	408.14	718	545	1.317
MMB40	2.80E-03	2.55E-02	390.4	4.76E-03	5.49E-03	no	0.000	2.784	3.137	0.353	452.66	994	757	1.314
											avg	895	668	1.340
											std	179	133	0.020
											n			10
c=58.92															
MMB41	3.10E-03	2.62E-02	353.2	4.70E-03	6.83E-03	no	0.000	2.537	2.962	0.426	368.94	849	383	2.216
MMB42	2.83E-03	2.56E-02	387.0	4.61E-03	6.22E-03	no	0.000	2.542	2.847	0.305	231.25	454	208	2.184
MMB43	3.05E-03	2.57E-02	359.0	4.84E-03	5.35E-03	no	0.000	2.723	3.045	0.323	293.63	664	304	2.186
MMB44	2.93E-03	2.63E-02	373.1	4.69E-03	5.59E-03	no	0.000	2.630	3.005	0.376	306.18	725	332	2.184
MMB45	2.92E-03	2.62E-02	375.0	4.99E-03	5.52E-03	no	0.000	2.881	3.107	0.226	314.49	919	427	2.153
MMB46	2.89E-03	2.54E-02	378.3	4.50E-03	4.48E-03	no	0.000	2.649	3.225	0.576	279.01	677	311	2.177
MMB47	2.94E-03	2.61E-02	371.9	4.97E-03	5.31E-03	no	0.000	2.924	3.473	0.549	281.61	747	347	2.151
MMB48	2.97E-03	2.57E-02	368.7	4.80E-03	5.29E-03	no	0.000	2.952	3.406	0.455	310.87	931	433	2.151
MMB49	2.85E-03	2.23E-02	383.6	4.40E-03	4.22E-03	no	0.000	3.045	3.463	0.418	241.26	880	413	2.130
MMB50	2.90E-03	2.61E-02	377.6	4.61E-03	5.40E-03	no	0.000	2.610	3.075	0.465	307.63	759	348	2.183
											avg	761	351	2.172
											std	145	68	0.025
											n			10

APPENDIX D: CALCULATION EXAMPLE

Conversion	$N := newton \quad J := joule \quad kJ := 10^3 J \quad GPa := 10^9 \cdot Pa$
The variable c	$c := 31.87 \cdot mm$
The half-span length	$L := 49.68 \cdot mm$
Critical Load	$P_c := 378.35N$
Half height	$h := 3.055 \cdot mm$
Width	$b := 24.15 \cdot mm$
Longitudinal Modulus	$E_{11} := 27.9 \cdot GPa$
Moment	$I := \frac{b \cdot h^3}{12} \qquad I = 5.738 \times 10^{-11} m^4$
Precrack position	$a := 32.17mm$
Transverse Modulus	$E_{22} := 7.44 \cdot GPa$
Inplane Shear Modulus	$G_{13} := 3.05 \cdot GPa$
Elastic Foundation Correction	$\lambda := \frac{1}{h} \cdot \sqrt[4]{\frac{6 \cdot E_{22}}{E_{11}}} \qquad \lambda = 368.145 m^{-1}$
Mode I Loading	$P_I := P_c \cdot \left(\frac{3c - L}{4 \cdot L} \right)$
Mode II Loading	$P_{II} := P_c \cdot \left(\frac{c + L}{L} \right)$
Mode I SERR	$G_I := \frac{12 \cdot P_I^2}{b^2 \cdot h^3 \cdot E_{11}} \cdot \left(a^2 + \frac{2 \cdot a}{\lambda} + \frac{1}{\lambda^2} + \frac{h^2 \cdot E_{11}}{10 \cdot G_{13}} \right) \qquad G_I = 242 \frac{J}{m^2}$
Mode II SERR	$G_{II} := \frac{9 \cdot P_{II}^2}{16 \cdot b^2 \cdot h^3 \cdot E_{11}} \cdot \left(a^2 + \frac{0.2 \cdot h^2 \cdot E_{11}}{G_{13}} \right) \qquad G_{II} = 492 \frac{J}{m^2}$

APPENDIX E: ANSYS INPUT FILE

```
/COM, *** IF Statement for "AUTOMATION" ***
/COM, ALL PRINTOUT IS SUPPRESSED FOR CALCULATION EFFICIENCY
*IF, menupass, EQ, 0, THEN
     /COM, "/CLEAR" command must be omitted for "/OPT"
     /CLEAR         ! Clear previous database
     /GOPR
     pass=0
*ELSEIF, menupass, EQ, 1, THEN
     /NOLIST
     /NOPR
     pass=1
*ENDIF

/COM, Filename: /usr/people/pagastra/MMB/MMB_geom5.inp
/COM,
***********************************************************
**********
/COM, ***                     MMB CRACK PROPAGATION
***
/COM,
***********************************************************
**********

/FILNAME, MMB_geom5

/COM, MMB_geom with no loading roller, no uneven
/TITLE, MMB v.5 (PLANE82 w/ Plane Strain Option)

/PREP7
/COLOR,PBAK,OFF               ! background shading off
/RGB,INDEX,100,100,100,0      ! 4 subsequent commands are
for reversing the video
/RGB,INDEX,80,80,80,13
/RGB,INDEX,60,60,60,14
/RGB,INDEX,0,0,0,15
/DEV,FONT,2,COURIER,MEDIUM,R,12

/COM, *** Model Specification ***
*IF,menupass,EQ,0,THEN
     multipro, 'start',3
          *CSET,1,3,spec,'1=DCB 2=ENF 3=MMB',1
          *CSET,4,6,MATR,'Matl 1=PE 2=VE 3=EE',1
          *CSET,7,9,NLGEOMV,'Large Defl Eff 0=OFF 1=ON',0
          *CSET,61,62,'Enter model spec'
     multipro, 'end'
```

```
     /COM, *** "T"-TABS OPTION ***
     *IF, spec, EQ, 3, THEN
          option=1
     *ELSEIF, spec, NE, 3, THEN
          *ASK, option, 1=inc--2=excl tabs, 1
          /COM, option to in/exclude tabs
          ! 1 = include; 2 = exclude tabs
     *ENDIF
*ENDIF

/COM, *** Correction factor for the crack length ***
/COM, ***      for sensitivity analysis         ***
fa=1.0

/COM, *** Code for Changing the Material Properties ***
/COM, ***          Online vs. Average              ***
mpreal=0       ! 0=use the average
               ! 1=use the online


/COM, *** Geometric Parameters ***
/COM, NOTE: ALL UNITS ARE IN SI
/COM, *** Variable Default Values ***
*IF, MATR, EQ, 1, THEN
     *IF, spec, EQ, 1, THEN
          g_tv=2*0.00293      ! DCB0202141850p
          g_wv=0.02491
          g_tlv=5.21E-3       ! Tab length into the crack
from tab hole's midpoint
          g_tlpv=5.09E-3      ! Tab height (from arm
midpoint to tab hole's midpoint)
          g_r1_av=0.02575*fa
          loadv=62.9
          g_cv=0

     *ELSEIF, spec, EQ, 2, THEN
          g_tv=2*0.00288      ! ENF0202161905
          g_wv=0.02493
          g_tlv=6.95E-3
          g_tlpv=4.60E-3
          g_r1_av=0.02782*fa
          loadv=-1464.0
          g_cv=0
```

```
     *ELSEIF, spec, EQ, 3, THEN
          g_tv=2*0.003055          ! MMB020217_c3187_1820
          g_wv=0.02415
          g_tlv=5.42E-3
          g_tlpv=4.31E-3
          g_r1_av=0.03217*fa
          loadv=-378.4
          g_cv=0.03187
          g_cll=0.03187
     *ENDIF
*ELSEIF, MATR,EQ, 2, THEN          ! Vinylester
     *IF, spec, EQ, 1, THEN
          g_tv=2*0.002985          ! DCB03p
          g_wv=0.02607
          g_tlv=5.29E-3       ! Tab length into the crack
from tab hole's midpoint
          g_tlpv=5.36E-3      ! Tab height (from arm
midpoint to tab hole's midpoint)
          g_r1_av=0.05772*fa
          loadv=45.4
          g_cv=0

     *ELSEIF, spec, EQ, 2, THEN
          g_tv=2*0.002855          ! ENF03p
          g_wv=0.02628
          g_tlv=4.83E-3
          g_tlpv=4.43E-3
          g_r1_av=0.02816*fa
          loadv=-1922.7
          g_cv=0

     *ELSEIF, spec, EQ, 3, THEN
          g_tv=2*0.00281      ! MMB13p
          g_wv=0.02628
          g_tlv=5.09E-3
          g_tlpv=4.79E-3
          g_r1_av=0.02941*fa
          loadv=-377.9
          g_cv=0.045085
          g_cll=0.045085
     *ENDIF
*ELSEIF, MATR, EQ, 3, THEN ! Epoxy
     *IF, spec, EQ, 1, THEN
          g_tv=2*0.00313      ! DCB021109_p b202p
          g_wv=0.02615
```

```
          g_tlv=4.62E-3       ! Tab length into the crack
from tab hole's midpoint
          g_tlpv=4.61E-3      ! Tab height (from arm
midpoint to tab hole's midpoint)
          g_r1_av=0.02902*fa
          loadv=104.9
          g_cv=0

     *ELSEIF, spec, EQ, 2, THEN
          g_tv=2*0.003145          ! ENF_B2_021110 ENF04
          g_wv=0.02527
          g_tlv=5.51E-3
          g_tlpv=4.88E-3
          g_r1_av=0.02680*fa
          loadv=-2442.0
          g_cv=0

     *ELSEIF, spec, EQ, 3, THEN
          g_tv=2*0.00293      ! MMB_B2_021204_c4560 MMB33
          g_wv=0.02626
          g_tlv=5.64E-3
          g_tlpv=4.62E-3
          g_r1_av=0.02424*fa
          loadv=-517.5
          g_cv=0.04560
          g_cll=0.04560
     *ENDIF
*ENDIF

*IF, pass, EQ, 0, THEN
     multipro, 'start',7
          *CSET,1,3,g_t,'tot thickness/m',g_tv
          *CSET,4,6,g_w,'width/m',g_wv
          *CSET,7,9,g_tl,'L-prime/m',g_tlv
          *CSET,10,12,g_tlp,'t-prime/m',g_tlpv
          *CSET,13,15,g_r1_a, 'crack length from
support/m',g_r1_av
          *CSET,16,18,load,'critical load/N',loadv
          *CSET,19,21,g_c, 'the variable c', g_cv
          *CSET,61,62,'Enter the correct dimension.'
     multipro, 'end'
*ELSEIF, pass, EQ, 1, THEN
     g_t=g_tv       ! MMB020217_c3187_1820
     g_w=g_wv
     g_tl=g_tlv
```

```
     g_tlp=g_tlpv
     g_r1_a=g_r1_av
     load=loadv
     g_c=g_cv
*ENDIF

/COM, *** Online Calculation of Modulus with ***
/COM, *** half height and ply number as the  ***
/COM, ***          only variables          ***
h=g_t/2             ! h is the half of total thickness in
meter
n=10                ! n is the number of layer
vf=.1033541363e-1*(1/h*n)**1.000100010  ! Vf is the fiber
volume percentage
ELstar=37E+09       ! ELstar is the longitudinal modulus at
45% fiber volume fraction
ETstar=8.99E+09          ! ETstar is the transverse modulus
at 45% fiber volume fraction
GLTstar=4.1E+09          ! GLT is the longitudinal-
transverse shear modulus at 45% fvf
vLTstar=0.31        ! vLT is the longitudinal-transverse
poisson ratio at 45% fvf
EL=(.3057169061e-1*ELstar/(1E+09)*(3.1+.6796005562e-
2*(1/h*n)**1.000100010))*1E+09
ET=(.4533091568*ETstar/(1E+09)*(1+.8634438677e-
4*(1/h*n)**1.000100010)/(1-.8634438677e-
4*(1/h*n)**1.000100010))*1E+09
GLT=(.3559985760*GLTstar/(1E+09)*(1+.1726887735e-
3*(1/h*n)**1.000100010)/(1-.8634438677e-
4*(1/h*n)**1.000100010))*1E+09
vLT=3.144654088*vLTstar*(.385-.1549241390e-
4*(1/h*n)**1.000100010)

/COM, *** Model Specification (continued) ***
g_l = 0.159              ! total length of specimen
g_r1 = 0.016        ! cracked-end to first support (roller-
1; r1)
g_sl = 0.09928      ! support length, MMB

!g_r1_a = crack length from first support to crack-tip
g_a =  g_r1 + g_r1_a     ! crack length from edge to crack-
tip

!g_tl = tab length at base (base-specimen interface)
g_ttb = 0.00156          ! tab thickness at base
```

```
!g_tlp = t in EXCEL Calculation Sheet

!pos=0+g_t/4-g_tlp

RD1=0.0038                    ! the radius of the clevis
g_tll = 0.02522               ! the thickness of the
loading lever
!g_hll = 0.075155             ! G_HLL based on LDPT, G_HLL
OPT, SUBP
g_hll = 0.075180              ! G_HLL based on LDPT, G_HLL
OPT, FIRST
!g_hll = 0.076          ! the height of loading lever
!g_hll=0.02
!g_c=the parameter c in the analysis

/COM, *** Element Default Size ***
nelem=4
elesize=(g_t/2)/nelem

/COM, *** Coefficient of Frictions ***
MU_BI=0.01          ! Coefficient of friction for Beam
Interface
MU_RI=0.01          ! Coefficient of friction for Roller
Interface

/COM, *** MATH constants ***
pi=2*asin(1)

/COM, *** Load Parameters ***
F_y=load/g_w

/COM, *** Creation of Geometry ***
/COM, *** Keypoints ***
K,1

/COM, Keypoints for the tabs
K,2, g_r1-(g_tl)
K,3, g_r1
K,4, g_r1+(g_tl)
K,5, g_a-(g_t/2),       0,0

/COM, Keypoint 6 is right under the singular KP
K,6, g_a,          0,0
K,7, g_a+(g_t/2),       0,0
```

```
K,8, g_r1+(g_sl/2)-0.007,     0,0


/COM, KP#9 is the mid-span of specimen
K,9, g_r1+(g_sl/2),      0,0
K,10, g_r1+(g_sl/2)+0.007,    0,0
K,11, g_r1+g_sl,         0,0
K,12, KX(11)+(KX(3)-KX(1)),            0,0

*IF, SPEC, EQ, 1, AND, KX(7), GT, KX(8), THEN
K,8, (KX(11)+KX(7))/2-0.007
K,9, (KX(11)+KX(7))/2
K,10, (KX(11)+KX(7))/2+0.007
*ENDIF

ALLS
! BSKP is the number of KP's at bottom of spec.
*GET,BSKP,KP,,NUM,MAX

/COM, Keypoints for the double cantilever (beam's
interface)
KGEN, 2, 1, 5,,,(g_t/2)
*REPEAT,2

/COM, Keypoints from crack-tip to crack-free edge at mid-
thickness
KGEN, 2, 6, BSKP,,,(g_t/2)

/COM, KPSING is KP at crack tip
KPSING=KP(g_a,g_t/2,0)
ALLS

/COM, Keypoints at top of spec
KGEN, 2, 1, BSKP,,,g_t

*IF, option, EQ,1, THEN
     /COM, *** keypoints for tabs ***
     K, 42, (g_r1-g_tl)+g_ttb,     -g_ttb, 0
     K, 43, g_r1,              -g_ttb, 0
     K, 44, (g_r1+g_tl)-g_ttb,     -g_ttb, 0
     KGEN,2,42,44,,,-(g_tlp-g_t/4-KY(3)+KY(43))

     /COM, keypoints for the top tabs using "KSYMM"
     WPOF,,g_t/2
     CSYS, 4
```

```
     KSYMM, Y, 42,47
     CSYS, 0
*ENDIF

/COM, The creation of geometry starts from
/COM, lines (instead of area), so that all numberings
/COM, can be better controlled.

/COM, horiz lines
L,1,2
*REPEAT, BSKP-1, 1, 1

/COM, *** T a r g e t  Lines ***
! lines for the lower arm at crack interface
L,13,14
*REPEAT, 4, 1, 1
L,17,23

/COM, *** C o n t a c t  Lines ***
/COM, lines for the upper arm at crack interface
L,18,19
*REPEAT, 5, 1, 1

/COM, lines for the mid-thickness (crack tip to crack-free
edge)
L, 23, 24
*REPEAT, 6, 1, 1
/COM, lines for the top of specimen
L,30,31
*REPEAT, BSKP-1, 1, 1

/COM, *** Vertical Lines ***
L, 1, 13
*REPEAT, 5, 1, 1
L, 6, 23
*REPEAT, 7, 1, 1
L, 18, 30
*REPEAT, 5, 1, 1
L, 23, 35
*REPEAT, 7, 1, 1

*IF, option, EQ, 1, THEN
/COM, Lines for the tabs
/COM, *** BOTTOM ***
L, 2, 42
```

```
*REPEAT, 3, 1, 1
L, 42, 45
*REPEAT, 3, 1, 1
L, 42, 43
*REPEAT, 2, 1, 1
L, 45, 46
*REPEAT, 2, 1, 1
/COM, *** TOP ***
L, 31, 48
*REPEAT, 3, 1, 1
L, 48, 51
*REPEAT, 3, 1, 1
L, 48, 49
*REPEAT, 2, 1, 1
L, 51, 52
*REPEAT, 2, 1, 1
*ENDIF

/COM, Creation of area from lines
AL,1,40,12,39
*REPEAT, 5, 1, 1, 1, 1
AL,6,45,22,44
*REPEAT, 6, 1, 1, 1, 1
AL,17,52,28,51
*REPEAT, 5, 1, 1, 1, 1
AL,22,57,33,56
*REPEAT, 6, 1, 1, 1, 1

*IF, option, EQ, 1, THEN
/COM, area for tabs
AL, 69, 64, 2, 63
*REPEAT, 2, 1, 1, 1, 1
AL, 71, 67, 69, 66
*REPEAT, 2, 1, 1, 1, 1
AL, 29, 74, 79, 73
*REPEAT, 2, 1, 1, 1, 1
AL, 79, 77, 81, 76
*REPEAT, 2, 1, 1, 1, 1
*ELSEIF, option, EQ, 2, EXIT
*ENDIF

*IF, spec, EQ, 3, THEN

/COM, *********************************
/COM, *** Creating the Loading Lever ***
```

```
/COM, **********************************
/COM, moving the working plane to KP52
/COM, and changing active CS to WP
KWPAVE, 52
CSYS, WP

/COM, *** Creating the Radius of the Clevice ***
K, 54, ,-RD1
K, 55, -RD1*COS(pi/4), -RD1*SIN(pi/4)
K, 56,  RD1*COS(pi/4), -RD1*SIN(pi/4)
K, 57,  -0.013/2
K, 58,  RD1*COS(pi)
K, 59,
K, 60,  RD1*COS(0)
K, 61,  0.013/2


/COM, *** Creating the loading lever roller ***
/COM, THE HIGHEST KP is 61
RD2=0.0095/2        ! RADIUS of loading lever roller
KGEN, 2, 57, 61, ,g_sl/2
K,67, KX(38), KY(38)+RD2
KWPAVE, 67

CSYS, WP
K, 62, ,-RD2
K, 63, -RD2*COS(pi/4), -RD2*SIN(pi/4)
K, 64,  RD2*COS(pi/4), -RD2*SIN(pi/4)
K, 65,  -0.03412/2
K, 66,  RD2*COS(pi)
K, 67,
K, 68,  RD2*COS(0)
K, 69,  0.03412/2

/COM, NOTE: KP70 is also temporarily defined and redefined
K,70,KX(67)+g_cll,KY(67)+0.0017+g_t/2
!K,70,KX(67)+g_cll,KY(67)+0.0010+g_t/2

KWPAVE, 70
!LDPT=0.028754      ! LDPT=Loading Point in y position
!LDPT=0.028344      ! from LDPT, G_HLL optimization
!LDPT=0.028512      ! from LDPT, G_HLL, optimization
OPTYPE, FIRST
LDPT=0
```

```
K, 70,-0.03814/2,-LDPT  ! KP70 is redefined here
K, 71,          ,-LDPT
K, 72, 0.03814/2,-LDPT

LDHT=KY(71)-KY(28)  ! LDHT is loading point height from
                    ! the mid-thickness of specimen

/COM, *** Creating the bottom of LOADING LEVER keypoints
***
/COM, NOTE: The variable "diff" is to accommodate the
changing
/COM,       tab heights from different specimens
diff=KY(65)-KY(57)
KGEN, 2, 57, 61, ,,g_hll+diff
KGEN, 2, 65, 69, ,,g_hll
KGEN, 2, 70, 72, ,,g_hll-(KY(70)-KY(69))
*GET,AA,KP,0,NUM,MAX          ! AA is a dummy variable
KSEL,,LOC,Y,KY(AA)
*GET, BB, KP, 0, NUM, MIN     ! BB is a dummy variable
K,AA+1,KX(BB)+0.16380,KY(BB)
ALLS

/COM, *** Creating the top of LOADING LEVER keypoints ***
KGEN, 2, 73, AA+1, ,,g_tll
*SET,AA
*SET,BB

/COM, *** horizontal lines first ***
L, 57, 58
*REPE, 4, 1, 1
L, 65, 66
*REPE, 4, 1, 1
L, 70, 71
*REPE, 2, 1, 1
L, 73, 74
*REPE, 13, 1, 1
L, 87, 88     ! KP87 does not exist at this point????
*REPE, 13, 1, 1

/COM, *** vertical lines secondly ***
L, 54, 59
L, 62, 67

/COM, vertical lines for the loading roller
L, 57, 73
```

```
*REPEAT, 5, 1, 1
L, 65, 78
*REPEAT, 5, 1, 1
L, 70, 83
*REPEAT, 3, 1, 1
L, 73, 87
*REPE, 14, 1, 1

/COM, *** arches finally ***
LARC, 58, 54, 55
LARC, 54, 60, 56
LARC, 66, 62, 63
LARC, 62, 68, 64

/COM, *** Area now ***
AL, 148, 119, 84
AL, 149, 85, 119
AL, 150, 120, 88
AL, 151, 89, 120

AL, 83, 122, 93, 121
*REPE, 4, 1, 1, 1, 1
AL,  87, 127, 98, 126
*REPE, 4, 1, 1, 1, 1
AL, 91, 132, 103, 131
*REPE, 2, 1, 1, 1, 1

/COM, Area for top part of loading lever
AL, 93, 135, 106, 134
*REPE, 13, 1, 1, 1, 1
*ENDIF

/COM, *** Elements ***
ET,1,PLANE82   ! Element Type, Ref#, name of El. type
KEYOPT,1,3,2
KEYOPT,1,5,2
KEYOPT,1,6,0

/COM, *** The specimen MP's, 5 MP's only <== transversely
isotropic ***
*IF,MPREAL,EQ,0,THEN
     *IF, MATR, EQ, 1, THEN
          e1=27.9E+09
          e2=7.44E+09
          v12=0.33
```

```
          v23=0.44
          g12=3.05E+09
          densc=1686     ! densc=density of composite
material
          vfa=36.7  ! average fiber volume percentage
     *ELSEIF, MATR, EQ, 2, THEN
          e1=31.1E+09
          e2=7.96E+09
          v12=0.33
          v23=0.44
          g12=3.05E+09
          densc=1585
          vfa=34.2
     *ELSEIF, MATR, EQ, 3, THEN
          e1=31.0E+09
          e2=7.38E+09
          v12=0.33
          v23=0.44
          g12=3.05E+09
          densc=1569
          vfa=32.4
     *ENDIF
*ELSEIF,MPREAL,NE,0,THEN
     e1=EL
     e2=ET
     g12=GLT
     v12=vLT
     v23=0.44
     vfa=vf         ! vfa=average fiber volume percentage
     *IF, MATR, EQ, 1, THEN
          densc=1686     ! densc=density of composite
material
     *ELSEIF, MATR, EQ, 2, THEN
          densc=1585
     *ELSEIF, MATR, EQ, 3, THEN
          densc=1569
     *ENDIF
*ENDIF

e3=e2
v13=v12
g13=g12
g23=e2/(2*(1+v23))

MPTEMP,,,,,,,,
```

```
MPTEMP,1,0
MPDATA,EX,1,,e1
MPDATA,EY,1,,e2
MPDATA,EZ,1,,e3
MPDATA,PRXY,1,,v12
MPDATA,PRYZ,1,,v23
MPDATA,PRXZ,1,,v13
MPDATA,GXY,1,,g12
MPDATA,GYZ,1,,g23
MPDATA,GXZ,1,,g13
MPDATA,DENS,1,,densc

/COM, The tabs' and part of loading lever MP's
e1_al=70E+09   ! aluminum young's mod
v12_al=0.3          ! al poisson ratio
dens_al=2710
MPDATA,EX,2,,e1_al
MPDATA,PRXY,2,,v12_al
MPDATA,DENS,2,,dens_al

/COM, Part of loading lever MP's
e1_fe=206.8E+09     ! steel modulus of elasticity
v12_fe=0.3          ! steel poisson ratio
dens_fe=7870
MPDATA,EX,3,,e1_fe
MPDATA,PRXY,3,,v12_fe
MPDATA,DENS,3,,dens_fe

/COM, *** Attribute assignment ***
/COM, NOTE: MUST BE BEFORE MESHING!!!
ALLS
ASEL, S, ,,1, 22
AATT, 1,, 1, 0
ALLS

/COM, retrieving the maximum numbers of area
*GET, anmax, AREA, 0, NUM, MAX

/COM, if tabs are included, then aluminum material props
/COM, are used
*IF, option, EQ, 1, THEN
     ASEL,S, AREA, ,23,30
     AATT, 2,, 1, 0
     ALLS
```

```
*ENDIF


*IF, spec,EQ,3, THEN
/COM, attribute assignment for steel and alum part of the
loading lever
ASEL, S, AREA, ,31,42
AATT, 3,,1,0
ASEL, S, AREA, ,43, anmax
AATT, 2,,1,0
*ENDIF

/COM, Initial Line-Mapping Operation for Specimen
ASEL,S, ,,1, 22
LSLA, R
LESIZE,ALL, elesize
ALLS

/COM, ===========================
/COM, ALTERNATIVE Mesh Refinement at KPSING
NDIVKP23=40  ! The number of division of lines emanating
from KP23
SPCRT23=0.2 ! The spacing ratio for lines emanating from
KP23
LSEL, ,,,16
LSEL, A,,,21
LSEL, A,,,44
LESIZE,ALL,,,NDIVKP23,SPCRT23,1,,0
ALLS
LSEL, S,,,22
LSEL, A,,,56
LESIZE,ALL,,,NDIVKP23,1/SPCRT23,1,,0  ! 1/SPCRT23 for
flipping the spacing ratio
ALLS
/COM, ===========================

/COM, Meshing Operation for Specimen FIRST
AMESH, 1,22
*GET, LINDIV2, LINE, 2, ATTR, NDIV

/COM, Line-Mapping Operation for the tabs (incl. the
specimen
/COM,where it is in contact with the tabs)
*IF, option, EQ, 1, THEN
ASEL,S, ,,23,anmax
```

```
LSLA, R
LSEL, R,,, 2, 3
LSEL, A,,, 13, 14
LSEL, A,,, 18, 19
LSEL, A,,, 29, 30
LSEL, A,,, 69, 72
LSEL, A,,, 79, 82
CM, _Y1, LINE
LSEL, ,,,_Y1
LESIZE,_Y1, , ,LINDIV2, ,4 , , ,1
ALLS

LSEL,S,,,63,68
LSEL,A,,,73,78
CM, _Y2, LINE
LSEL, ,,,_Y2
LESIZE,_Y2, , ,LINDIV2/2, ,1 , , ,1

ALLS

/COM, Meshing operation for the tabs ONLY
MSHKEY, 1
AMESH, 23, 30
*ENDIF

/COM, Initial Line-Mapping for the Loading Lever
*IF, spec, EQ, 3, THEN
ALLS
ASEL, S, AREA, ,31, anmax
LSLA, R
CM, _Y3, LINE
LSEL, ,,,_Y3
LESIZE, _Y3, 0.005,,,,,,,1
MSHAPE, 0, 2D

/COM, Line-Mapping on the loading lever mid-roller
/COM, and the hinges
ALLS
LSEL, S,,, 148, 151
CM, _Y4, LINE
LSEL, ,,,_Y4,
LESIZE, _Y4, 0.001,,,,,,,1

/COM, Meshing Operation for the Loading Lever
ALLS
```

```
MSHKEY, 1
AMESH, 31, anmax
*ENDIF

/COM, Deleting line components for mesh control
CMDELE, _Y1
CMDELE, _Y2
*IF, spec, EQ, 3, AND, option, EQ, 1, THEN
     CMDELE, _Y3
     CMDELE, _Y4
*ENDIF

!ALLS
!============================
! Mesh Refinement at KPSING
!N=4
!*DO, count, 1, N
!KREF, KPSING,,,1,1,1,1
!*ENDDO
!============================

*IF, spec, EQ, 3, THEN
/COM, *** Coupling the nodes at "T" tabs + Loading Lever
***
WPAVE, 0,0,0
CSYS, WP
KSEL, S, KP, ,52
NSLK, R
KSEL, A, KP, ,59
NSLK, A
CP,2001, UX, ALL
CP,2002, UY, ALL
ALLS
*ENDIF

/COM, Creating target component
/COM, Target of crack interface
/COM, ### RESTORING THE COORDINATE SYSTEM ###
CSYS, 0
ASEL, S, LOC, X, 0, g_a
ASEL, R, LOC, Y, 0, g_t/2
LSEL, R, EXT
LSEL, R, LOC, Y, g_t/2
NSLL, R, 1
```

```
/COM, removing the two nodes closest to the crack tip
*GET, MXTG, NODE,,MXLOC, X
NSEL, U, LOC, X, MXTG
*GET, MXTG2, NODE,,MXLOC, X
NSEL, U, LOC, X, MXTG2
CM, TARGET, NODE
ALLS

*IF, spec, EQ, 3, THEN
/COM, target of loading lever mid-roller
/COM, ###  THIS MUST BE THE TARGET, BECAUSE IT'S COARSER
###
/COM, ###                THAN THE SPECIMEN
###
LSEL, S, , , 150,151
NSLL, R, 1
CM, TARGET2, NODE
ALLS
*ENDIF

/COM, creating contact component
ALLS
ASEL, S, LOC, X, 0, g_a
ASEL, R, LOC, Y, g_t/2, g_t
LSEL, R, EXT
LSEL, R, LOC, Y, g_t/2
NSLL, R, 1

/COM, removing the two nodes closest to the crack tip
*GET, MXCT, NODE,,MXLOC, X
NSEL, U, LOC, X, MXCT
*GET, MXCT2, NODE,,MXLOC, X
NSEL, U, LOC, X, MXCT2
CM, CONTACT, NODE
ALLS

*IF, spec, EQ, 3, THEN
/COM, contact of loading lever mid-roller (with specimen)
ALLS
LSEL,S,LOC,X,KX(37),KX(39)
LSEL,R,LOC,Y,KY(37)
NSLL, R, 1
CM, CONTACT2, NODE
ALLS
*ENDIF
```

```
*IF, spec, EQ, 2, THEN
/COM, ##################################
/COM, ### CONTACT AT CRACK INTERFACE ###
/COM, ##################################
/COM, *** Contact Pair Creation - START ***
CM,_NODECM,NODE
CM,_ELEMCM,ELEM
CM,_LINECM,LINE
CM,_AREACM,AREA
/GSAV,cwz,gsav,,temp
MP,MU,1,MU_BI       ! MU = coefficient of friction of Beam
Interface
MAT,1
R,3
REAL,3
ET,2,169
ET,3,172
RMODIF,3,1,,,0.1,0.1,,   ! FKN=0.1, FTOLN=0.1 GOOD
NUMBERS!!!
                    ! FKN=0.01, FTOLN=0.01 BETTER
NUMBERS!!!
                    ! FTOLN=0.01 ==> TOO MUCH PENETRATION
                    ! Original numbers, 0.1 and 1
RMODIF,3,7,,,1.0e20,-1E-8,0.01
KEYOPT,3,1,0   ! UX, UY  DOF
KEYOPT,3,2,0   ! Penalty function + Lagrange multiplier
(default)
KEYOPT,3,3,0   ! use with h-element, no superelements
KEYOPT,3,4,0   ! On Gauss point (for general cases)
KEYOPT,3,5,3   ! 3=close gap/reduce penetration
               ! 2=reduce penetration
               ! 0=no adjustment
KEYOPT,3,6,0   ! symm/unsymm stiffness matrix
KEYOPT,3,7,2   ! 1=auto-bisect 2=Reason time/load 3=min
KEYOPT,3,8,0   ! 0=no prevention of spurious contact,1=yes
KEYOPT,3,9,0   ! 0=include geom pen and offset
               ! 1=exclude geom pen and offset
KEYOPT,3,10,2  ! update stiffness matrix every substep
KEYOPT,3,11,0
KEYOPT,3,12,0  ! 0=standard 2=sliding (no sepa)

/COM, Generate the target surface
NSEL,S,,,TARGET
CM,_TARGET,NODE
```

```
TYPE,2
ESLN,S,0
TSHAP, LINE
ESURF,ALL
CMSEL,S,_ELEMCM

/COM, Generate the contact surface
NSEL,S,,,CONTACT
CM,_CONTACT,NODE
TYPE,3
ESLN,S,0
TSHAP, LINE
ESURF,ALL
ALLSEL
ESEL,ALL
ESEL,S,TYPE,,2
ESEL,A,TYPE,,3
ESEL,R,REAL,,3
/PSYMB,ESYS,1
/PNUM,TYPE,1
/NUM,1

ESEL,ALL
ESEL,S,TYPE,,2
ESEL,A,TYPE,,3
ESEL,R,REAL,,3
CMSEL,A,_NODECM
CMDEL,_NODECM
CMSEL,A,_ELEMCM
CMDEL,_ELEMCM
CMSEL,S,_LINECM
CMDEL,_LINECM
CMSEL,S,_AREACM
CMDEL,_AREACM
/GRES,cwz,gsav
CMDEL,_TARGET
CMDEL,_CONTACT
/COM, *** Contact Pair Creation - END ***

*ELSEIF, spec, EQ, 3, THEN
     /COM, ###################################
     /COM, ### CONTACT AT ROLLER INTERFACE ###
     /COM, ###################################
     /COM, *** Contact Pair Creation - START ***
     CM,_NODECM,NODE
```

```
     CM,_ELEMCM,ELEM
     CM,_LINECM,LINE
     CM,_AREACM,AREA
     /GSAV,cwz,gsav,,temp
     MP,MU,1,MU_RI                ! Coefficient of
friction of Roller Interfaces
     MAT,1
     R,4
     REAL,4
     ET,4,169
     ET,5,172
     RMODIF,4,1,RD2,,0.01,0.1,,        !
RD2=R1,,FKN=1,FTOLN=1
     !RMODIF,4,7,5e-5,1e-5,1.0e20,,1.0  ! CNOF is not
defined, but will be
                                  ! automatically defined
because
                                  ! KEYOPT(5)=3
     RMODIF,4,7,,,1.0e20,-1E-8,0.01
     KEYOPT,5,1,0   ! UX, UY  DOF
     KEYOPT,5,2,0   ! Penalty function + Lagrange
multiplier (default)
     KEYOPT,5,3,0   ! use with h-element, no superelements
     KEYOPT,5,4,0   ! On Gauss point (for general cases)
     KEYOPT,5,5,3   ! 2=reduce penetration, 3=close
gap/reduce penetration
     KEYOPT,5,7,2   ! 1=bisection, 2=reasonable time/load
increment
     KEYOPT,5,8,1   ! 1=spurious contact is detected and
ignored
     KEYOPT,5,9,2   ! 2=include geom pen and off with ramp
effect
     KEYOPT,5,10,2  ! 2=update contact stiffness at every
substep
     KEYOPT,5,12,0  ! 0=standard contact
                    ! 2=no separation sliding permitted

     ! Generate the target surface
     NSEL,S,,,TARGET2
     CM,_TARGET,NODE
     TYPE,4
     ESLN,S,0
     TSHAP, CARC
     ESURF,ALL
     CMSEL,S,_ELEMCM
```

```
     ! Generate the contact surface
     NSEL,S,,,CONTACT2
     CM,_CONTACT,NODE
     TYPE,5
     ESLN,S,0
     TSHAP, LINE
     ESURF,ALL
     ALLSEL
     ESEL,ALL
     ESEL,S,TYPE,,4
     ESEL,A,TYPE,,5
     ESEL,R,REAL,,4
     /PSYMB,ESYS,1
     /PNUM,TYPE,1
     /NUM,1
     ESEL,ALL
     ESEL,S,TYPE,,4
     ESEL,A,TYPE,,5
     ESEL,R,REAL,,4
     CMSEL,A,_NODECM
     CMDEL,_NODECM
     CMSEL,A,_ELEMCM
     CMDEL,_ELEMCM
     CMSEL,S,_LINECM
     CMDEL,_LINECM
     CMSEL,S,_AREACM
     CMDEL,_AREACM
     /GRES,cwz,gsav
     CMDEL,_TARGET
     CMDEL,_CONTACT
     /COM, *** Contact Pair Creation - END ***
*ENDIF

ALLS

/COM, *** Performing mass test of loading lever ***
loadpass=0
*IF, loadpass, EQ, 0, THEN
     /COM, *** Boundary Conditions ***
     *IF, spec, EQ, 1, THEN
          *IF, option, EQ, 1, THEN

               DK,46,UY,0     ! DOF, KP46, UY, Fix
               DK,46,UX,0     ! DOF, KP46, UY, Fix
```

```
                DK,52,UX,0     ! DOF, KP52, UY, Fix
                FK,52,FY, F_y  ! KP52, y-dir, mag
           *ELSEIF, option, EQ, 2, THEN
                DK,3,UY,0       ! DOF, KP3, UY, Fix
                DK,3,UX,0       ! DOF, KP3, UX, Fix
                DK,32,UX,0          ! DOF, KP32, UX, FIX
                FK,32,FY, F_y  ! KP32, y-dir, mag
           *ENDIF
      *ELSEIF, spec, EQ, 2, THEN
           *IF, option, EQ, 1, THEN
                DK,46,UY,0      ! DOF, KP46, UY, Fix
                DK,46,UX,0      ! DOF, KP46, UX, Fix
           *ELSEIF, option, EQ, 2, THEN
                DK,3,UY,0       ! DOF, KP3, UY, Fix
                DK,3,UX,0      ! DOF, KP3, UX, Fix
           *ENDIF
           DK,11,UY,0     ! DOF, KP11, UY, Fix
           FK,38,FY, F_y
      *ELSEIF, spec, EQ, 3, THEN
           DK,46,UY,0      ! DOF, KP46, UY, Fix
           DK,46,UX,0      ! DOF, KP46, UX, Fix
           DK,11,UY,0      ! DOF, KP11, UY, Fix
           FK,71,FY, F_y  ! Loading Lever Load, KP71, y-dir,
mag
      *ENDIF
*ELSEIF, loadpass, EQ, 1, THEN
      *IF, spec, EQ, 1, THEN
           *IF, option, EQ, 1, THEN
                DK,46,UY,0     ! DOF, KP46, UY, Fix
                DK,46,UX,0     ! DOF, KP46, UY, Fix
                DK,52,UX,0     ! DOF, KP52, UY, Fix
           *ELSEIF, option, EQ, 2, THEN
                DK,3,UY,0       ! DOF, KP3, UY, Fix
                DK,3,UX,0       ! DOF, KP3, UX, Fix
                DK,32,UX,0          ! DOF, KP32, UX, FIX
           *ENDIF
      *ELSEIF, spec, EQ, 2, THEN
           *IF, option, EQ, 1, THEN
                DK,46,UY,0      ! DOF, KP46, UY, Fix
                DK,46,UX,0      ! DOF, KP46, UX, Fix
           *ELSEIF, option, EQ, 2, THEN
                DK,3,UY,0       ! DOF, KP3, UY, Fix
                DK,3,UX,0      ! DOF, KP3, UX, Fix
           *ENDIF
           DK,11,UY,0     ! DOF, KP11, UY, Fix
```

```
     *ELSEIF, spec, EQ, 3, THEN
          DK,46,UY,0      ! DOF, KP46, UY, Fix
          DK,46,UX,0      ! DOF, KP46, UX, Fix
          DK,11,UY,0      ! DOF, KP11, UY, Fix
     *ENDIF
*ENDIF

/COM, #### Node selection for postprocessing BEGIN###
KSEL, ,,,KPSING
/PNUM, KP, 1
/PNUM, NODE, 1
/PNUM, ELEM, 1
NSLK, R
ESLN, R, ,
NSLE, A, ALL
LSEL,S,,,21
NSLL, R
*GET, NJ, NODE, 0, NUM, MAX
*GET, NI, NODE, NJ, NXTL
ALLS

LSEL,S,,,16
NSLL, R
*GET, NJP, NODE, 0, NUM, MAX
*GET, NIP, NODE, NJP, NXTL
ALLS

KSEL, ,,,KPSING
NSLK, R
*GET, NK, NODE, 0, NUM, MAX
ALLS

LSEL,S,,,KPSING-1
NSLL, R  !select only interior nodes, witty!
*GET, NL, NODE, 0, NUM, MIN
*GET, NM, NODE, NL, NXTH
ALLS

DELTA=NX(NM)-NX(NK)

/PNUM, KP, 0
/PNUM, NODE, 0
/PNUM, ELEM, 0
/COM, #### Node selection for postprocessing END###
```

```
WPSTYLE,,,,,,,,0                ! turning off WP
ALLS                            ! Select All Entities

! *** Selection of Deflection point ***
*IF, spec, EQ,1, THEN
     *IF, option, EQ, 1,  THEN   ! include tabs
          KSEL,,,,52
     *ELSEIF, option, EQ, 2, THEN
          KSEL,,,,32
     *ENDIF
*ELSEIF, spec, EQ, 2, THEN
     KSEL,,,,38
*ELSEIF, spec, EQ, 3, THEN
     KSEL,,,,71
*ENDIF

NSLK,R
*GET,DFLN,NODE,0,NUM,MAX
ALLS
FINISH

/SOLU
!EQSLV, SPARSE      ! Already default
ANTYPE,0
NLGEOM,NLGEOMV
SOLCONTROL, ON, ON!FF    ! Enhanced internal solution
algorithms

KBC, 0              ! Ramped
OUTPR, ALL, ALL         ! To output file(.out), all
results, LS freq.
OUTRES, ALL, ALL

/COM, ###################################################
/COM, ###### UNSYMMETRIC NEWTON RAPHSON METHOD IS #######
/COM, ##### ACCURATE BUT CAN CONSIDERABLY MORE TIME #####
/COM, ### CONSUMING IF APPLICATION IS NOT APPROPRIATE ###
/COM, ###################################################
*IF, spec, EQ, 1, THEN
     NSUBST,,,,ON   ! Specifying the number of substeps to
be taken in this load step
     NROPT, FULL,,OFF    ! Full Newton Raphson Method
                    ! with ("ON") Adaptive Descent
                    ! Automatically "OFF" with ARCLEN
*ELSEIF, spec, EQ, 2, THEN
```

```
     NSUBST,10,1000,3,ON
     NROPT, UNSYM,,OFF
*ELSEIF, spec, EQ, 3,THEN
     NSUBST,20,1000,3,ON ! Specifying the number of
substeps to be taken in this load step
     NROPT, UNSYM,,OFF   ! with ("OFF") no Adaptive Descent
                    ! Adaptive descent may cause
                    ! convergence problem in ENF spec
                    ! While Unsymmetric NRM is accurate
                    ! but requires smaller time steps
*ENDIF

ARCLEN,ON           ! AGGRESSIVE TIME STEPPING!

ACEL,,9.8           ! including acceleration field==> mass
matters!

ALLS

/COM, *** Retrieving the STARTING TIME of Solution ***
*GET, TINIT, ACTIVE, 0, TIME, CPU
SAVE,MMB_geom5,db,MMB
/GROPT,VIEW,1
/GST, ON
/STAT, SOLU

SOLVE
FINISH

/COM, *** Retrieving the ENDING TIME of Solution ***
*GET, TFINAL, ACTIVE, 0, TIME, CPU

/COM, *** Calculating the SOLUTION TIME ***
SOLTIME=TFINAL-TINIT
FINISH

/POST1
/DSCALE,1,1              ! No displacement Scaling

/COM, *** Retrieving SERR from each substep ***
SET,LAST
*GET,LASTST,ACTIVE,,SET,SBST

/COM, *** retrieving the reaction forces ***
/COM, NOTE:  the sequence of NFORCE, NSEL .., FSUM, *GET is
```

```
/COM,           is very important
ALLS
ASEL,, LOC, Y, g_t/2, g_t,,1
NFORCE
NSEL,,,,NK
FSUM
*GET, F_KY, FSUM,,ITEM,FY
*GET, F_KX, FSUM,,ITEM,FX
NSEL,,,,NL
FSUM
*GET, F_LY, FSUM,,ITEM,FY
*GET, F_LX, FSUM,,ITEM,FX
ALLS

VI=UY(NI)
VJ=UY(NJ)
VIP=UY(NIP)
VJP=UY(NJP)
UI=UX(NI)
UJ=UX(NJ)
UIP=UX(NIP)
UJP=UX(NJP)

/COM, *****************************
/COM, **** MBT SERR Calculation ***
/COM, *****************************
*IF, spec, EQ, 1, THEN
lam=1/(g_t/2)*(6*e2/e1)**0.25
GICx_1=12*load**2
GICx_2=g_w**2*(g_t/2)**3*e1
GICx_31=g_r1_a**2+2*g_r1_a/lam+1/lam**2
GICx_32=(g_t/2)**2*e1/(10*g13)
GICx_3=GICx_31+GICx_32
GICx=GICx_1/GICx_2*GICx_3
!GICx=(12*load**2)/(g_w**2*(g_t/2)**3*e1)*(g_r1_a**2+2*g_r1
_a/lam+1/lam**2+(g_t/2)**2*e1/(10*g13))
*ELSEIF, spec, EQ, 2, THEN
GIICx=(9*load**2)/(16*g_w**2*(g_t/2)**3*e1)*(g_r1_a**2+0.2*
(g_t/2)**2*e1/g13)
*ELSEIF, spec, EQ, 3, THEN
lam=1/(g_t/2)*(6*e2/e1)**0.25
/COM, NOTE: GICx has to be split because of "too many
parameters"
GICx_1=(3*load**2*(3*g_c-g_sl/2)**2)
GICx_2=(4*g_w**2*(g_t/2)**3*(g_sl/2)**2*e1)
```

```
GICx_31=(g_r1_a**2+2*g_r1_a/lam+1/lam**2)
GICx_32=(g_t/2)**2*e1/(10*g13)
GICx_3=GICx_31+GICx_32
GICx=GICx_1/GICx_2*GICx_3
!GICx=(3*load**2*(3*g_c-
g_sl/2)**2)/(4*g_w**2*(g_t/2)**3*(g_sl/2)**2*e1)*(g_r1_a**2
+2*g_r1_a/lam+1/lam**2+(g_t/2)**2*e1/(10*g13))
GIICx=(9*load**2*(g_c+g_sl/2)**2)/(16*g_w**2*(g_t/2)**3*(g_
sl/2)**2*e1)*(g_r1_a**2+0.2*(g_t/2)**2*e1/g13)
*ENDIF

/COM, ************************************
/COM, ***  MBT Deflection Calculation  ***
/COM, ************************************
*IF, spec, EQ, 1, THEN
     part1=64*1/e1/g_t**3/g_w*g_r1_a**3*load
     part2=24/5/g_t/g_w/g13*g_r1_a*load
     part3=192/e1/g_t**3/lam/g_w*g_r1_a**2*load
     part4=192/e1/g_t**3/lam**2/g_w*g_r1_a*load
     part5=96/e1/g_t**3/lam**3/g_w*load
     ddcbmbt=part1+part2+part3+part4+part5
*ELSEIF, spec, EQ, 2, THEN
     part1=2*(9/40*g_r1_a+3/20*g_sl)*load/g_t/g_w/g13
     part2=8*(3/8*g_r1_a**3+1/32*g_sl**3)/e1*load/g_t**3/g_
w
     denfmbt=part1+part2
*ELSEIF, spec, EQ, 3, THEN
     dmmbmbt=0
*ENDIF

/COM, **************************************
/COM, *** Required Element Size (DELTA) ***
/COM, **************************************
/COM, d_req is the required DELTA size
d_req=g_r1_a*0.005  ! ANSYS Recommendation

/COM, **************************************
/COM, **** FEA SERR Calculation, VCCT_1 ***
/COM, **************************************

GIC=1/(2*DELTA)*(F_KY*(VI-VIP)+F_LY*(VJ-VJP))
GIIC=1/(2*DELTA)*(F_KX*(UI-UIP)+F_LX*(UJ-UJP))
!*GET,defl_ans,NODE,DFLN,U,Y
defl_ans=UY(DFLN)
```

```
*IF, spec, EQ, 3, THEN
/COM, *** Selection of Variables for OPTIMIZATION (OBJ) ***
GIDIFF=1/GIC   ! GIDIFF the inverse of GIC
               ! Objective variable for optimization
RES_RG=ABS(ABS(GICx/GIICx)-ABS(GIc/GIIC))    ! RES_RG
residual Rg=GI/GII
RES_GI=ABS(GIC-GICx)
RES_GII=ABS(GIIC-GIICx)
SSE_G=RES_GI**2+RES_GII**2
*ENDIF

*IF, spec, EQ, 3, AND, option, EQ, 2, THEN
     defl_ans=0
*ENDIF

*DIM,LABEL1,CHAR,1,2
*DIM,LABEL2,CHAR,1,2
*DIM,LABEL3,CHAR,3,2
*DIM,LABELMP,CHAR,5,2
*DIM,LABELVF,CHAR,1,2
*DIM,LABELMU,CHAR,2,1
*DIM,VALUE1,,1,3
*DIM,VALUE2,,1,5
*DIM,VALUE3,,3,3
*DIM,VALUEMP,,5,3
*DIM,VALUEVF,,1,3
*DIM,VALUEMU,,2,1
LABEL1(1,1) = 'elesize'
LABEL1(1,2) = 'm'
LABEL2(1,1) = 'deflectn'
LABEL2(1,2) = 'm'
LABEL3(1,1) = 'GI','GII','G-ratio'
LABEL3(1,2) = 'J/m2','J/m2','unitless'
LABELMP(1,1) = 'E11','E22','G12','v12','G23'
LABELMP(1,2) = 'Pa','Pa','Pa','unitless','Pa'
LABELVF(1,1) = 'Vf'
LABELVF(1,2) = '%'
LABELMU(1,1) = 'mu_bi','mu_ri'
*VFILL,VALUEMP(1,1),DATA,EL,ET,GLT,vLT,g23
*VFILL,VALUEMP(1,2),DATA,e1,e2,g12,v12,g23
*VFILL,VALUEMP(1,3),DATA,e1/EL,e2/ET,g12/GLT,v12/vLT,g23/g2
3
*VFILL,VALUEVF(1,1),DATA,vf
*VFILL,VALUEVF(1,2),DATA,vfa
*VFILL,VALUEVF(1,3),DATA,vf/vfa
```

```
*VFILL,VALUEMU(1,1),DATA,MU_BI,MU_RI

*IF, MATR, EQ, 1, THEN
     ddcb=0.000836
     denf=-0.003835
     dmmb=-0.003429
*ELSEIF, MATR, EQ, 2, THEN
     ddcb=0.004491
     denf=-0.004324
     dmmb=-0.004073
*ELSEIF, MATR, EQ, 3, THEN
     ddcb=0.001310
     denf=-0.006129
     dmmb=-0.005261
*ENDIF

*IF, spec, EQ, 1, THEN
     *VFILL,VALUE1(1,1),DATA,d_req
     *VFILL,VALUE1(1,2),DATA,delta
     *VFILL,VALUE1(1,3),DATA,delta/d_req
     *VFILL,VALUE2(1,1),DATA,ddcb
     *VFILL,VALUE2(1,2),DATA,ddcbmbt
     *VFILL,VALUE2(1,3),DATA,defl_ans
     *VFILL,VALUE2(1,4),DATA,ABS(ddcbmbt/ddcb)
     *VFILL,VALUE2(1,5),DATA,ABS(defl_ans/ddcb)
     *VFILL,VALUE3(1,1),DATA,GICx,0, 0
     *VFILL,VALUE3(1,2),DATA,GIC ,GIIC, GIC/GIIC
     *VFILL,VALUE3(1,3),DATA,ABS(GIC/GICx), 0, 0
*ELSEIF, spec, EQ, 2, THEN
     *VFILL,VALUE1(1,1),DATA,d_req
     *VFILL,VALUE1(1,2),DATA,delta
     *VFILL,VALUE1(1,3),DATA,delta/d_req
     *VFILL,VALUE2(1,1),DATA,denf
     *VFILL,VALUE2(1,2),DATA,denfmbt
     *VFILL,VALUE2(1,3),DATA,defl_ans
     *VFILL,VALUE2(1,4),DATA,ABS(denfmbt/denf)
     *VFILL,VALUE2(1,5),DATA,ABS(defl_ans/denf)
     *VFILL,VALUE3(1,1),DATA,0, GIICx, 0
     *VFILL,VALUE3(1,2),DATA,GIC, GIIC , GIC/GIIC
     *VFILL,VALUE3(1,3),DATA,0, ABS(GIIC/GIICx),0
*ELSEIF, spec, EQ, 3, THEN
     *VFILL,VALUE1(1,1),DATA,d_req
     *VFILL,VALUE1(1,2),DATA,delta
     *VFILL,VALUE1(1,3),DATA,delta/d_req
     *VFILL,VALUE2(1,1),DATA,dmmb
```

```
     *VFILL,VALUE2(1,2),DATA,dmmbmbt
     *VFILL,VALUE2(1,3),DATA,defl_ans
     *VFILL,VALUE2(1,4),DATA,ABS(dmmbmbt/dmmb)
     *VFILL,VALUE2(1,5),DATA,ABS(defl_ans/dmmb)
     *VFILL,VALUE3(1,1),DATA,GICx,GIICx,GICx/GIICx
     *VFILL,VALUE3(1,2),DATA,GIC, GIIC, GIC/GIIC
     *VFILL,VALUE3(1,3),DATA,ABS(GIC/GICx),
ABS(GIIC/GIICx), (GICx/GIICx)/(GIC/GIIC)
*ENDIF

/COM, *** Filename Convention ***
/COM, First initials of filename: type of test
*IF,spec,EQ,1,THEN
     anfile='DCB_'
     andir='DCB'
*ELSEIF,spec,EQ,2,THEN
     anfile='ENF_'
     andir='ENF'
*ELSEIF,spec,EQ,3,THEN
     anfile='MMB_'
     andir='MMB'
*ENDIF
anext='vrt'

/COM, Second initials of filename: type of material
*IF, MATR, EQ, 1, THEN
     MA='PE_'
*ELSEIF, MATR, EQ, 2, THEN
     MA='VE_'
*ELSEIF, MATR, EQ, 3, THEN
     MA='EE_'
*ENDIF

/COM, Third initials of filename: type of solution
*IF, NLGEOMV, EQ, 0, THEN
     SLN='LIN_'
*ELSEIF, NLGEOMV, EQ, 1, THEN
     SLN='NL_'
*ENDIF

*IF, option, EQ, 1, THEN
     OP='TAB'
*ELSEIF, option, EQ, 2, THEN
     OP='NT'
*ENDIF
```

```
*IF,LDPT,EQ,0,THEN
     FIX=''
*ELSEIF,LDPT,NE,0,THEN
     FIX='_ADJ'
*ENDIF


/COM, *** SUBTITLE FOR GRAPHING ARCHIVE ***
/STITLE, %anfile%%OP%%MA%%SLN%%FIX%

/COM, *** PLOTTING EQUIVALENT STRESS ***
/AUTO,1

/EFACE,2  ! 2 = for midside node elements
/PLOPTS,INFO,2
/PLOPTS,LOGO,ON     ! ANSYS logo, instead of ansys
text+version
/PLOPTS,DATE,0 ! No date+time
/PLOPTS,FRAME,OFF   ! No frame around graph
/TRIAD,OFF          ! No triad
AVPRIN,0.E+00,0,
/PBC,ALL,,1    ! ON all bc
/PBC,NFOR,,0   ! except nodal forces
/PBC,NMOM,,0   ! except nodal moment
/PBC,RFOR,,0   ! except reaction forces
/PBC,RMOM,,0   ! except reaction moment
/PBC,PATH,,0   ! except path
ETABLE,SEQV1,S,EQV
SMULT,SEQV_W,SEQV1,,g_w
PLETAB,SEQV_W,AVG
!PLNSOL,S,EQV,2,1

/COM, *** Getting the TIME and DATE signature ***
*GET, DATEDONE, ACTIVE, ,DBASE, LDATE
*GET, TIMEDONE, ACTIVE, ,TIME, WALL

/OUT,%anfile%%MA%%SLN%%OP%%FIX%,anext,andir,APPEND
/COM,========================== SUMMARY BEGIN
=========================
/COM,                        required        used
Ratio
/COM,
used/required
```

```
*VWRITE,LABEL1(1,1),LABEL1(1,2),VALUE1(1,1),VALUE1(1,2),VAL
UE1(1,3)
(1X,A8,1X,A8,1X,E14.5,1X,E14.5,1X,F8.3)
/COM,------------------------------------------------------------
------------
*VWRITE,LABEL2(1,1),LABEL2(1,2)
(1X,A8,1X,A8)
/COM,     Experimental        MBT            FEA
Ratio    Ratio
/COM,
MBT/Exp  FEA/Exp
*VWRITE,VALUE2(1,1),VALUE2(1,2),VALUE2(1,3),VALUE2(1,4),VAL
UE2(1,5)
(4X,E14.5,1X,E14.5,1X,E14.5,1X,F8.3,1X,F8.3)
/COM,------------------------------------------------------------
------------
/COM,                         MBT         FEA(VCCT)
Ratio
/COM,
FEA/MBT
*VWRITE,LABEL3(1,1),LABEL3(1,2),VALUE3(1,1),VALUE3(1,2),VAL
UE3(1,3)
(1X,A8,1X,A8,1X,F14.5,1X,F14.5,1X,F8.3)
/COM,====================== Material Properties
=======================
/COM,                  ACTUAL SPECIMEN       USED
Ratio
/COM,
USED/ACTUAL
*VWRITE,LABELMP(1,1),LABELMP(1,2),VALUEMP(1,1),VALUEMP(1,2)
,VALUEMP(1,3)
(1X,A8,1X,A8,1X,E14.5,1X,E14.5,1X,F8.3)
*VWRITE,LABELVF(1,1),LABELVF(1,2),VALUEVF(1,1),VALUEVF(1,2)
,VALUEVF(1,3)
(1X,A8,1X,A8,1X,F14.1,1X,F14.1,1X,F8.3)
/COM,-------------------- Coefficient of Friction ---------
------------
*VWRITE,LABELMU(1,1),VALUEMU(1,1)
(1X,A8,1X,E14.5)
/COM,========================= Analysis Types
=========================
/COM, SPECIMEN--MATERIAL---SOLUTION_TYPE---OPTION
*VWRITE, SPEC, MATR, NLGEOMV, OPTION
%I     %I     %I    %I
/COM, SPEC          ==> 1=DCB, 2=ENF, 3=MMB.
```

```
/COM, MATERIAL      ==> 1=ISOPHTHALIC POLYESTER,
2=VINYLESTER, 3=EPOXY
/COM, SOLUTION TYPE ==> 0=LINEAR, 1=NONLINEAR
/COM, TABS OPTION   ==> 1=INCLUDE, 2=EXCLUDE
/COM,============================ Time etc.
============================
/COM,    DATEDONE   |     TIMEDONE   |   SOL_TIME (mins)  |
SUBSTEP
*VWRITE, DATEDONE, TIMEDONE, SOLTIME/60, LASTST
(F14.0,'  ',F14.5,'  ',F14.2,'  ',F14.0)
/COM,=========================== SUMMARY  END
=========================
/OUT
SAVE,MMB_geom5,db,MMB
*LIST,%anfile%%MA%%SLN%%OP%%FIX%,anext,andir
FINISH
/EOF
```